The Role of Interstitial Nitrogen in the Precipitation Hardening Reactions in High-Chromium Ferritic Steels

by

John Edward Leitch

Thesis submitted to the Faculty of Engineering of the University of Cape Town in fulfilment of the requirements for the degree of Master of Science (Applied Science).

September 1987

Acknowledgements

Dr D Waters, Dept. of Geology, University of Cape Town, for the use of x-ray diffraction facilities.

Dr D Williams, Director of the Institute for Electron Microscopy, Medical Research Council, for the use of electron microscopy facilities.

Mrs S Cooper for typing the manuscript.

Mr B Greaves for assistance with photographic printing.

The Council of Mintek, for provision of financial support.

Prof A Ball, for his able supervision.

My wife, for her patience.

Dedicated to my parents.

ABSTRACT

The effects of exposure to temperatures in the range 475 - 800 C on the hardness and associated microstructure of high chromium ferritic steels has been investigated. Low-carbon 26Cr-1Mo steels containing 0,02 - 0,04% nitrogen were found to constitute an age hardening system when quenched from a temperature of nitrogen solubility and exposed at temperatures in the range 600 - 700 C. TEM observations on thin foils revealed that hardening was associated with the formation of a high density of Cr-N zones. These grew on over-ageing into disc-shaped Cr-N precipitates situated on {100} lattice planes, and ultimately became large incoherent precipitates.

Ageing at 475 C and 550 C produced hardening due to the formation of chromium-rich ferrite phases α' as a result of the miscibility gap in the Fe-Cr phase diagram. However the presence of interstitial nitrogen in solution in the steel considerably reduced the rate of hardening, especially at 475 C. TEM examination confirmed that this effect was due to the formation of Cr-N zones in preference to α'. This type of decomposition occurs by a mechanism of nucleation and growth, forming zones similar to those formed during an ageing at 600 C. When depleted of interstitial nitrogen, through precipitation at 800 C or through zone formation at 475 C, the specimens aged at 475 C underwent spinodal decomposition. Thus nitrogen in solid solution was found to have a significant effect on the 475 C hardening reaction.

Precision X-ray diffraction measurements revealed the presence of secondary diffraction peaks associated with the Bragg peaks, which comfirmed the formation of Cr-rich phases during ageing at 475 C. The calculated associated lattice parameter measurements allowed estimates of the compositions of the decomposition phases to be made. These were calculated to be about 6-18% Cr in the Fe-rich and 60-80% Cr in the Cr-rich phases of the 26Cr-1Mo steel.

CONTENTS

Chapter 1

INTRODUCTION

Ferritic stainless steels are, by the simplest definition, binary alloys of iron and between 12 and 30% by weight of chromium, with interstitial (carbon and nitrogen) contents low enough to preclude the formation of significant amounts of retained austenite or martensite during cooling from high temperatures. They are cheaper than and are generally considered to be inferior to the widely used austenitic stainless steels, which are based on 18% chromium and 8% nickel; this inferiority is considered to apply to their weldability and corrosion resistance. Under optimum conditions the ferritics have good corrosion resistance, good tensile strength, reasonable impact energy and sufficient ductility to meet numerous fabrication requirements. However, exposures to two different elevated temperature ranges can have detrimental effects on their mechanical properties and corrosion resistance, to the extent that serviceability is greatly impaired. Despite this the ferritics are attractive in their advantages over the austenitics: they are cheaper (nickel is an expensive alloying element) and they are not susceptible to stress corrosion cracking in chloride environments, which can be a major drawback with the austenitics.

Impairment of impact toughness and of resistance to intergranular corrosion after exposure to temperatures above about 1000 C, such as after a welding procedure, have always been problems associated with ferritic stainless steels. The causes of these are complex, but are related primarily to the presence in the steel of interstitials (carbon and nitrogen), which have decreasing solubility in ferrite solid solution with decreasing temperature. Other aggravating factors are the rapid grain growth at high temperature, and the inherent increase in flow stress that results from increasing amounts of chromium alloyed with iron. The overall degradation is

known as **high temperature embrittlement.**

The **475 C hardening** reaction occurs under very different conditions from the above. Exposure for very long periods (of the order of tens of hours) to temperatures around 475 C results in increased hardness and flow stress, decreased ductility, and degradation of room temperature impact toughness to virtually zero. These effects are often accompanied by a loss of corrosion resistance. The extent of the reaction is dependent on the chromium content of the steel, and in fact its origin is the presence of a miscibility gap below about 550 C in the iron-chromium phase diagram.

Both of these phenomena have been the subject of numerous publications, particularly during the 1970's, with research in these areas having been given impetus by the development of progressively more sophisticated steelmaking techniques such as argon-oxygen decarburization, vacuum melting and electron-beam refining. Two very comprehensive reviews covering the properties and microstructures of the ferritic stainless steels have been published by Rajkay (1967) and Demo (1977); the volume of information published recently is so great that only papers quite relevant to the present study are reviewed in the following pages.

Both the high temperature embrittlement and the 475 C hardening have been studied in the present work, and they are different enough as regards the circumstances under which each presents itself, to be dealt with separately. It should be noted that this study is confined to high chromium ferritics (in practice 26Cr-1Mo steel and to a lesser extent, 30Cr steel); the varieties stabilized with titanium or niobium are also excluded.

1.1 The High Temperature Embrittlement Reaction

It has long been known that exposure to high temperatures can

result in the degradation of the toughness, ductility and corrosion resistance of the ferritic stainless steels, and that subsequent annealing at about 700 to 800 C reduces these effects, to a large extent restoring the original properties. The elements carbon and nitrogen, generally present as interstitial impurities in small amounts, have a powerful effect on the structure of these steels and on the resulting mechanical properties and corrosion resistance.

Figure 1.1 shows a section of the phase diagram for the Fe-26Cr-N system (Brewer and Chang, 1972). From a very small solubility at 900 C and below, the amount of nitrogen that is soluble in the alpha phase at 1100 C is quite considerable at about 0,14 weight % (1400 ppm). Clearly if any more than about 100 ppm of nitrogen (0,01%) is present in solid solution at low temperatures, it will exist as a non-equilibruim concentration. Similar limits apply to carbon in solid solution: data by Grubb and Wright (1979) give solubilities in 26% chromium steel at 800 C, of 10 ppm for nitrogen and at least an order of magnitude lower for carbon. These low solubilities at the lower temperatures should have an effect on the structure and properties of these steels. Nevertheless, prior to the important publication by Binder and Spendelow (1951), the detrimental properties that follow high temperature exposure were attributed to the high chromium contents of these steels.

Binder and Spendelow (1951) used vacuum-melted steels to show that a 25% chromium steel could indeed have high impact strength provided the total interstitial (carbon and nitrogen) content was kept below 350 ppm. In fact it was shown that the 25% chromium steel had a higher impact energy and lower impact ductile-brittle transition temperature than vacuum-melted steels of lower chromium content. (They also demonstrated the increase in hardness - from Rockwell B60 to B80 - which occurs on increasing the chromium content of vacuum-melted steels from 12% to 26%, and which is a consequence of solid-solution hardening.) Thus some of the

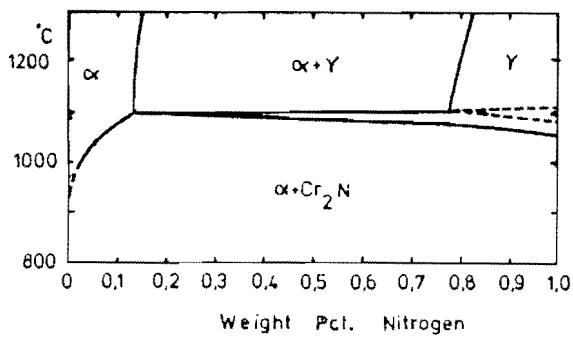

Figure 1.1 Section of the phase diagram of the Fe-26Cr-N system (Brewer and Chang, 1972).

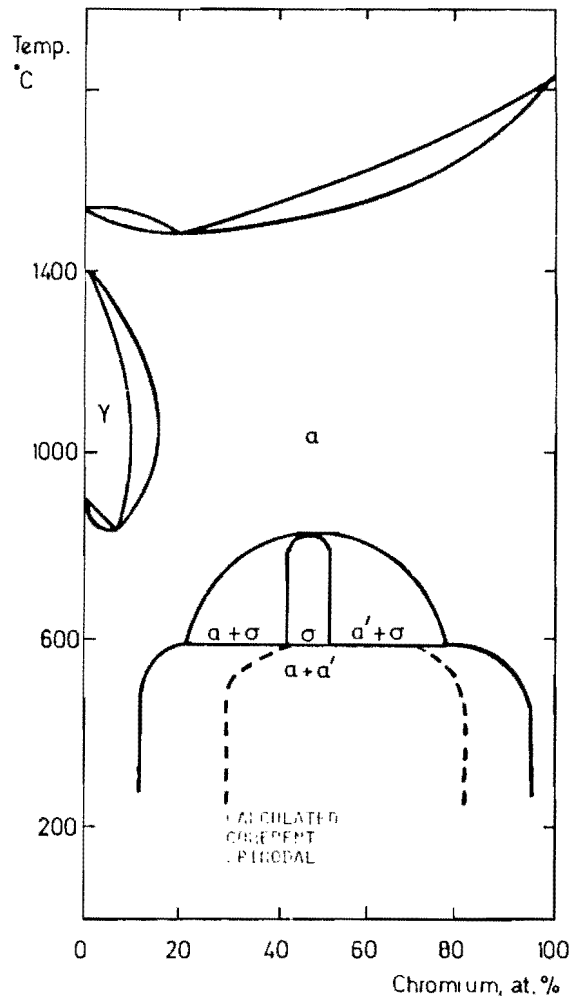

Figure 1.2 The iron-chromium phase diagram, showing the miscibility gap below about 560 C and, inside it, the calculated coherent spinodal (Hendry et al, 1979).

potentially detrimental effects of interstitials were proven. Thielsch (1955) gave guidelines for welding ferritic stainless steels: noting the embrittlement associated with the solution of carbides at elevated temperatures, he recommended a one-hour anneal at 705 to 790 C to restore ductility. However, no reason was given for this treatment.

Susceptibility to intergranualar corrosion was studied by Lula, Lena and Kiefer (1954): the high chromium ferritics are sensitized when cooled rapidly after exposure to temperatures above 950 C, an effect that can be removed by a short annealing treatment at 700 to 850 C. Their proposed mechanism for sensitization was the grain boundary precipitation of carbides or nitrides which results in the presence of matrix strains, and consequently a susceptiblity to grain boundary corrosion. Annealing relieved the stresses and thus restored corrosion resistance.

An important study by Baerlecken, Fischer and Lorenz (1961) showed that the resistance of ferritic stainless steels to intergranular corrosion is a function of the carbon content. These steels become sensitized after quenching from high temperatures if they contain more than about 100 ppm of carbon in solution in the ferrite. Any carbon content above that amount is precipitated even when the steel is quenched quite rapidly from the temperatures at which the carbon is soluble.

The intergranular corrosion problem received much attention towards the end of the 1960's, and was the subject of publications by Bond (1969), Hodges (1971) and Demo (1971), all of whom worked with high-purity (low interstitial) steels containing at 18 to 26% chromium. In general they found that, contrary to experience with commercial grades (high interstitial contents), as described above, corrosion resistance after quenching from around 1100 C was very good. Air cooling of these low-interstitial steels degraded their resistance to intergranular corrosion, while furnace cooling

produced intermediate results which depended upon alloying elements. They concluded that at high temperatures (ie. above 950 C) all of the interstitials are in solution; if the interstitial contents are low enough they can be kept in solid solution during a rapid quench, resulting in good resistance to intergranular corrosion. However, air cooling these steels allows precipitates of chromium carbides and nitrides to form at the grain boundaries, thus depleting the adjacent matrix of chromium and causing sensitization. Furnace cooling or annealing at 700 to 950 C allows diffusion of chromium to the depleted grain boundary regions to occur, thus restoring good corrosion resistance.

In the case of commercial grades of high-chromium steels, the high interstitial contents force precipitation even during a rapid quench; the large supersaturation of interstitials at intermediate temperatures, and their rapid rate of diffusion, result in grain boundary precipitation. Because of the considerably slower rate of diffusion of chromium, depletion of this element occurs in the grain boundary regions, leaving them susceptible to corrosion.

Demo (1971) investigated the ductility of a commercial grade (high-interstitial) 26% chromium steel after exposures at high temperature (1100 C) followed by either water quenching, air cooling, furnace cooling, or annealing after quenching. Quenching resulted in severe reductions in ductility and resistance to intergranular corrosion. Optical microscopy and transmission electron microscopy (TEM) examinations revealed the presence of a duplex structure, which included retained austenite, and of heavy precipitation on dislocations. Both of these microstructural features were considered to contribute to the undesireable properties encountered after quenching. Good ductility followed the high temperature exposure when slower cooling rates were used - air or furnace cooling - or when an 850 C anneal had been carried out after the quenching. This annealing treatment also restored the corrosion resistance of the quenched

specimen.

Demo (1971) concluded that the 26% chromium steel was sensitized to intergranular corrosion following high temperature exposure, because the interstitials dissolved in solid solution form precipitates at intermediate temperatures, leaving chromium-depleted areas at the grain boundaries. Thus precipitation of chromium carbides and nitrides occurs in the temperature range 500-950 C, although annealing above about 700 C allows chromium diffusion to occur, restoring this element to the grain boundary areas. An interesting TEM observation was the absence of precipitation on the dislocations present in the air-cooled specimen, which had good ductility, in contrast to the quenched specimen with poor ductility and heavy precipitation on dislocations.

Semchyshen, Bond and Dundas (1971) examined the impact test behaviour of the high-chromium ferritics as a function of heat treatment and interstitial content. They found a slight deterioration in impact properties of a low-interstitial 25% chromium steel when quenched from 1150 C, compared with after an annealing treatment at 980 C. On the other hand the high-interstitial equivalent of this steel (800 ppm of C+N) had very much higher ductile-brittle transition temperatures, and furthermore after the 1150 C quench the impact energies attained in this case were very low. The last observation is consistent with the findings of Demo (1971) of poor ductility in quenched high-interstitial steels. The authors concluded, from studies on 17% chromium steels, that precipitation of chromium carbo-nitrides, mainly at grain boundaries, is the principal cause of increased transition temperatures when high-interstitial alloys are quenched from high temperatures.

Wright (1971) researched the weldability of 26Cr-1Mo steels as a function of interstitial contents, using material with a wide range of carbon and nitrogen contents (C+N 65-900 ppm). In tests of reaction to annealing treatments, in all cases

water quenching from the anneal at 800-980 C produced a lower impact ductile-brittle transition temperature than did air cooling. This effect was expecially noticeable both at the lower interstitial levels and with stabilizing titanium additions. When steels of different interstitial contents were compared, the effects of carbon and nitrogen on impact properties were quite pronounced, with increases in interstitial content raising the transition temperature, particularly at the lower carbon and nitrogen levels and at thicker gauges of material. Concerning tensile properties, the effects of an increase in total carbon and nitrogen from 65 to 300 ppm were an increase in yield strength of about 80 MPa and decrease in elongation of about 13%. It was concluded that for acceptable properties in 12,7 mm plate gauges, the 26Cr-1Mo steel required total interstitial (C+N) contents to be kept below about 125 ppm.

Plumtree and Gullberg (1974) examined the influence of variations in interstitial content on the ductile-brittle transition temperature of a 25% chromium steel. The final stages of heat treatment, which were applied to all the alloys used, were a 30 minute anneal at 850 C followed by either a water quench or air cooling. Increased ductile-brittle transition temperatures resulted from increases in interstitial contents. Microscopy revealed the presence of very thin grain boundary films, increasing in extent and size with interstitial content, while in the alloys with higher carbon or nitrogen contents, larger discrete particles were present within the grains. Tensile test results showed that the yield stress and the slope of the Petch equation did not vary with interstitial content of the water-quenched specimens. It was concluded that the presence of hard precipitates, particularly at the grain boundaries, promoted brittle fracture; this accounted for the decreased elongations and increased ductile-brittle impact transition temperatures which occurred with increased interstitial contents.

The investigation by Wright (1971) referred to above was extended (Grubb and Wright, 1979) in a more specific research into the microstructures, tensile and impact properties, and modes of fracture of two 26% chromium steels of low and high interstitial contents respectively. A number of different heat treatments were used, based on variations in cooling rate from a 1290 C solution treatment, or variations in the annealing temperature in the range 540-955 C carried out after the solution treatment and quenching. Optical microscopy and TEM examinations showed that rapid quenching prevented carbide and nitride precipitation in the low-interstitial (67 ppm C+N) alloy, but not in the high-interstitial case. However in the low-interstitial alloy, decreased cooling rate from solution treatment temperature did produce small quantities of grain boundary precipitation. The ten-minute anneals of the quenched material produced variations in microstructure with changes in annealing temperature: at 870 C, both intragranular and grain-boundary precipitates were formed; at 620 to 790 C, only semi-continuous grain boundary precipitates; and at 540 C only a plate-like intragranular species which was identified as chromium nitride. The high-interstitial steel specimens, on the other hand, were found to have both continuous grain boundary films and angular or globular intragranular precipitates after the various heat treatments.

These authors found, as expected, that changes in the state of the carbon and nitrogen in the two steels could be related to large variations in the ductile-brittle transition temperature. The low-interstitial steel had its lowest transition temperature in the as-quenched condition. It was embrittled by grain boundary carbide precipitation which occurred during the post-quench intermediate temperature (620-870 C) anneal. However, much greater increases in transition temperature were associated with the presence of plate-like intragranular precipitates formed at 540 C, which played a strong embrittling role both as crack initiation sites, and through their tendency to increase the flow stress

of the specimen, possibly by dislocation immobilization. In the high interstitial steel, although quenching from the high temperature suppressed precipitation, embrittlement resulted from increased yield and flow stresses due to solid solution hardening. Intermediate temperature annealing in this case also causes embrittlement through the formation of grain boundary carbides and intragranular nitrides, both of which act as crack initiation sites.

While this work of Grubb and Wright (1979) was, as far as is known, the most comprehensive study of the microstructural developments associated with high temperature embrittlement published at that time, many unanswered questions remained. These included the temperatures and kinetics of nucleation of precipitates, the role of existing dislocations, and the relative importances of dislocation locking, solid solution strengthening and precipitation hardening. Demo (1977), in his comprehensive review, has come to the following conclusion which summarizes the uncertainty concerning the mechanism of embrittlement:

> "Baerlecken et al, Demo, Semchyshen et al, and Plumtree et al all conclude from their data that the so-called high-temperature embrittlement phenomenon of high-chromium ferritic stainless steels is due to precipitation of chromium-rich carbides and nitrides caused by relief of supersaturation when the alloys are exposed to high temperatures. Baerlacken et al and Semchyshen et al find the embrittlement occurs because the chromium-rich precipitate forms on grain boundaries, while Demo and Plumtree claim the embrittlement occurs because a finely dispersed precipitate in the grain matrix hinders dislocation motion, and precipitates in the grain boundaries do not necessarily indicate alloy embrittlement. Perhaps the difference in thought resides in testing severity. A grain boundary precipitate may be detrimental to the high-rate energy absorbing requirement of the impact test but perhaps not detrimental to the

slow-rate energy absorbing requirement of the tensile or slow bend test. The important point, however, is the general agreement that the high-temperature embrittlement phenomenon observed in ferritic stainless steels is dependent upon the levels of carbon and nitrogen in the alloys. The embrittlement problem in chromium-iron alloys will manifest itself whenever alloys containing moderate or high interstitial levels are heated to temperatures above about 950 C. The embrittlement is caused by precipitation of chromium-rich carbides and nitrides on grain boundaries or dislocations or both. It is at once apparent that the same precipitation mechanism causing embrittlement also produces the serious loss of corrosion resistance when ferritic alloys are heated to high temperatures"

This present work is an attempt to clarify some aspects of the role of nitrogen in the hardening and resultant embrittlement of low-interstitial 26Cr-1Mo steels. The reader is referred to the paper given by Leitch and Ball (1979) on some of the results obtained here. A copy of this paper is included as Appendix A.

1.2 The 475 C Hardening Reaction

The name "475 C hardening reaction" derives from the substantial increase in hardness and yield strength, with a corresponding reduction in ductility and impact toughness, which occurs in high-chromium ferritic steels on prolonged exposure to temperatures around 475 C. A further deleterious effect is the associated loss of corrosion resistance which can considerably reduce the serviceability of these steels after intermediate temperature exposure. While the phenomenon is undoubtably of great practical importance to engineers seeking to use high-chromium steels in intermediate temperature applications, it is also of interest to metallurgists concerned with the fundamentals of alloy formation.

The iron-chromium phase diagram (fig. 1.2) shows the existence of the intermetallic sigma phase at temperatures above about 560 C and compositions centred around 50%Fe-50%Cr. This phase is naturally quite hard and brittle and hence undesireable. At temperatures below about 560 C there is a miscibility gap which extends from chromium contents of about 16% to about 80%, and it is within this gap that the 475 C hardening reaction occurs. The important changes in mechanical properties and corrosion resistance, referred to above, occur slowly: typically they are detected after periods of ageing of the order of 10 hours, and have significant effect after 100 hours, depending in general on the chromium content of the alloy. Ageing of a 25% chromium steel for long periods such as 1000 hours can result in hardness increases of up to 200 points (HV); however after only 9 hours, increases in impact ductile-brittle transition temperatures of as much as 250 C have been reported (Plumtree and Gullberg, 1976).

Because of its profound effect on the properties of high-chromium ferritic steels, the reaction has been the subject of much research since the early 1950's. Comprehensive literature surveys of the subject have been written by Rajkay (1967) and Demo (1977). In this work we shall briefly survey the important papers which contributed to the understanding of the nature of the 475 C hardening and in particular those in which TEM on thin foils was used as an experimental technique to obtain an understanding of the underlying solid state reactions.

The 475 C Hardening: Early Experimental Work

One of the major advances in the understanding of the nature of the reaction was the publication by Williams and Paxton (1957) of data obtained from measurements of electrical resistivity, hardness, magnetic behaviour and x-ray diffraction. It followed from these results that the 475 C hardening is an age-hardening reaction, which is associated

with the precipitation of small coherent particles rich in chromium, as a result of the existence of a miscibility gap in the binary Fe-Cr system. They proposed the phase diagram which forms the basis of that shown in fig. 1.2, and pointed out that this incompatibility between iron and chromium is somewhat surprising considering the smallness of the atomic size difference of these two elements (about 0,5%) and the fact that both are considered to have the same valence in the metallic state.

Williams and Paxton (1957) attributed the miscibility gap to chemical or magnetic energies, or a combination of the two. The precipitate - known as α' phase - may be considered to be bcc chromium containing small amounts of iron, and its rate of formation appears unaffected by either the presence of the usual impurity species in the alloy, or by differences in heat treatment prior to ageing. They concluded that both matrix and precipitate are strained, the former in tension and the latter in compression, to a common lattice parameter which is that of the unaged material.

Further work by Williams (1958) showed that the miscibility gap in the phase diagram appears to be almost flat between chromium contents of 30 and 75%. He concluded that this marked flatness arises from a cooperative phenomenon, presumeably of magnetic origin; the chromium-rich precipitate is anti-ferromagnetic and thus exhibits a new hardening mechanism analogous to atomic ordering, in which a unit dislocation passing through an anti-ferromagnetic domain would create a domain wall and thereby require an input of energy. However, Marcinkowski, Fisher and Szirmae (1964), analyzing the contributions of various strengthening mechanisms applicable to an Fe-48%Cr alloy, concluded that lattice friction within the chromium-rich phase, and the interfacial energy due to a dislocation passing through a precipitate ("chemical strengthening"), together account for 60% of the observed hardening. Coherency strains and differences in elastic moduli were thought to contribute the

remaining strengthening.

Spinodal Decomposition in the Iron-Chromium System

The existence of the miscibility gap in the iron-chromium phase diagram has been confirmed by other techniques. Calculations based on thermodynamic measurements by Kubaschewski and Chart (1964) proved the existence of the gap and showed that spinodal decomposition should indeed occur. Magnetization measurements (Imai, Izumiyama and Masumoto, 1966) have shown the existence of two Curie points after ageing, with a temperature differential increasing with ageing time. It could therefore be concluded that decomposition into zones respectively rich and poor in chromium occurs by a mechanism of spinodal decomposition. These experimental results confirmed statistical-thermodynamical calculations which had suggested both the existence of the miscibility gap and the likelihood of the mechanism of spinodal decomposition occurring.

When a homogeneous alloy is quenched into the miscibility gap of the phase diagram, a phase separation may occur by one of two processes: spinodal decomposition, or nucleation and growth. The two differ in that the former occurs when the material is inherently unstable to small fluctuations in composition, and hence decomposes spontaneously, while nucleation is associated with a thermodynamic barrier to phase separation and therefore involves a thermally activated step. The kinetics of spinodal decomposition are governed solely by diffusion of the atomic species and no incubation time or activation energy is associated with the transformation; the atomic species in solution rearrange in a continuous fashion to form like-atom clusters (LaSalle and Schwartz, 1986).

The relationship of free energy to composition at a particular temperature has a characteristic form when inside the spinodal, with the second derivative of free energy with

respect to composition being a negative quantity. (This allows the free energy of the system to decrease continuously when infinitely small phase separations occur.) Outside of the spinodal curve on the phase diagram, d^2F/dC^2 is positive, reflecting the need to form a critical-sized nucleus with increased overall free energy as the first stage of phase separation. The boundary between the two types of phase change on the phase diagram, known as the spinodal curve, is the loci of points on the free energy/composition curves, for different temperatures, where $d^2F/dC^2=0$ (see for example Martin and Doherty, 1976).

The approximate spinodal curve within the miscibility gap in the Fe-Cr phase diagram can be seen in fig. 1.2. It is clear that at temperatures around 475 C, ferritic stainless steels of 25-30% chromium lie close to the spinodal on this phase diagram, and thus either of the two phase separation processes might occur.

Mossbauer spectroscopy is not only able to confirm the existence of the miscibility gap, but can also differentiate between the possible mechanisms of decomposition. Chandra and Schwartz (1971) showed that when aged at 475 C, an Fe-60%Cr alloy undergoes spinodal decomposition, while for an Fe-24%Cr alloy the mechanism is nucleation and growth. The solubility of chromium in iron at 475 C is estimated to be 12%; at this temperature alloys with chromium contents between 12% and 30% should separate by nucleation and growth, and higher chromium contents by spinodal decomposition.

Similar results were found by De Nys and Gielen (1971) using the same experimental technique: at a temperature of 470 C a 20% chromium steel decomposes by nucleation and growth, while alloys with chromium contents of 30% and greater undergo extremely slow spinodal decomposition. At 540 C, the mechanism of nucleation and growth applies to all compositions and it can be concluded that this temperature is in fact above the coherent spinodal.

In another study using Mossbauer spectroscopy, Roy and Solly (1973) confirmed the tendency towards decomposition when alloys containing 17, 25 and 30% chromium are aged at 475 C. However no evidence of a process of nucleation and growth was found, even in the 17% chromium alloy.

TEM Examinations of Iron-Chromium Alloys Aged at 475 C

The technique of transmission electron microscopy (TEM) has been used by a number of researchers on thin foils taken from ferritic stainless steels aged at appropriate temperatures within the miscibility gap. The question of the nature of the TEM image formed in this case is a very interesting one, and in the past some erroneous interpretations have been made of features found on micrographs. Therefore before reviewing some of the published results, we shall briefly consider the nature of the TEM image likely to be formed in thin foils where decomposition has produced chromium-rich precipitates within a chromium-depleted matrix.

Consider a 30% chromium steel aged at 475 C long enough for decomposition to occur, resulting in the formation of small coherent precipitates of α' phase containing 80% chromium, balance iron, within an iron-rich matrix containing 20% chromium. The two possible origins of the contrast which produces the TEM image are structure factor contrast and strain field contrast (Hirsch, Howie, Nicholson, Pashley & Whelan, 1965). The former arises when precipitate and matrix have different unit cell structure factors, arising from differences in the atomic scattering factors of the constituent atoms. In this case contrast in the image arises from what is equivalent to an effective foil thickness difference in the presence of a precipitate. As there is little difference between the atomic scattering factors of iron and chromium, it can be shown that structure factor contrast should not be visible when the α' precipitates are below 10 nm (nanometers) in size.

Strain field contrast arises from the displacement of lattice planes from their normal positions as a result of the difference in the lattice parameters of precipitate and matrix. The result is a phase shift of the diffracted beam which has passed through the precipitate, relative to the beam that has passed through the matrix only. For the precipitate and matrix compositions assumed above, the lattice mismatch is about 0,2%. It can be shown that a 20% change in image intensity of the precipitate relative to the matrix, is only exceeded when there is sufficient strain such as would be caused by a precipitate at least 15 nm in diameter. Thus to be visible in thin foil TEM, the chromium-rich precipitates would have to be relatively large; even then they would not display a dot-like structure, but each would appear as an area little different in contrast to the matrix, and of size approximately equal to the actual size of the precipitate.

The first published study of thin foils taken from 475 C hardened Fe-Cr alloys, examined by means of the technique of TEM, is attributed to Marcinkowski et al (1964). A 48% chromium alloy aged at 500 C for over 3000 hours, was found to have a high density of roughly spherical centres of contrast which were only visible when the foil was orientated so as to diffract strongly. These features, which were about 7 nm in size and distributed throughout the matrix, were considered to be the chromium-rich precipitates of α'.

In the same year, a TEM study of thin foils prepared from a 21% chromium ferritic stainless steel aged at 475 C, was published by Blackburn and Nutting (1964). They found a very fine uniformly-distributed precipitate visible after 80-100 hours of ageing. After further ageing, to a total of 1000 hours at 475 C, the microstructure comprised small disc-like precipitates, lying on {100} planes of the ferrite matrix, and accompanied by relatively large strain fields. It was concluded that the precipitates were chromium-rich ferrite, although the authors acknowledged the difficulty in

accounting for the large strain fields indicated by the contrast visible in the surrounding matrix, particularly in view of the smallness of the coherency strain expected from the formation of chromium-rich precipitates within a chromium-depleted matrix.

Lagneborg (1967) examined the microstructures of a 30% chromium alloy aged at 475 C and at 550 C. Ageing at 475 C gave a hardness increase from about HV 200 to a final value of HV 350. Associated with the hardening was a finely-dispersed uniform precipitation which became visible in TEM after periods of ageing as short as one hour. These precipitates were of spherical shape irrespective of ageing time, from which observation it was concluded that they had formed by a process of spinodal decomposition. In addition preferential precipitation occurred at grain boundaries and adjacent to them, at inclusions and at dislocations; this was analysed and found to consist of chromium nitrides.

Ageing at 550 C gave less of a hardness increase - at the most about HV 50 - and was subject to softening on over-ageing. The microstructure corresponding to the 550 C ageing comprised a coarser general precipitation, in the shape of discs with large associated strain fields. These precipitates were identified as chromium-rich α' situated on $\{100\}$ planes, and their disc-shaped morphology attributed to their formation by a nucleation-and-growth mechanism, in which vacancies or vacancy clusters constitute a preferred nucleation site.

The large matrix strain fields observed by both Blackburn & Nutting (1964) and Lagneborg (1967) to be associated with disc-shaped precipitates of α', appear inconsistent with the relatively small amount of lattice expansion that should occur normal to the disc, when it is formed through the replacement of iron atoms with chromium. This aspect is covered in more detail later.

Roy and Solly (1973) reported TEM observations on various iron-chromium alloys aged at 475 C for 1000 hours. The 16% chromium alloy showed no significant microstructural features; alloys with chromium contents of 25% or more produced a very fine disperse intragranular precipitation which was particularly visible in TEM under strongly diffracting conditions. The mean precipitate size increased with chromium content. Electron diffraction measurements on extraction replicas of the precipitates identified them as Fe-Cr, of the same crystallographic orientation and the same lattice parameter as the matrix (although the precision of this technique is limited).

A study of the effects of variations in the nitrogen content of a 22% chromium steel, on its age hardening reaction at 500 C, was reported by Hendry, Mazur and Jack (1979). The degree of hardness increase with ageing was found to be dependent on the nitrogen content: a negligible amount of hardening was associated with a near-zero nitrogen content, but the highest nitrogen content of 800 ppm gave a hardness increase of about HV 150 after about 200 hours of ageing. TEM examination of the material aged for only five hours showed a fine modulated structure in all specimens, irrespective of nitrogen content. Further ageing of the nitrogen-containing specimens revealed the formation of disc-shaped precipitates, lying on {100} matrix planes and accompanied by strong strain field contrast; no such microstructural changes were found in the nitrogen-free specimen after further ageing. The discs were identified as mixed substitutional-interstitial solute-atom clusters, ie. chromium-nitrogen Guinier-Preston zones.

Hendry et al (1979) concluded that the presence of interstitial nitrogen in the interstices of the matrix distorts the surrounding lattice considerably; this accounts for the size of the strain fields, associated with the zones, and which could not reasonably be produced by pure chromium-rich zones within a chromium-depleted matrix. (The

observations of large strain fields by Blackburn and Nutting (1964) and Lagneborg (1967) are also explained by this mechanism). A new model of 475 C embrittlement of the 22% chromium steel was proposed: during ageing, chromium-nitrogen clustering occurs, resulting in extreme hardening arising from the strength of the Cr-N bonds which must be broken by mobile dislocations during the deformation process. It is proposed that outside of the spinodal, disc-shaped Cr-N clusters are formed by a mechanism of nucleation and growth, while inside of the spinodal spherical Cr-N clusters are formed.

A comprehensive study of the 475 C reaction in commercial ferritic stainless steels with chromium contents of 11-29% was carried out by Nichol, Datta and Aggen (1980). Among the steels examined was a 26Cr-1Mo steel with a moderately high interstitial content (C+N of 500 ppm), although these interstitials had been effectively removed from solid solution through precipitation with titanium which had been added to the steel for that purpose. Exposure of the 26Cr-1Mo steel to a temperature of 482 C for 1000 hours resulted in large increases in hardness and yield strength, in the case of the latter parameter by a factor of 3. The associated microstructures after periods of ageing of 100 and 1000 hours were examined by TEM.

After the shorter period (100 hours) there was no evidence of microstructural change; however after 1000 hours at 482 C, microstructure consisting of net matrix contrast striations was visible along the traces of {100} matrix planes, when viewed under two-beam conditions using a 200 g-vector. This type of contrast has been reported in other alloy systems which have undergone spinodal decomposition; these include Cu-Ni-Fe (Livak & Thomas, 1971); Cu-Ti (Krull, Starke and Newman, 1972, and Cornie, Datta and Soffa, 1973); and Fe-Mo (Miyazaki, Takagishi, Mori and Kozakai, 1980). In these cases spinodal decomposition produces a modulated structure in which solute atoms are distributed periodically along the

orthogonal <100> directions, and the associated TEM images show corresponding contrast modulations in the <100> direction when an appropriate diffraction condition is used.

In the alloy examined by Nichol et al (1980), the modulations in the TEM image are considered to arise from wave-like clusters of chromium atoms associated with spinodal decomposition along the elastically soft <100> directions. It is usual for satellite spots (sidebands) to be present flanking the matrix diffraction spots obtained in TEM on spinodally decomposed alloys. These were not observed, possibly because of the smallness of the mismatch parameter (0,04) and because of the similarity in the atomic scattering factors of iron and chromium, as shown below.

The Bragg Reflections Associated with Spinodal Decomposition

A spinodally decomposed crystalline material, with periodic fluctuations in composition and usually in lattice parameter as well, produces particular effects when subjected to x-ray or electron diffraction. The microstructure can be characterized by three parameters representing the amplitude and wavelength of the compositional fluctuations, and the volume fraction of the phases present. These compositional modulations give rise to sidebands or satellites about the Bragg reflection during x-ray or electron diffraction. As decomposition proceeds, the wavelength of the modulations increases resulting in the disappearance of the sidebands from the parent Bragg reflection. With further phase separation the sidebands are replaced by very diffuse satellite spots (or peaks, as appropriate) which eventually evolve towards the sharp spots characteristic of the co-existing non-coherent equilibrium phase which is produced (De Fontaine, 1969).

Examples of sidebands in electron diffraction patterns are given by Livak and Thomas (1971), Cornie et al (1973) and Miyazaki et al (1980), all in alloy systems other than Fe-Cr.

The sidebands occur when the TEM image of the spinodally decomposed material shows contrast modulations or striations perpindicular to <100> directions. In the case of the Fe-Mo alloy, further decomposition leads to growth of the modulations and eventually the formation of incoherent Mo-rich precipitates, while the diffraction spots become asymmetric in both position and intensity. Finally the relection maximum splits into two spots, each corresponding to the different lattice parameters of matrix and precipitate. When ageing is carried out above the coherent spinodal, plate-shaped zones form on {100} matrix planes. In this case no periodic modulations are found in the TEM image, nor do any satellites appear: this corresponds to a nucleation and growth process.

When sidebands are present as a result of periodic compositional fluctuations, the wavelength of the latter may be calculated using the Daniel and Lipson relationship (Cornie et al, 1973):

$$\frac{\Delta g}{g} \qquad \frac{h\ a}{h + k + l}$$

where a is the lattice parameter and $\Delta g/g$ the ratio of the distances from origin and satellite to the hkl spot.

Applying the above equation to the ferritic stainless steels, if we have compositional fluctuations with a period of 10 nm then $\Delta g/g$ should be about 0,014 for the 200 reflection. In a TEM electron diffraction pattern this represents typically about 0,4 mm between (hkl) and the satellite (if spot (hkl) is 30 mm from the origin), and will thus not be easily observed. In XRD for the above parameters the distance from the 200 peak to the satellite should be about 0,9 degrees of 2θ.

Conclusion

It can be concluded that the 475 C hardening reaction does indeed occur at appropriate temperatures and compositions

within the miscibility gap of the Fe-Cr phase diagram. It results from segregation into chromium-rich precipitates within a chromium-depleted matrix, with associated changes in mechanical properties which are wide-ranging and severe. It has been established by Mossbauer spectroscopy that both spinodal decomposition, and nucleation and growth, are mechanisms for the reaction, the former tending to occur at lower temperatures and higher chromium contents (on the iron-rich side of the phase diagram) than the latter mechanism. However, the compositions of ferritic stainless steels (up to 30% chromium) and the temperatures used in investigations (around 475 C) together tend to represent a position on the phase diagram that is close to the spinodal.

There is some discrepancy concerning the reported influence of interstitials, particularly nitrogen, on the hardening reaction: Hendry et al (1979) find that a 22Cr steel only undergoes the reaction when there is some nitrogen present as an impurity, and that hardening is associated with the formation of Cr-N GP zones. On the other hand, hardening has been reported in a low-interstitial 25Cr steel (Plumtree and Gullberg, 1974), and in 18Cr and 26Cr-1Mo steels containing titanium which effectively removes the interstitials from solid solution through precipitation prior to ageing (Nichol et al, 1980). Finally, Grobner (1973) found considerable hardening in an 18Cr steel with very low interstitial levels.

This ambiguity in the role of nitrogen also applies to the actual mechanism of hardening. Three different types of structure have been observed by TEM on thin foils taken from bulk aged material (subject to the use of two-beam or other strongly diffracting conditions). These are:

(1) matrix contrast striations along <100> matrix directions as imaged with a 200 g-vector;

(2) very small dot-like strain centres with high specific strain fields in the surrounding matrix;

(3) small planar precipitates, coherent with a strained

matrix, on {100} planes. (These could be the same species as the strain centres after further growth).

There is a difficulty in accounting for the sizes of the strain fields in (2) and (3) above if they are due to chromium clustering alone, especially in the case of the planar precipitates. Furthermore, the lattice mismatch between chromium clusters and matrix is so small that the formation of a planar morphology, in preference to spherical, seems unlikely, particularly if one considers the extra interfacial energy that should be associated with the planar species.

Chapter 2

THE EXPERIMENTAL TECHNIQUES

2.1 Materials Used

Ferritic stainless steels of 26 and 30 weight percentage chromium were used exclusively in this study. They were obtained from three different sources and embraced three different melting techniques, which resulted in significant differences between them as regards their interstitial (carbon and nitrogen) contents: these varied from very low to somewhat higher than usual in a commmercial grade of ferritic stainless steel. The compositions of these steels are given in Table 1.1; the following is a brief description of them.

(1) A 26% chromium-1% molybdenum vacuum-melted steel (ASTM grade XM27) obtained from Allegheny Ludlum Corporation. This low-interstitial steel contains nominally 0,02% nitrogen and 0,001% carbon. The 2,5 mm thick plate was cold rolled down to 1 mm with intermediate anneals at 820 C in vacuum.

TABLE 2.1

Element	26Cr-1Mo* Allegheny Ludlum	26Cr-1Mo* Climax Molybdenum	30Cr Experimental
Carbon	0,01	0,001	0.04
Nitrogen	0,02	0,01	0,06
Chromium	26,0	26,0	30,6
Molybdenum	1,0	1,0	-
Silicon	0,3	0,25	0,4
Manganese	0,1	0,02	0,4
Iron	balance	balance	balance

Table 2.1: Compositions (by weight) of steels used in this study. * denotes manufacturer's specification.

(2) A similar composition to the above, known as E-Brite 26-1 obtained from Climax Molybdenum Company. This steel is electron-beam refined to ensure low interstitial levels, in this case a carbon content of 0,001% and nitrogen of 0,01%. The 1,7 mm thick sheet was cold rolled down to 1 mm.

(3) A 30% chromium steel obtained from Southern Cross Steel Company as an experimental melt; it had been melted under argon but contained the quite high interstitial levels of 0,04% carbon and 0,06% nitrogen. This steel was in the form of an ingot which was hot rolled and cold rolled down to strip 1 mm thick.

2.2 Heat Treatment and Nitriding

In preparation for the age hardening experiments, the specimens were subjected to one of a choice of three different types of heat treatment as described below. Prior to the preliminery heat treatment, the specimen of size about 50 mm by 15 mm by 1 mm was cleaned thoroughly by degreasing in trichloroethylene vapour, immersing in concentrated sulphuric acid and electropolishing as described in Section 2.4 below.

The heat treatments and nitriding were carried out in a vertical ceramic tube placed inside a resistance-heated furnace. The furnace temperature was controlled by a thermocouple and controller, while another thermocouple situated inside the tube gave an accurate measurement of the specimen temperature. High vacuum inside the ceramic tube was provided by a Balzers turbo-molecular pump, which maintained the system at about 10-7 millitorr. The specimen in the tube was suspended from a length of wire, which itself was hooked over a fuse wire connected between two terminals outside of the heated zone. On completion of the heat treatment period, argon was admitted into the furnace tube until atmospheric pressure was reached, thus allowing removal of the base of the furnace tube. Quenching was effected by

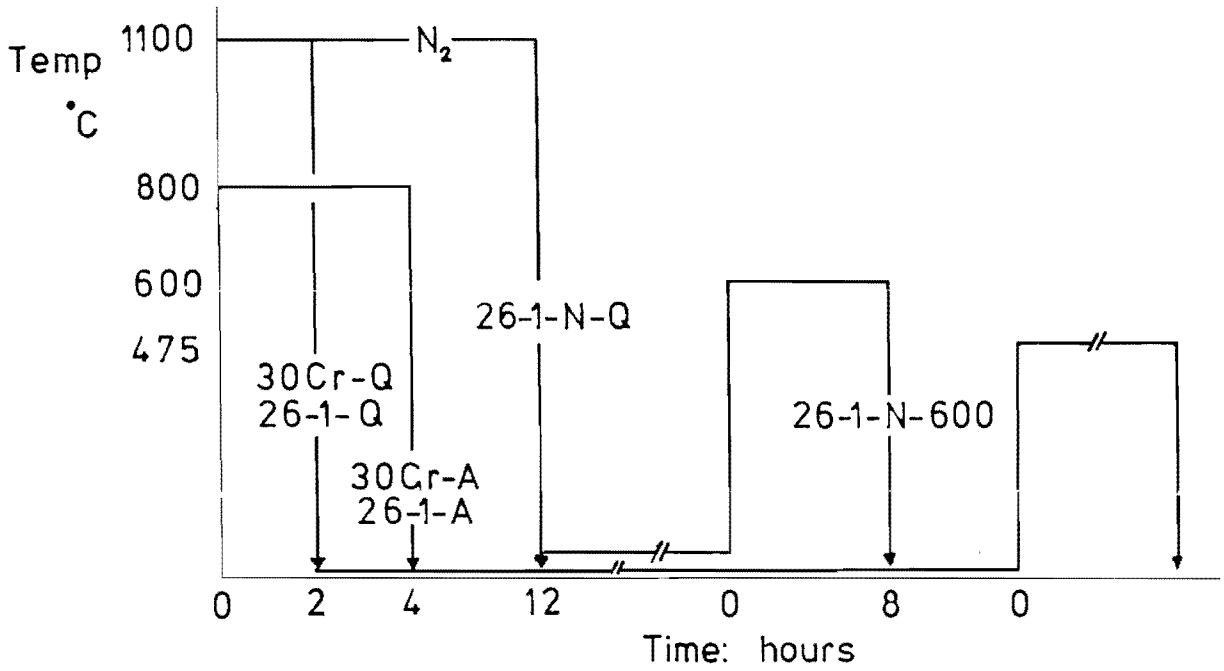

Figure 2.1 Schematic of preliminery heat treatments and the 475 C age hardening.

melting the fuse wire, thus allowing the specimen to drop down the tube into chilled water. While the cooling rate was not measured, it was considered to be quite rapid due to the thinness of the specimen (ie. 1 mm).

Details of each of the three heat treatment procedures, which are referred to as annealing, nitriding and quenching, and solution treatment and quenching, follow.

Annealing was performed at a temperature of 800 C in vacuum for a period of 4 hours followed by quenching. The temperature was chosen in accordance with the phase diagram for a similar composition of ferritic stainless steel, viz. a Fe-26% Cr alloy, which is shown in fig. 1.1. It follows from this phase diagram that the solubility of nitrogen at 800 C is very small, and thus this interstitial should be removed from solid solution quite rapidly at that temperature, through precipitation as chromium nitride. Similarly the interstitial carbon present in the steel should precipitate out as chromium carbide.

Nitriding and quenching were carried out by soaking at a low pressure of pure nitrogen at 1100 C followed by quenching into chilled water. The temperature was chosen for the associated substantial solubility of nitrogen in this steel (see fig. 1.1) and the high diffusion rate. It was assumed that the nitrogen would be retained in solid solution during the quench to low temperatures. The equipment used for nitriding has been described above: the ceramic tube was evacuated and high purity nitrogen (containing less than 10 ppm of oxygen) which had been passed through magnesium perchlorate as a dessicant, was bled into the specimen tube to a pressure of 100 millitorr. This was maintained at temperature for 12 hours, when argon was admitted and quenching carried out as described above. This treatment increased the nitrogen content of the specimen, while the rapid quenching should have ensured that all interstitials remained in solid solution.

Solution treatment and quenching was performed in order to place the interstitials present in the as-received material into solid solution. The solution treatment comprised a two-hour soak at 1100 C in vacuum followed by a water quench as described above.

2.3 Age Hardening and Hardness Measurements

Specimens used in the age hardening experiments were in the form of small sheets, about 15 mm square in size, cut from the 1mm thick strips which had been given one of the preliminery heat treatments described above. Ageing was carried out at various temperatures between 475 C and 750 C in a quartz tube placed inside a resistance furnance, the specimens being maintained under argon. The subsequent cooling was effected by quenching into water.

Hardness measurements were taken as an indication of the change in mechanical properties of these specimens, using a Vickers diamond pyramid under a 5 kg load (increased to 10 kg when hardness values above HV 250 were encountered). Any hardness value reported was the average of at least four indentations.

2.4 Optical Microscopy

Specimens for optical microscopy were prepared by standard metallographic techniques: grinding on successively finer silicon carbide papers from #180 grit down to #600, and polishing on cloths impregnated with diamond pastes from 3 micron down to 0,25 micron. The specimens were then either electro-polished or electro-etched, the former procedure giving specimens which on examination under a metallurgical microscope tended to be devoid of all features excepting precipitates, while the latter invariably etched the grain boundaries (especially when grain boundary precipitation was present).

Electropolishing was carried out in a mixture of butyl oxitol, ethanol and perchloric acid chilled to a temperature of about -10 C, at a potential of about 15 volts. Electro-etching was done using the well-known oxalic acid etchant (a 10% solution in water) at room temperature at 7 volts. The specimens thus prepared were examined under a Reichert metallurgical microscope using objective magnifications of either 16 or 63 times. Photographs were taken using standard 35 mm film in an integrated camera system.

2.5 Transmission Electron Microscopy (TEM)

TEM was used to examine the microstructures of a number of specimens, both after the preliminery heat treatment and after the subsequent age hardening. Suitable thin foils were prepared by electropolishing using the well-known "window" technique, although in the initial stages of the study this technique was modified to include argon ion-beam milling as the final step in obtaining electron transparency. The TEM specimens were prepared from the small sheets, 1 mm thick, as follows:

(1) The specimens were mounted on a solid block and ground on successively finer silicon carbide papers to a thickness of about 0,15 mm, then removed from the block and cleaned.

(2) Electropolishing was carried out in the butyl oxitol-ethanol-perchloric solution described in Section 2.4. The edges of the specimen were masked with lacquer and electropolishing carried out until a small hole was formed. The hole was masked and electropolishing continued until another hole formed; this hole was masked and the process repeated until a rapid rate of formation of holes indicated that the foil was very thin.

(3) The lacquer was dissolved from the foil using a suitable solvent and the foil placed between filter papers under ethanol. The foil was cut into pieces using the

rolling action of a curved scalpel blade and apparently suitable pieces placed on standard TEM grids using a fine-haired artist's brush, and stored awaiting TEM examination.

(4) During the early stages of this study the skills necessary to prepare good TEM specimens by the above technique had not yet been acquired. Thus some of the pieces cut from the electropolished foils were fixed to TEM specimen support discs and subjected to argon ion-beam milling. This generally produced electron-transparent specimens, although it had the disadvantage of introducing artefacts into the specimen due to ion-beam damage.

The TEM examinations were carried out on either a Philips EM 300 instrument, operated at 100 kV, or a Siemens S102 operated at up to 125 kV. The instruments were equiped with double-tilt and rotation-tilt goniometer stages respectively. Photographs were taken using the standard cameras built into these instruments, using electron-sensitive sheet film.

The specimens were almost always viewed under two-beam diffraction conditions, using a low-index reflection in bright field, and occasionally also in dark field. The associated selected area diffraction pattern was invariably photographed with the bright field image. The basic principles of TEM as outlined in the standard textbook by Hirsch et al (1965), were followed as far as possible.

2.6 X-Ray Diffraction Measurements (XRD)

Precision lattice parameter measurements were taken and diffraction peak profiles obtained using the technique of x-ray diffraction (XRD). The equipment comprised a diffractometer which was usually operated at a scan speed of 0,125 degrees of 2θ per minute, and was equiped with a single crystal monochromator and 0,17 degree receiving slit. Both copper and molybdenum $K\alpha$ radiation were used. The instrument was carefully aligned and resolution was such that on

suitable specimens, the $\alpha_1 - \alpha_2$ doublet of Cu K radiation was resolved for the 110 reflection, ie. at a diffraction angle as low as 44 degrees of 2θ.

Specimens were prepared for XRD by grinding on silicon carbide papers, polishing with diamond paste down to 0,25 micron size, and electropolishing as applied during preparation of the TEM specimens. (This specimen preparation was designed to remove the strained surface layer). The overall experimental technique was considered to be of high precision: in certain specimens the diffraction peak positions could be determined from the diffractometer trace to within 0,01 degrees of 2θ, which corresponds to a difference in lattice parameter of 0,02 picometers. The instruments used in this study had a stated precision and reproducibility of better than 0,003 degrees of 2θ.

Chapter 3

RESULTS: PART A
AGE HARDENING DUE TO PRECIPITATION OF INTERSTITIALS

This chapter describes the microstructural features of the 26Cr-1Mo steel after preliminery heat treatment comprising either solution treatment at 1100 C and quenching, nitriding at 1100 C and quenching, or annealing at 800 C and quenching. The microstructures were determined by optical microscopy and by transmission electron microscopy (TEM). The results of age hardening experiments which were performed on the solution-treated steel in the temperature range 600-800 C, are presented together with the associated microstructures as determined by TEM. Each preliminery heat treatment was repeated several times, and all subsequent age hardening experiments and TEM examinations were at least repeated using material subjected to preliminery heat treatment at a different time.

As regards the 30Cr steel used in this study, the high carbon and nitrogen contents resulted in a very high hardness after quenching, and in a considerable volume fraction of precipitates after either quenching from the solution treatment at 1100 C or from the annealing at 800 C. As such a composition is unlikely to be used successfully as a wrought alloy, the 30Cr steel was only examined in the context of the 475 C hardening, which is discussed in the following chapter.

3.1 Measurement of Interstitial Nitrogen

Interstitial nitrogen causes a lattice expansion in ferritic stainless steels to the extent of 2,85 picometer (pm) per weight percent of nitrogen (Hendry et al, 1979). (In the present context interstitial includes nitrogen present in non-random solid solution, ie. in zones or pre-precipitation phases as defined by Krawitz and Sinclair (1975)). In order

to establish the interstitial nitrogen content of the 26Cr-1Mo steel after quenching from solution treatment or from nitriding, x-ray diffraction (XRD) scans of the 211 diffraction peaks were made on specimens subjected to the different preliminery heat treatments. The lattice parameters were calculated from the Bragg equation. In accordance with the phase diagram for the ferritic stainless steel-nitrogen system (fig. 1.1), the interstitial nitrogen content of the specimen annealed at 800 C (in vacuo for 4 hours) was taken as zero. Thus the interstitial nitrogen contents of the quenched specimens were calculated from their lattice expansions relative to the annealed specimen.

The results obtained for the 26Cr-1Mo steel from Allegheny Ludlum, using both the 211 and 200 Bragg reflections, are presented in Table 3.1

The interstitial nitrogen content of the specimen which had been solution treated and quenched, as determined by the XRD technique, agrees with the manufacturer's figure of 0,02%.

TABLE 3.1

	Annealed (800 C)	Quenched (1100 C)	Nitrided & Quenched
211 Diffraction Peak			
Lattice Parameter (nm)	0,28794	0,28799	0,28803
Change (pm)	-	0,05	0,09
Nitrogen Content (%)	-	0,02	0,03
200 Diffraction Peak			
Lattice Parameter (nm)	0,28818	0,28830	0,28866
Change (pm)	-	0,12	0,48

Table 3.1: Results of lattice parameter measurements on the 26Cr-1Mo steel, showing calculated interstitial N contents (by mass) after solution treatment and after nitriding.

The nitriding process increased the interstitial nitrogen contents to measured values of 0,03 to 0,035%. While these measurements were obtained using the 211 diffraction peak, measurements of lattice parameters were also done on a set of the specimens, using the 200 peak. A much greater lattice expansion in the presence of interstitial nitrogen was found with the 200 peak, compared with the 211 as reported above. These results suggest that interstitial nitrogen is present at octahedral lattice sites (Hendry et al, 1979), thereby causing a lattice expansion along <100>.

3.2 The Hardness and Microstructure after Preliminery Heat Treatment

Vickers hardness measurements were made on specimens subjected to the preliminery heat treatments, the value for each treatment given here being the average of measurements on several different specimens. The results, together with the calculated standard deviations, were:

Annealed at 800 C and quenched ("26-1-A"):	HV 164 $\pm$2
Solution-treated at 1100 C and quenched ("26-1-Q"):	HV 172 $\pm$3
Nitrided at 1100 C and quenched ("26-1-N-Q"):	HV 171 $\pm$1

There is a small, but none the less valid, increase in hardness due to solution treatment and quenching relative to the annealed specimens.

The various specimens were examined by optical microscopy, after preparation by electropolishing in acetic-perchloric acid mixture or by etching in oxalic acid. The latter technique particularly revealed, in the form of grain boundary etching, any loss of corrosion resistance at grain boundaries due to removal of chromium from solid solution through precipitation in the vicinity of the boundary. Both electropolishing and etching revealed differences between the

specimens annealed at 800 C and those quenched from solution treatment or nitriding. In general the TEM examinations not only showed microstructures consistent with those observed by optical microscopy, but also revealed essential differences between specimens according to preliminery heat treatment.

The specimen 26-1-A (ie. annealed at 800 C and quenched) was found after electropolishing to contain numerous small particles, possibly precipitates, about 0,5 μm in size. These are visible in the optical micrograph fig. 3.1(a). Electro-etching in oxalic acid confirmed the presence of these particles, and revealed some loss of grain boundary corrosion resistance as demonstrated by the etching of grain boundaries, shown in fig. 3.1(b).

TEM examination of the specimens of 26-1-A showed a substantial population of relatively large precipitates, about 0,05 to 0,3 μm in size, which are incoherent with the matrix. Their distribution is random within the grains, but quite dense along grain boundaries, as shown in figs. 3.2(a) and 3.2(b) respectively. The matrix itself is completely clean and any dislocations present are free of precipitates or strain centres. Examination of a thin foil using the energy dispersive x-ray analysis technique in conjunction with STEM, proved these precipitates to be very rich in chromium, most likely as chromium carbo-nitrides. These TEM results are consistent with the optical microscopy observations of precipitates about 0,5 μm in size and of noticeable etching at the grain boundaries, the latter phenomenon being attributable to depletion of chromium within the matrix near the grain boundary due to formation of precipitates containing chromium.

The optical microscopy examination of specimens 26-1-Q and 26-1-N-Q (ie. solution-treated at 1100 C and quenched, and nitrided at 1100 C and quenched, respectively), revealed no significant difference between the two and they are therefore discussed together. In the electro-polished condition there

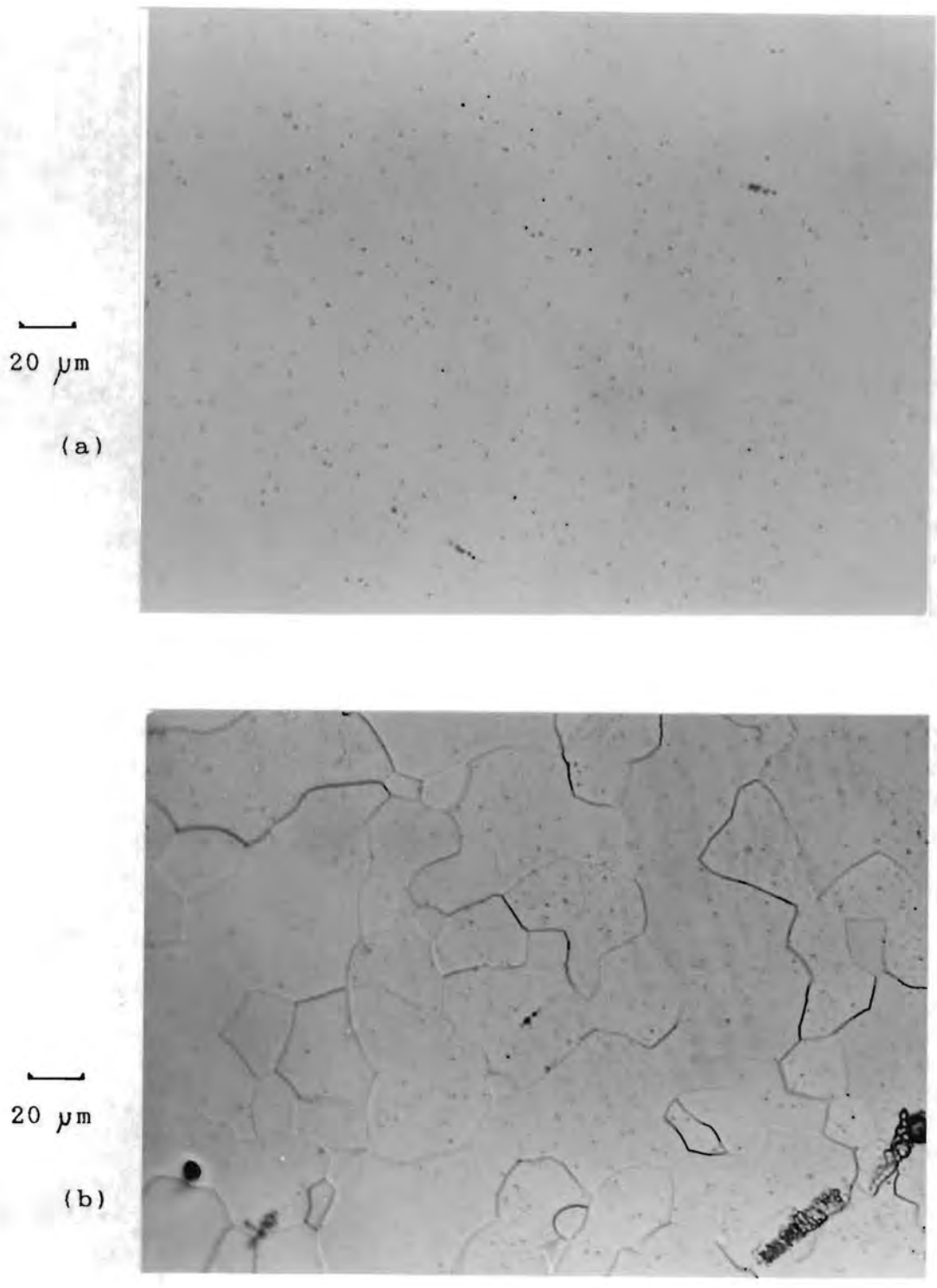

Figure 3.1. Optical micrograph of the annealed 26Cr-1Mo steel (specimen 26-1-A) prepared for microscopy by (a) electropolishing and (b) electro-etching in oxalic acid. The latter preparation reveals grain boundary etching.

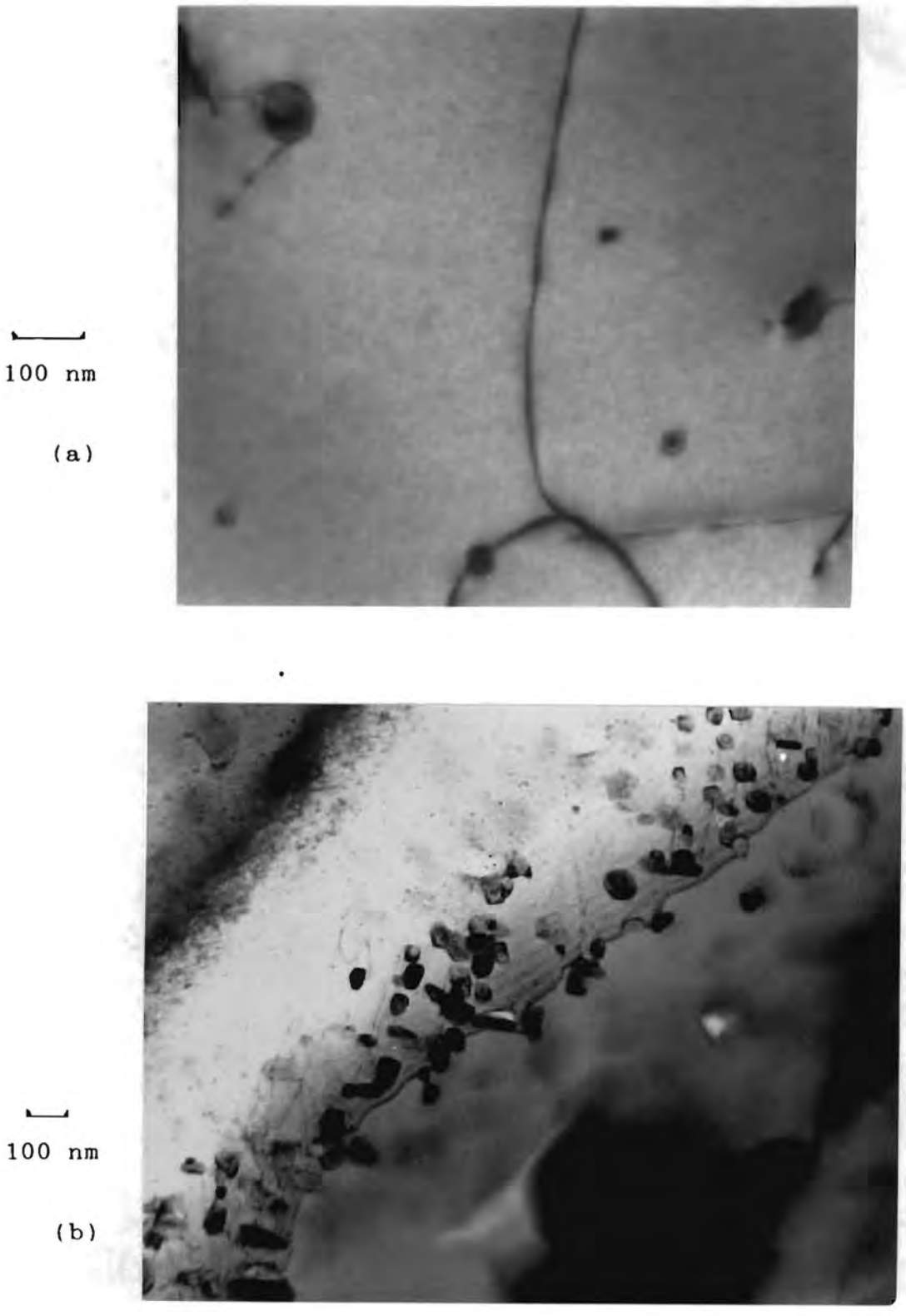

Figure 3.2 Thin foil TEM micrograph of the 26Cr-1Mo steel, showing large incoherent chromium nitride precipitates formed during annealing at 800 C. (b) shows heavy grain boundary precipitation present in another specimen of this heat treatment.

were no features present except for the occasional large inclusion such as are visible in fig. 3.3(a). Electro-etching in oxalic acid had little effect on the grain boundaries, as can be seen in figs. 3.3(b) and 3.4, indicating an absence of grain boundary precipitation.

TEM examination revealed that the nitrided and quenched specimens (26-1-N-Q) were free of precipitates and their grain boundaries were clean: this observation confirms the absence of grain boundary precipitation as suggested by the optical microscopy observations. However a high density of dislocations with specific crystallographic orientations was frequently observed within the grains. With a (111) foil orientation, these dislocations assume one of three different directions, with each of the three projecting at an angle of 60 degrees to another. This indicates that they lie in $\langle 110 \rangle$ directions. An example of these dislocations in specimen 26-1-N-Q is shown in fig. 3.5, where one particular orientation (lying normal to the g-vector) predominates.

The specimens of 26-1-Q showed similar microstructural features to those of 26-1-N-Q as described above.

The nature of the specimens after preliminary heat treatment can be summarized as follows. Rapid quenching, from solution treatment or nitriding at 1100 C, leaves the interstitials in solid solution, although in many cases dislocations lying on $\{110\}$ planes are produced. Annealing at 800 C produces incoherent precipitates up to about 0,3 μm in size, situated within the grains and especially at the grain boundaries where they are associated with decreased corrosion resistance as evidenced by the observed grain boundary etching. The precipitates are chromium rich, most probably chromium carbo-nitrides, and are large enough and far enough apart to be unlikely to have any effect on the deformation properties of the steel. The annealed condition has in fact a lower hardness than the solution-treated and quenched condition.

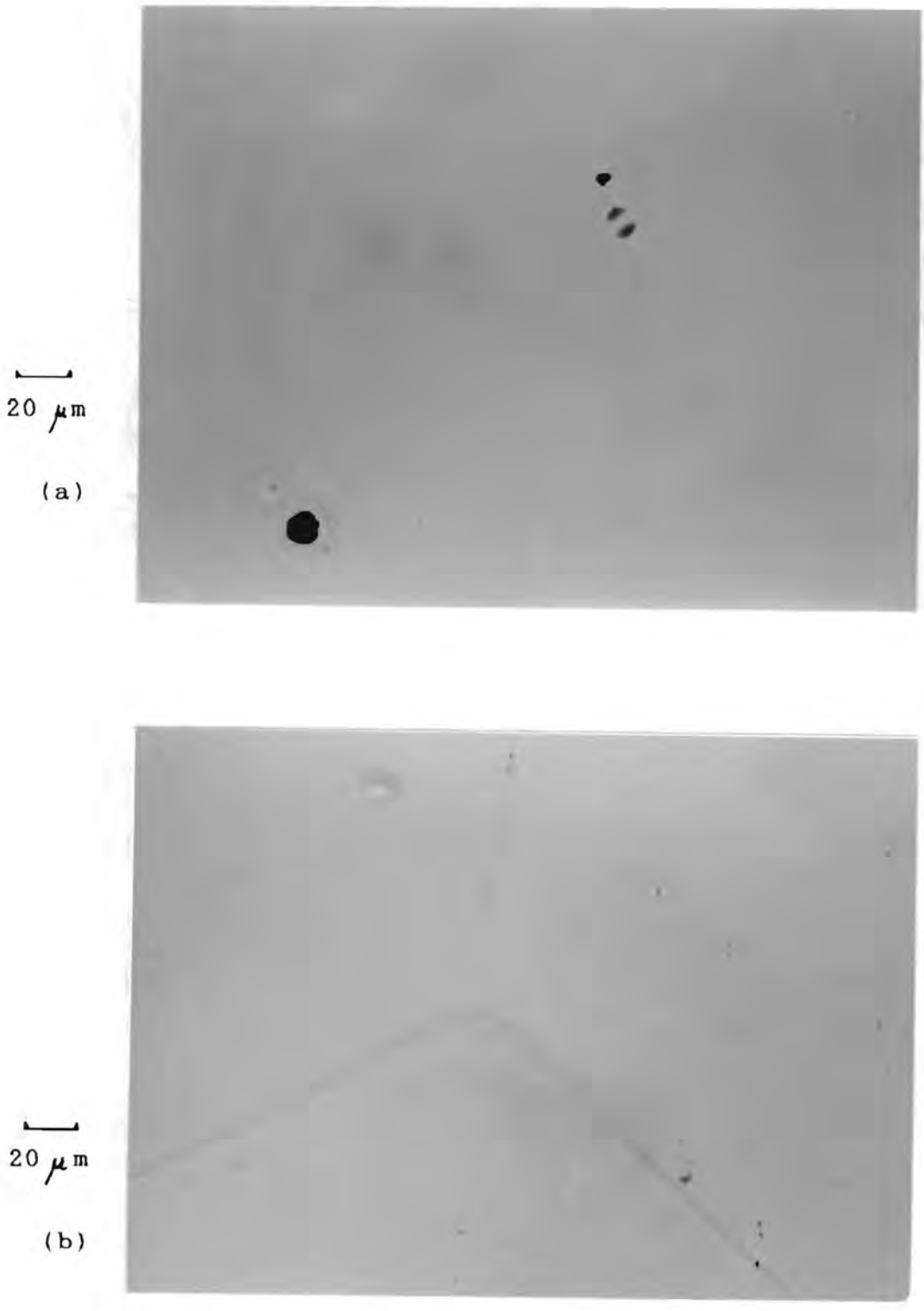

Figure 3.3. The nitrided and quenched 26Cr-1Mo steel (specimen 26-1-N-Q) prepared by (a) electropolishing and (b) electro-etching in oxalic acid. There is no grain boundary etching.

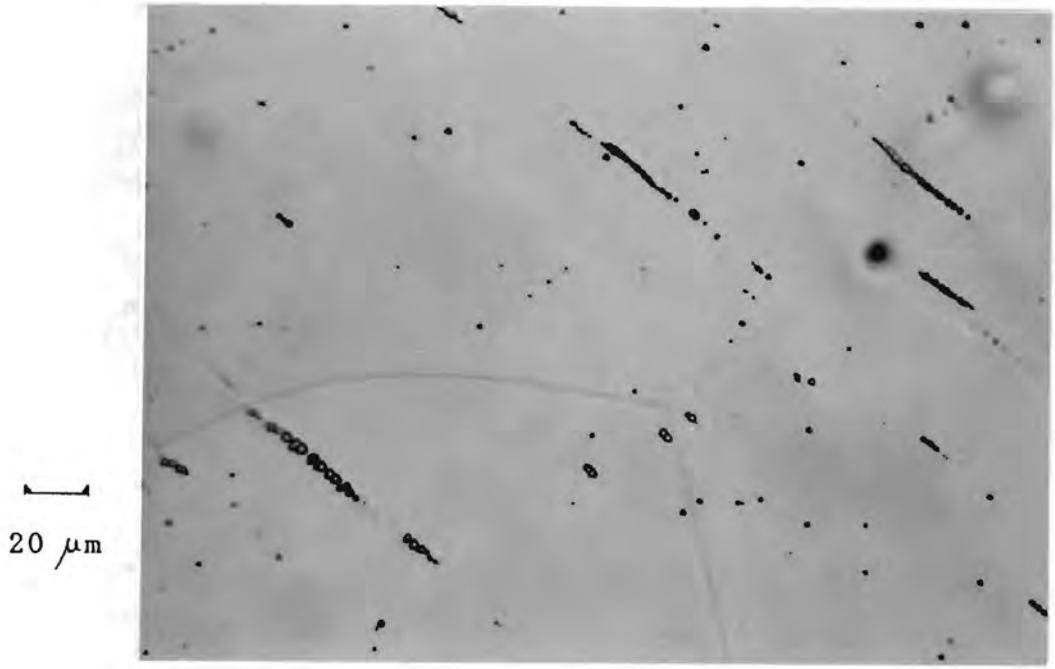

Figure 3.4. The 1100 C quenched 26Cr-1Mo steel (specimen 26-1-Q) electro-etched in oxalic acid, showing clean grain boundaries.

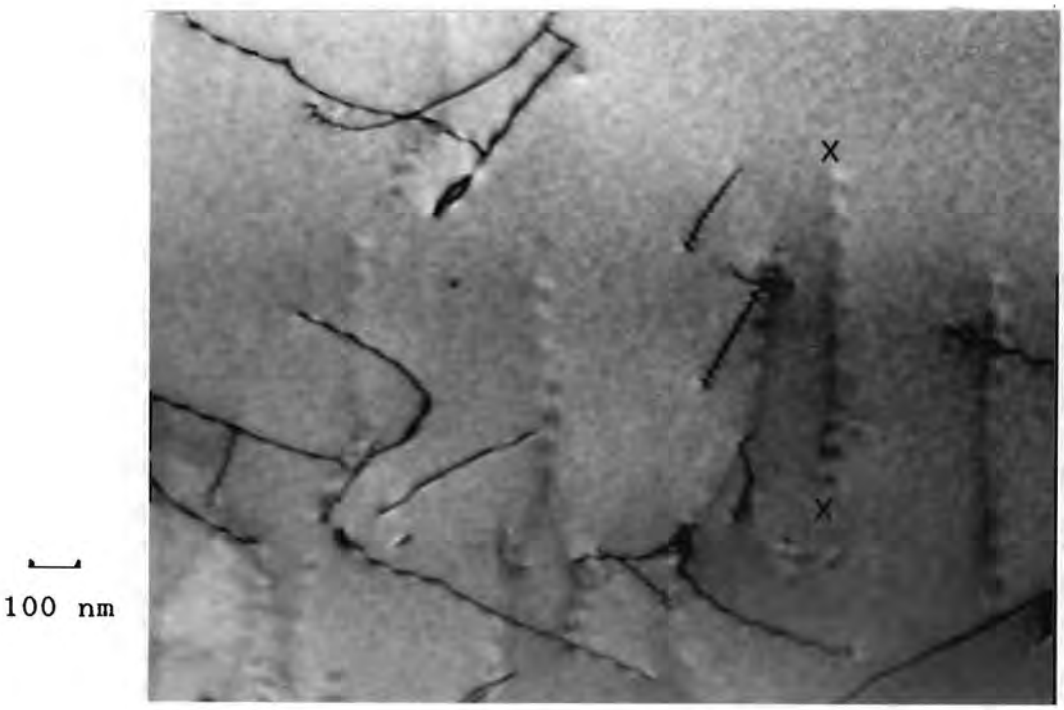

Figure 3.5. Thin foil TEM micrograph of specimen 26-1-N-Q, showing dynamical effects along out-of-contrast dislocations, with an example marked X-X.

3.3 Age Hardening in the Temperature Range 600 to 800 C

The purpose of the experiments described here was to determine what reactions occurred in the as-quenched steel (containing as it does, a non-equilibrium interstitial nitrogen content) when aged at intermediate temperatures. It will become evident from the results described here that this ferritic stainless steel containing interstitial nitrogen (and a lesser quantity of carbon) forms a classical age-hardening system.

Ageing at 800 C produces a rapid but small increase in hardness followed by over-ageing: typically a hardness increase of up to 18 points (HV) occurs within a period of 0,1 hour, followed after a further 0,1 hour period by a drop in the hardness to the original as-quenched value. Finally, the over-aged condition of the specimen 26-1-A (annealed at 800 C for 4 hours) is reached.

Ageing at temperatures below 800 C gives greater hardness increases and longer times to peak hardness. At 700 C an average hardness increase of 28 points (HV) was measured on a number of specimens, with a time to peak hardness of about 0,2 hours. Prolonged ageing, eg. for 8 hours, does not reduce the hardness to less than 10 points above the as-quenched value. The age hardening curves for two of the 700 C ageing experiments are shown in fig. 3.6.

At 600 C the hardness increase on ageing is quite large: averaged over five different experiments this amounts to 39 points (HV) with an ageing time to peak hardness of 6-10 hours. Thereafter some decrease in hardness is found; however even after an ageing period of as long as 200 hours the hardness is at least 20 points above the as-quenched value. Typical hardening curves for this temperature are shown in fig. 3.7.

Age hardening at other temperatures between 600 and 800 C was

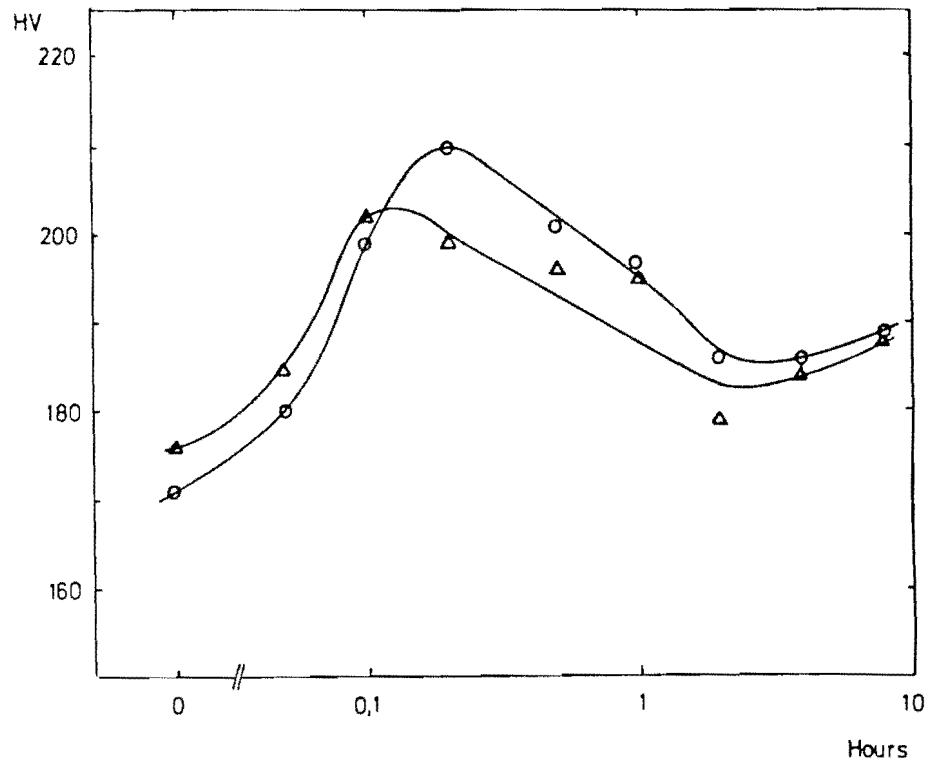

Figure 3.6. The 700 C age hardening curves of different specimens of the 26Cr-1Mo steel, quenched and nitrided from 1100 C.

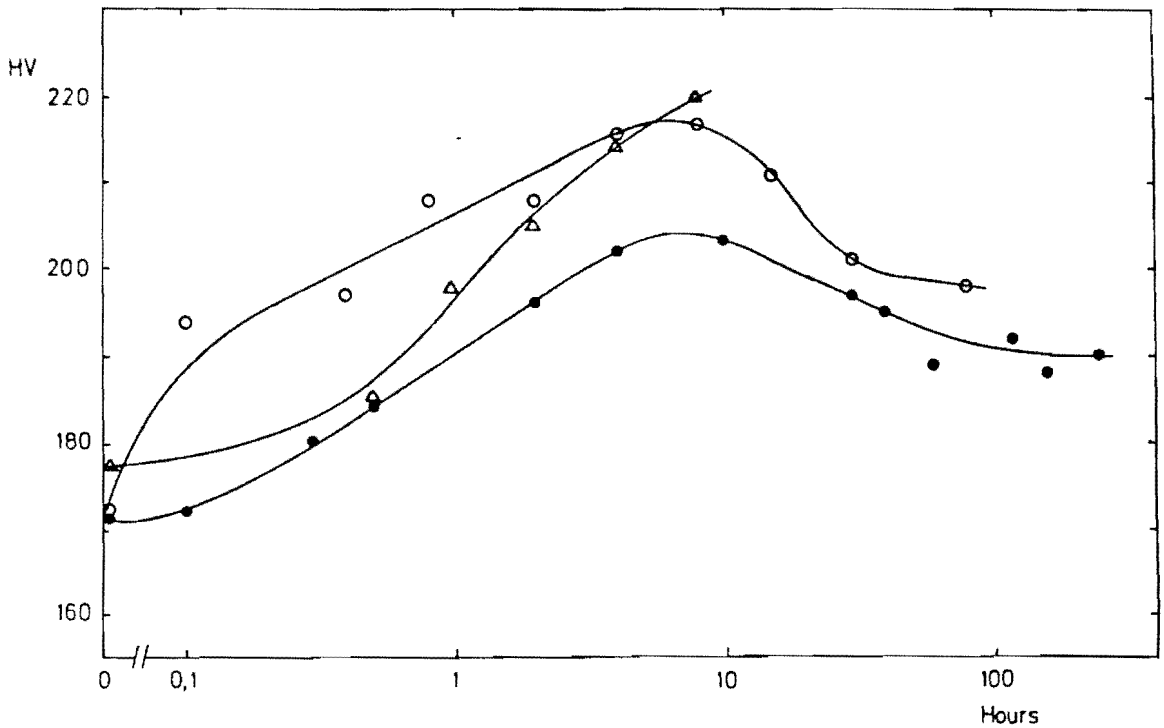

Figure 3.7. The 600 C age hardening curves of different specimens of the 26Cr-1Mo steel, nitrided and quenched from 1100 C.

investigated and found to be consistent with the results reported above. The behaviour at temperatures below 600 C is discussed in Chapter 4 of this thesis.

3.4 The Microstructures after Age Hardening in the Temperature Range 600-750 C

TEM examinations were carried out on a number of specimens age hardened at 600, 700 and 750 C to approximately their respective peak hardness values, and for longer periods which represented over-aged conditions. The microstructures produced at any particular ageing temperature were consistent from one specimen to the next; no significant difference was noticed among specimens which had been nitrided during their preliminery heat treatment, and those which had only been solution treated prior to quenching. The differences in observed microstructures between specimens aged at these lower temperatures, and those which had simply been given the preliminery heat treatment, were quite pronounced and unambiguous.

Ageing at 600 C for a period of 6 hours, ie. to approximately peak hardness for this temperature, produced an exceptionally high density of very small centres of contrast. An example is shown in fig. 3.8. which represents a hardness of HV 193. The TEM contrast from small coherent particles which strain the surrounding lattice, has been discussed by Ashby and Brown (1963). The dot-like contrast observed here is consistent with the appearance of small precipitates with large strain fields, including the characteristic of the black-white contrast existing in only one sense in the dark-field image, but in both senses in bright field.

Measurement of exact precipitate size is difficult because the structures visible in fig. 3.8 are in fact the associated strain fields; these are about 5-10 nm in size, with the precipitates themselves considerably smaller. The substantial overall matrix strain present in this aged

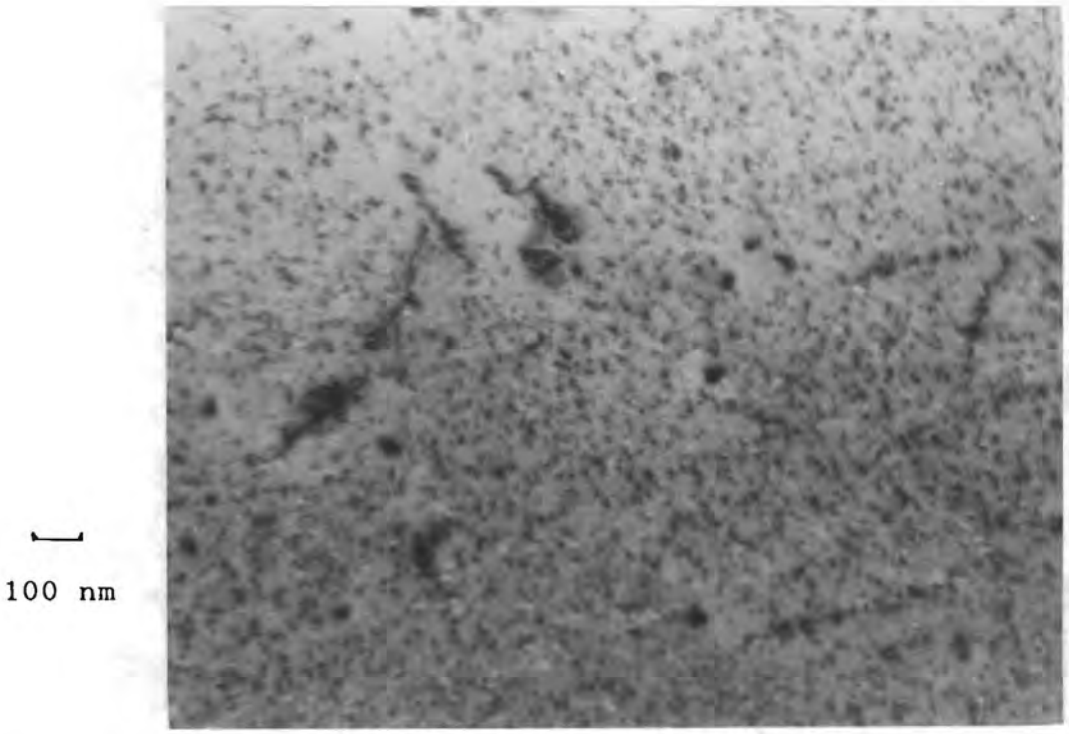

Figure 3.8 The nitrided and quenched 26Cr-1Mo steel aged at 600 C for 6 hours. A high density of small strain centres (zones), including many formed on dislocations, are present.

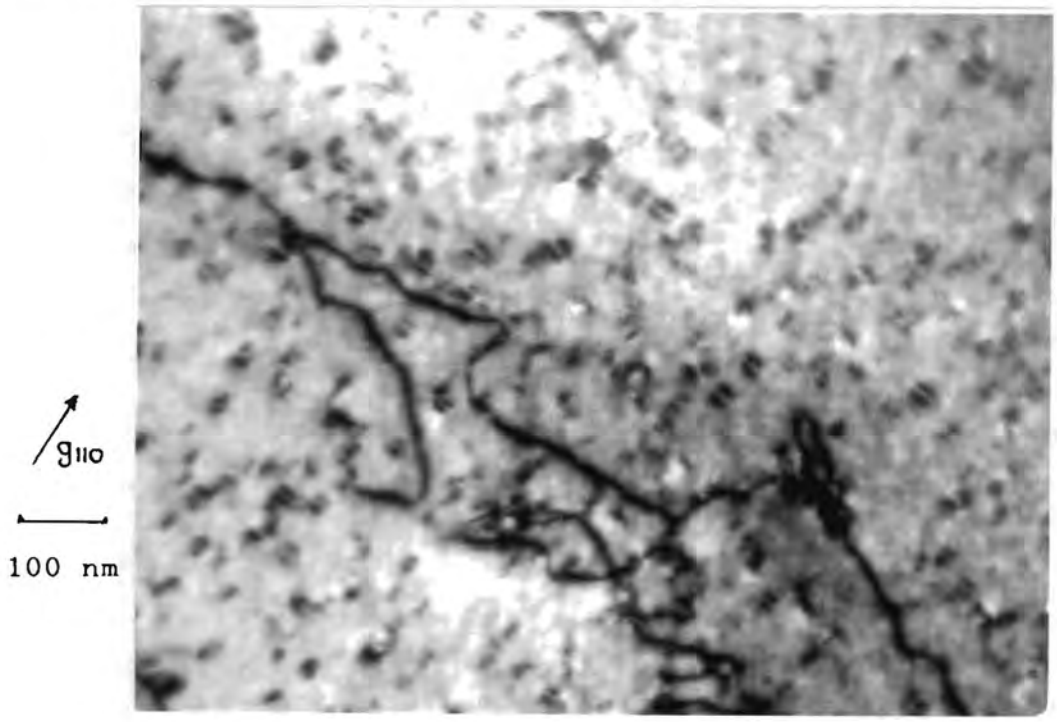

Figure 3.9(a). Specimen as for fig. 3.8, but total ageing time was 270 hours. The precipitate strain fields are large enough to show line of no contrast normal to g-vector.

specimen is probably a significant source of hardening, through the increased resistance to dislocation movement that it would present compared with the defect-free material.

Also of interest in fig. 3.8 is the reduction in density of precipitation in the vicinity of dislocations, which themselves are highly decorated with precipitates through having acted as preferential nucleation sites. This immobility of existing dislocations due to precipitation probably also contributes to the increased hardness of aged material relative to the as-quenched condition.

The gradual decrease in measured hardness found on extended ageing at 600 C, is accompanied by a subtle microstructural change. TEM examination of the specimen aged at this temperature for 270 hours, reveals a reduction in the density of the precipitates and an increase in the size of the strain fields associated with them, compared with the specimen aged for 6 hours to approximately peak hardness. The strain fields have grown large enough to show a line of no contrast through the image, normal to the g-vector, when viewed under two-beam diffraction conditions. (The line of zero contrast is the edge-on view of the plane comprising the points where the lattice distortion vector does not have a component parallel to the g-vector.) Examples of these can be seen in the micrograph shown in fig. 3.9(a) which represents an area of the specimen aged for 270 hours. The maximum size of the strain fields of the precipitates present after the extended ageing at 600 C, is about 15 nm.

Although fig. 3.9(a) represents a somewhat overaged condition it is demonstrated, by the apparent pinning of dislocations, that these precipitates contribute to the increased flow stress (and hence hardness) of the material shown in this micrograph. This precipitate-dislocation interaction was frequently observed during TEM examinations of specimens aged under time-temperature conditions such as led to the formation of small precipitates with large strain fields.

Newly-introduced dislocations, such as formed during preparation of specimens for TEM or during subsequent handling, were undoubtably restricted in their movement because of their interaction with the precipitate strain fields.

The precipitates which nucleated and grew on dislocations during ageing at 600 C for 6 hours, as shown in fig. 3.8, were observed to have grown in size during the extended ageing period and to appear in large numbers in the specimen aged for 270 hours. Examples of this precipitate-dislocation structure are present in fig. 3.9(b). One of the dislocations which is invisible due to a $\mathbf{g.b} = 0$ diffraction condition, is represented by a line of closely-spaced strain centres. Such dislocations will be highly immobile at ambient temperature and they probably contribute to the hardened and embrittled properties of the aged steel.

Ageing at 700 C produced a rapid initial hardness increase followed by softening or over-ageing, as reported in Section 3.3. The associated microstructural changes were equally specific and quite consistent, in so far as changes in microstructure were observed to correspond to the different trends in measured hardness. These specimens were examined by TEM both after a short period of ageing (0,15 hours), which corresponded to a near-peak hardness of HV 189, and after the over-aged periods of 4 and 47 hours.

The 0,15 hour specimen, whose hardness of HV 189 was slightly past the peak of HV 199 but significantly harder than the as-quenched value of HV 156, revealed a high density of fine dot-like strain field centres, apparently identical to those present after ageing at 600 C for 6 hours. This similarity in appearance is not unexpected as both specimens have a similar hardness.

Over-ageing at 700 C (for 4 hours) to a hardness of about HV 160, a value close to that measured prior to ageing, resulted

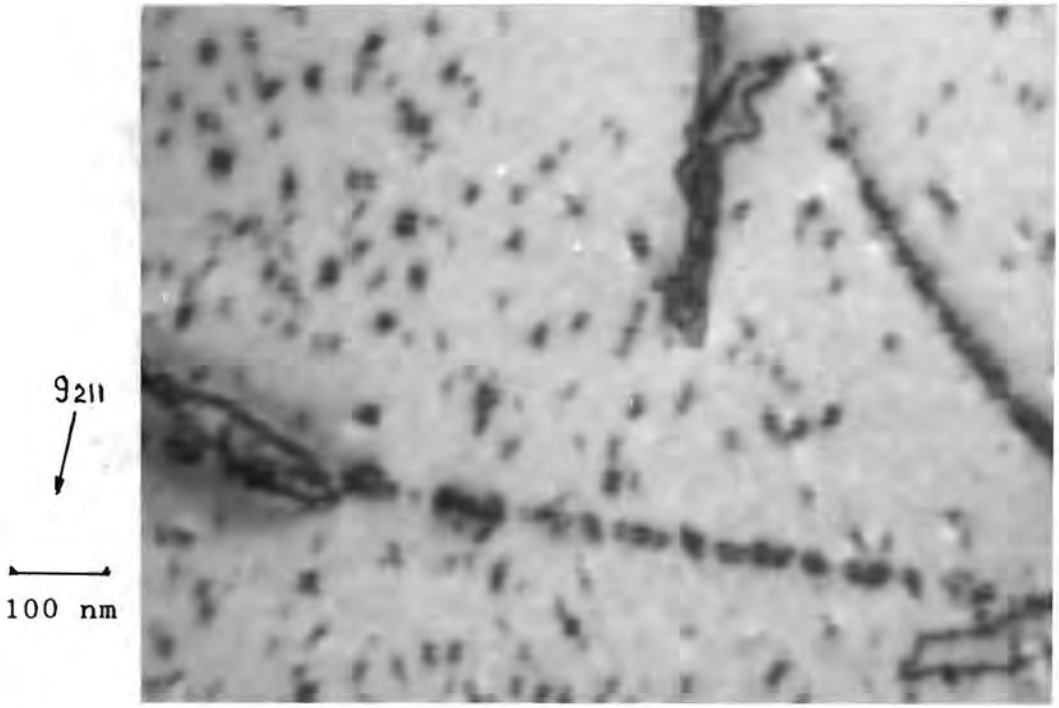

Figure 3.9(b) Specimen and heat treatment as for fig. 3.9(a) ie. 26-1-N-Q aged at 600 C for 270 hours. A line of precipitates define an out-of-contrast dislocation.

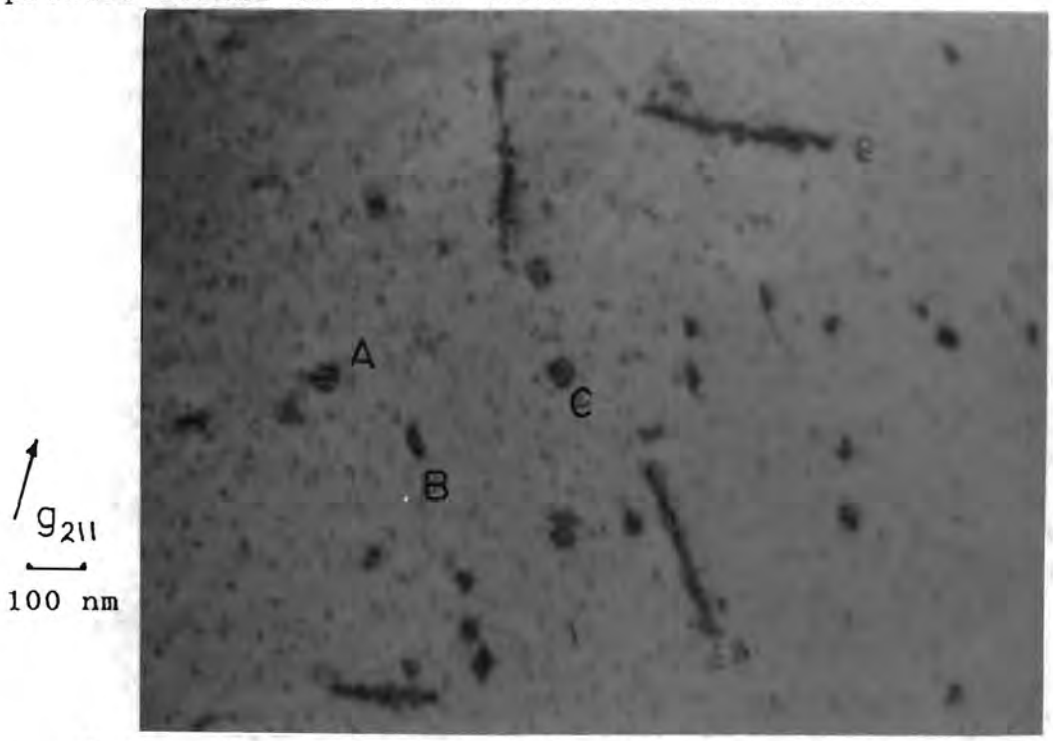

Figure 3.10 The nitrided and quenched 26Cr-1Mo steel (specimen 26-1-N-Q) aged at 700 C for 4 hours to produce {100} planar precipitates, with the three different orientations marked A,B & C. The dot-like features are radiation damage from ion-beam milling.

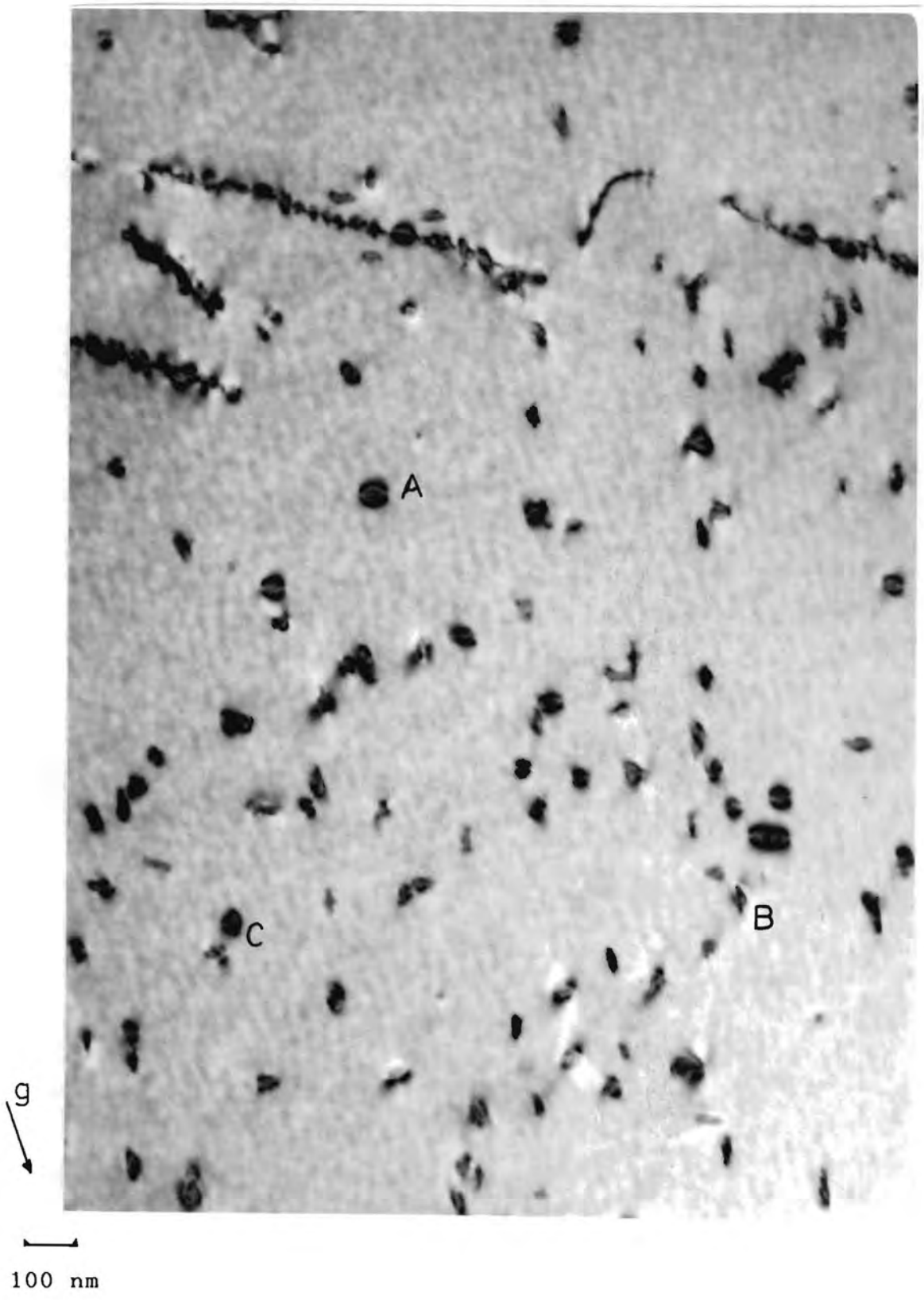

Figure 3.11 The nitrided and quenched 26Cr-1Mo steel aged at 700 C for 47 hours produced a microstructure of planar precipitates. The three orientations are marked A-C; existing dislocations are heavily decorated with precipitates.

in growth of the precipitate size with an associated reduction in distribution density. An example of this can be seen in fig. 3.10, where the precipitates are up to about 40 nm in size. They are coherent with the matrix and are associated with quite large strain fields. (The fine dots present in this micrograph are radiation damage caused by ion-beam milling). The foil orientation is close to [111]: three different orientations of precipitates are visible, labelled A to C, and analysis of these confirms that they are disc-shaped and lie on the three $\{100\}$ planes. This conclusion is supported by examination of other micrographs taken of this specimen.

Further exposure to the temperature of 700 C, for a total period of 47 hours, increased the size of the precipitates to 50-60 nm as shown in fig. 3.11. The disc-like morphology of the precipitates is confirmed, as is their occurrence on the three mutually orthogonal lattice planes (examples are marked A-C on the micrograph). As expected, this growth in size is accompanied by a small reduction in precipitate density. Another feature of interest is the presence of dislocations which are heavily decorated with precipitates and consequently would be quite immobile.

The precipitates pin or restrain new dislocations as shown in fig. 3.12, where the "new" dislocations (introduced subsequent to the ageing treatment) are well defined and are free of the numerous precipitates that characterize the pre-ageing species. One of the dislocations visible here is bowed out between four restraining precipitates; however, despite this constraint on dislocation movement, apparent in the specimen, the measured hardness of HV 150 was equal to the lowest of any specimen measured in this study.

Ageing at higher temperatures such as 750 C gave even larger precipitates, such as those in fig. 3.13 which are up to 80 nm in size. They are still disc shaped and lie on the three (orthogonal) $\{100\}$ planes, one of which is almost

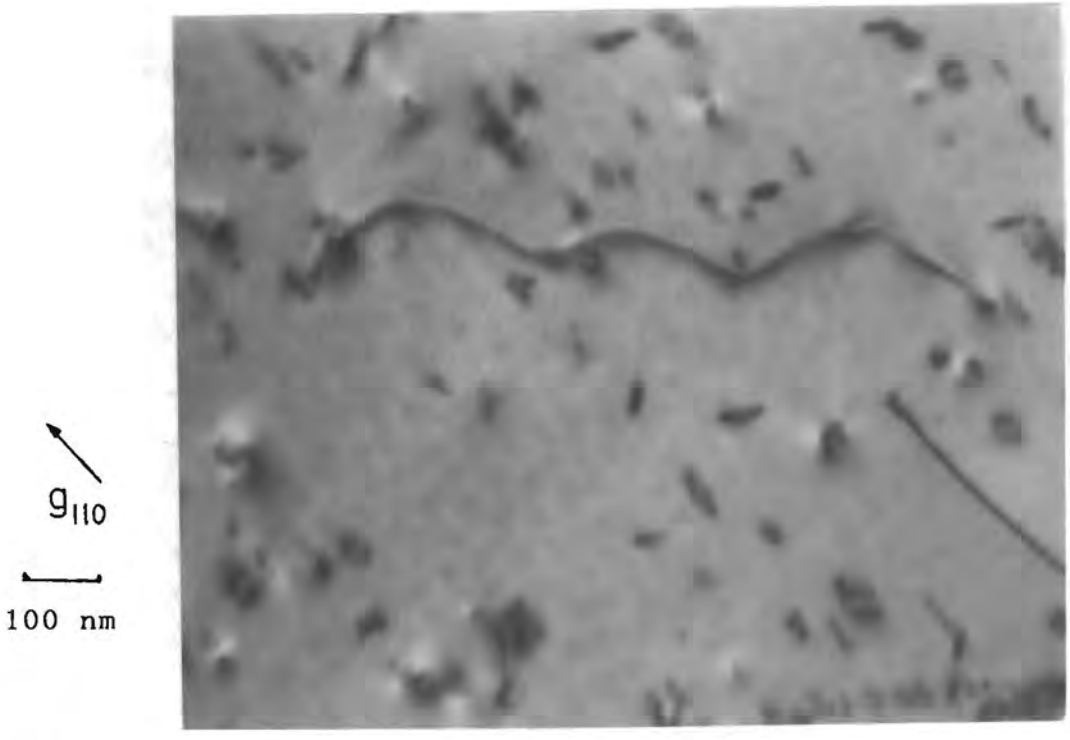

Figure 3.12 The specimen as in fig. 3.11 (ie. 26-1-N-Q aged at 700 C for 47 hours) showing pinning of a dislocation by precipitates.

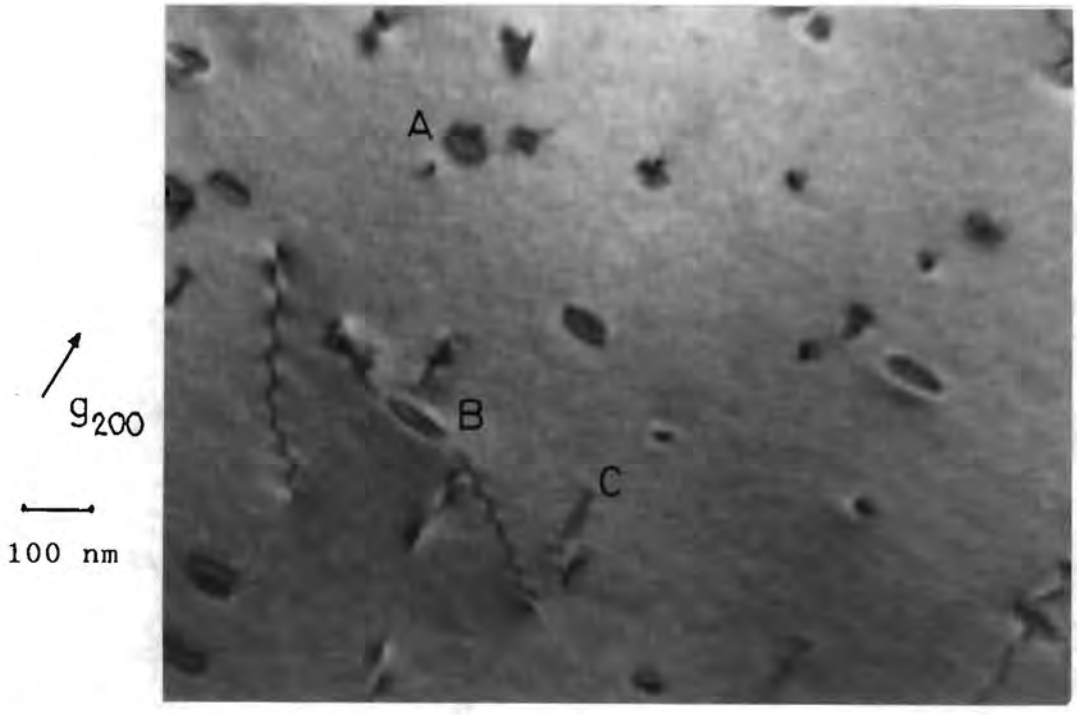

Figure 3.13 Planar chromium nitride precipitates formed in the specimen 26-1-N-Q during ageing at 750 C. The foil orientation is (100). Examples of precipitates on the three {100} planes are marked A-C.

coincidental with the plane of the foil in this particular micrograph. The one precipitate species (marked A) almost coincides with the foil, the other two species (B and C) are normal to the foil. As the g-vector is 200, one species of precipitate is parallel to the g-vector and thus has very little contrast visible due to the lattice distortion being mostly normal to the g-vector.

Any higher ageing temperature results in a loss of coherency with the matrix, due to rapid three-dimensional growth of the precipitates into the structures shown in the micrographs of 800 C annealed specimens (Fig. 3.7).

Chapter 4

RESULTS: PART B
THE 475 C HARDENING REACTION

This chapter describes the age hardening experiments performed on the 26Cr-1Mo steels at the temperatures of 475 C and 550 C, and on the 30Cr steel at the lower temperature. The materials used had been subjected to one of the following preliminery treatments (which were shown schematically in fig. 2.1):

Specimen 26-1-Q: solution treated at 1100 C followed by water quench.

Specimen 30Cr-Q: as above, but refers to the 30Cr steel.

Specimens 26-1-A and 30Cr-A: annealed at 800 C and quenched

Specimen 26-1-N-Q: nitrided at 1100 C and quenched.

Specimen 26-1-N-600: as for specimen 26-1-N-Q, but with a 600 C ageing treatment to give a hardness of about HV 220, ie about 50 points above that of specimen 26-1-N-Q, through the formation of small chromium nitride precipitates.

Graphs showing the changes in hardness with ageing time are presented, with optical and transmission electron micrographs showing the microstructural changes associated with age hardening. The results of precision x-ray diffraction measurements on the aged materials are discussed.

4.1 The 475 C Hardening: 26Cr-1Mo Steel ex Allegheny Ludlum

Prolonged ageing at 475 C resulted in a substantial hardening in all of the specimens, irrespective of prior heat treatment. However, the various specimens did demonstrate different trends in hardening, not only because of differences in composition (ie. 30Cr relative to 26Cr-1Mo steel), but also because of differences in prior heat treatment. We consider first the vacuum-melted 26Cr-1Mo steel from Allegheny Ludlum.

The age hardening behaviour of two different samples each of specimens 26-1-Q and 26-1-N-Q, and of three different samples of 26-1-A, are shown graphically in fig. 4.1. These results, which were obtained during two separate ageing experiments, show clearly the different trends followed by the annealed compared with the quenched specimens:

The annealed specimens (26-1-A) hardened at a fairly rapid rate, the change in hardness being measureable after a few hours of ageing. As shown in the age hardening curves (fig. 4.1), hardening continued until a peak value of about HV 360 was reached after about 1000 hours. No further increase was found during ageing for an additional 400 hours (ie. to a total period of 1400 hours).

There was no difference of any significance between the ageing behaviours of the quenched specimens 26-1-Q and 26-1-N-Q as regards the development of hardness with time, and while results of both are shown in fig. 4.1, they will be discussed as one (referred to as 26-1-(N)-Q). Exposure at 475 C resulted in a slower rate of increase of hardness than that of specimen 26-1-A until about 500 hours of ageing had elapsed. During this period the hardness increased from the as-quenched value of about HV 170 to the value of HV 220. (By comparison, at 500 hours, specimen 26-1-A measured HV 330-350). Thereafter the hardening rate increased and by 1400 hours a value of about HV 270 was reached.

In both cases, 26-1-A and 26-1-(N)-Q, the rate of increase in hardness slowed down as ageing proceeded. The graphs showing variations in the rate of change of hardness, expressed as a function of ageing time, are shown in fig. 4.2. The annealed specimens show a fairly consistent decrease in their rate of hardening over the total ageing time, this rate being approximately

$$\frac{d(HV)}{dt} \doteq \frac{1}{t^k} \quad \text{where } k = 0,8$$

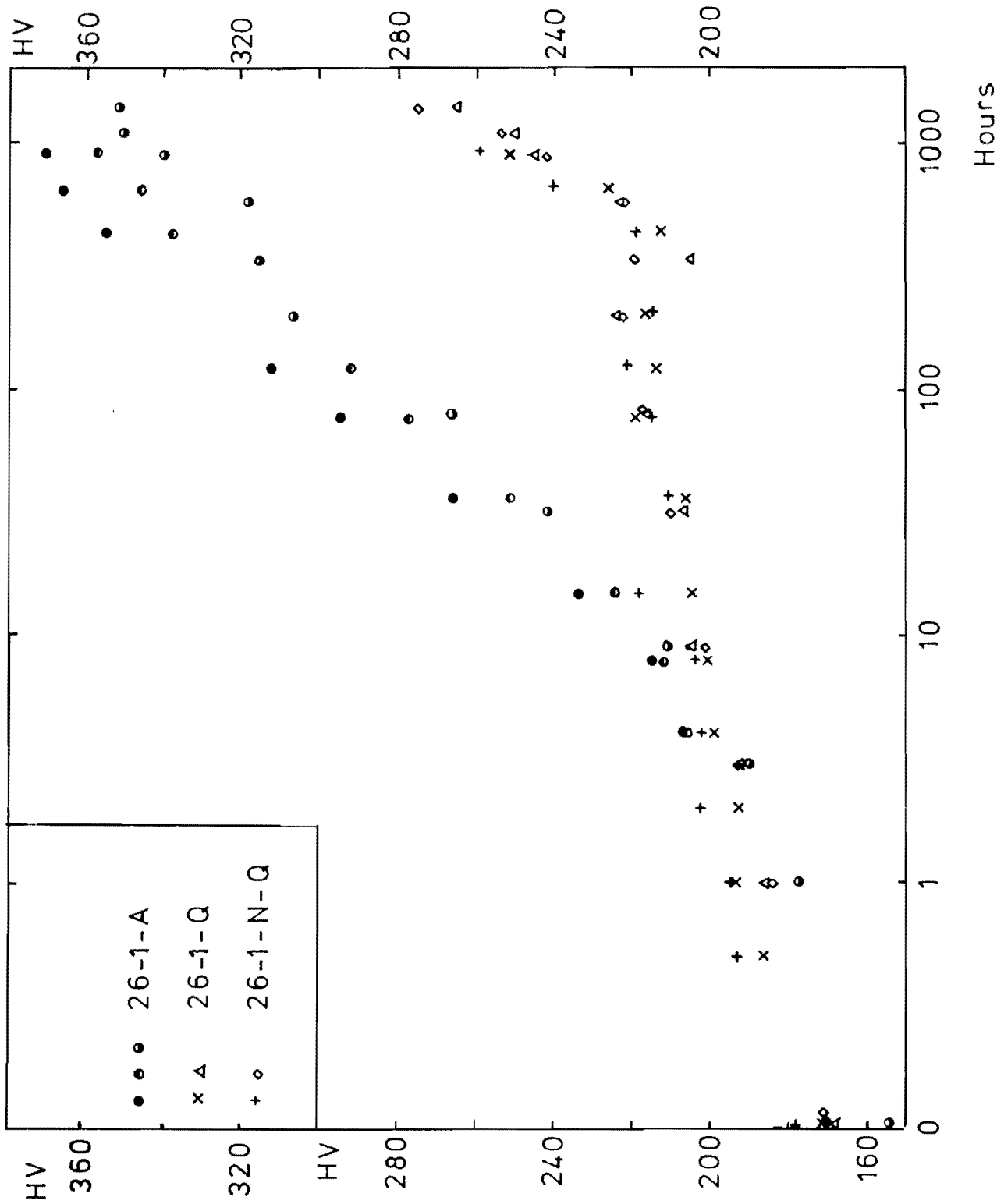

Figure 4.1. The results of 475 C age hardening experiments on a number of different specimens of the 26Cr-1Mo steel in either the annealed (26-1-A), the quenched (26-1-Q), or the nitrided and quenched (26-1-N-Q) condition. Vickers hardness is shown as a function of ageing time.

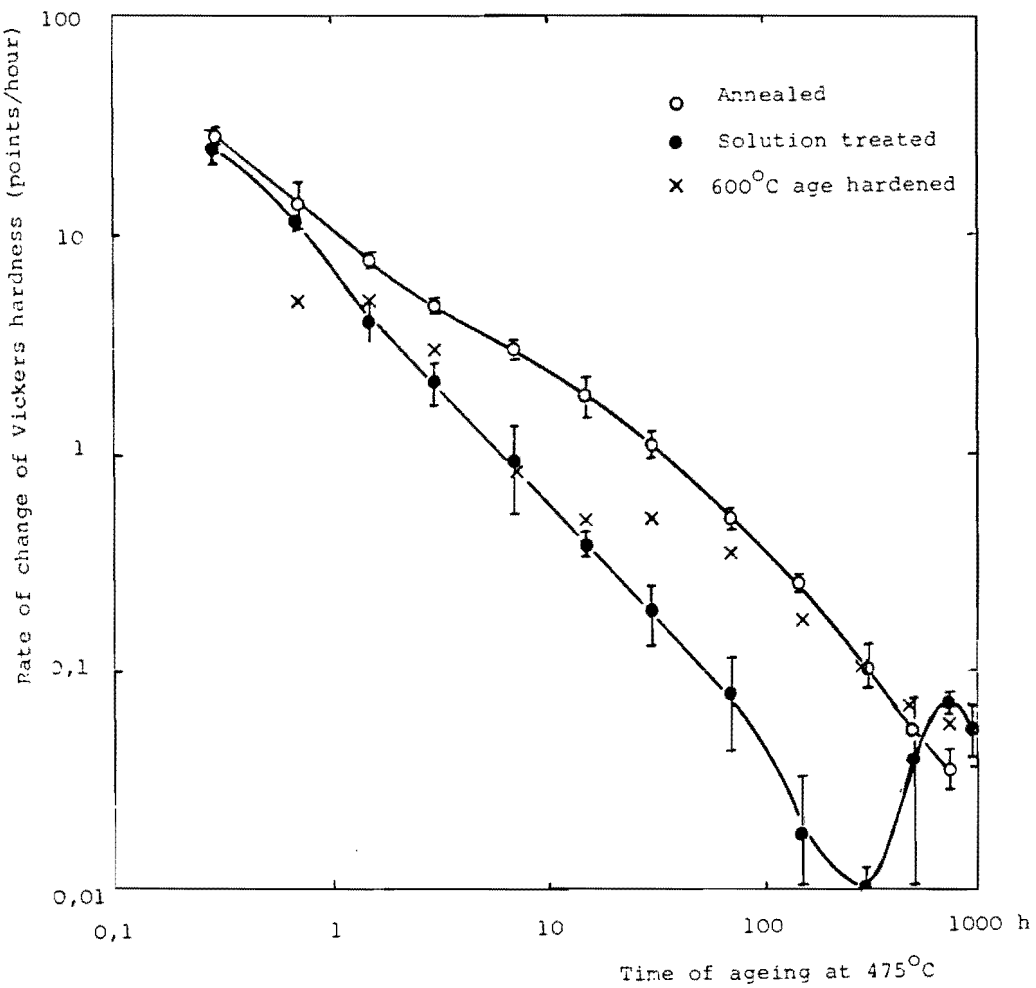

Figure 4.2 The rate of change of hardness at 475 C, as a function of ageing time, for the preliminery treatments of annealing, quenching, and 600 C hardening. In the annealed and the quenched cases points were derived from data for more than one specimen, and the associated standard deviations are denoted by bars.

The specimens 26-1-Q and 26-1-N-Q had a more pronounced decrease in their rate of hardening for the initial 300 hour period, with k being approximately 1,1 in the above equation. After about 300 hours there was a discontinuity in their rate graph which is associated with a sudden increase in hardening rate, shown in fig. 4.2, which might be indicative of a change in hardening mechanism.

The ageing behaviour of the 600 C hardened specimen (26-1-N-600) is shown in fig. 4.3 together with curves derived from fig. 4.1. It can be seen that this specimen had the slowest initial rate of hardness increase when aged at 475 C. This rate increased after about 20 hours, after which it tended to follow the age hardening curve of the annealed specimen. It is clear from fig. 4.2 that 26-1-N-600 initially followed the behaviour of the quenched specimens, but after about 20 hours the rate deviated from this tendency and it assumed the behaviour of the annealed specimen. The value of HV 340 was reached at 900 hours, at which point ageing was terminated and thin foils for TEM were prepared.

There can be no question as to the validity of the results shown in fig. 4.1: a total of seven different preliminery heat treatment experiments, followed by two sets of ageing experiments, were carried out to obtain these results. In fig. 4.2 the differences in ageing behaviour of the annealed and the solution treated specimens are validated by the standard deviations included with the data points.

4.2 The Optical Microscopy Observations

The 475 C ageing process caused a pronounced deterioration in the resistance of this steel to grain boundary attack during electro-etching in oxalic acid. This effect was evident in both the annealed (26-1-A) and the solution-treated specimens (26-1-(N)-Q), but especially in the latter case. The prominent attack, which occurred at grain boundaries and inclusions in the aged specimen of 26-1-N-Q during

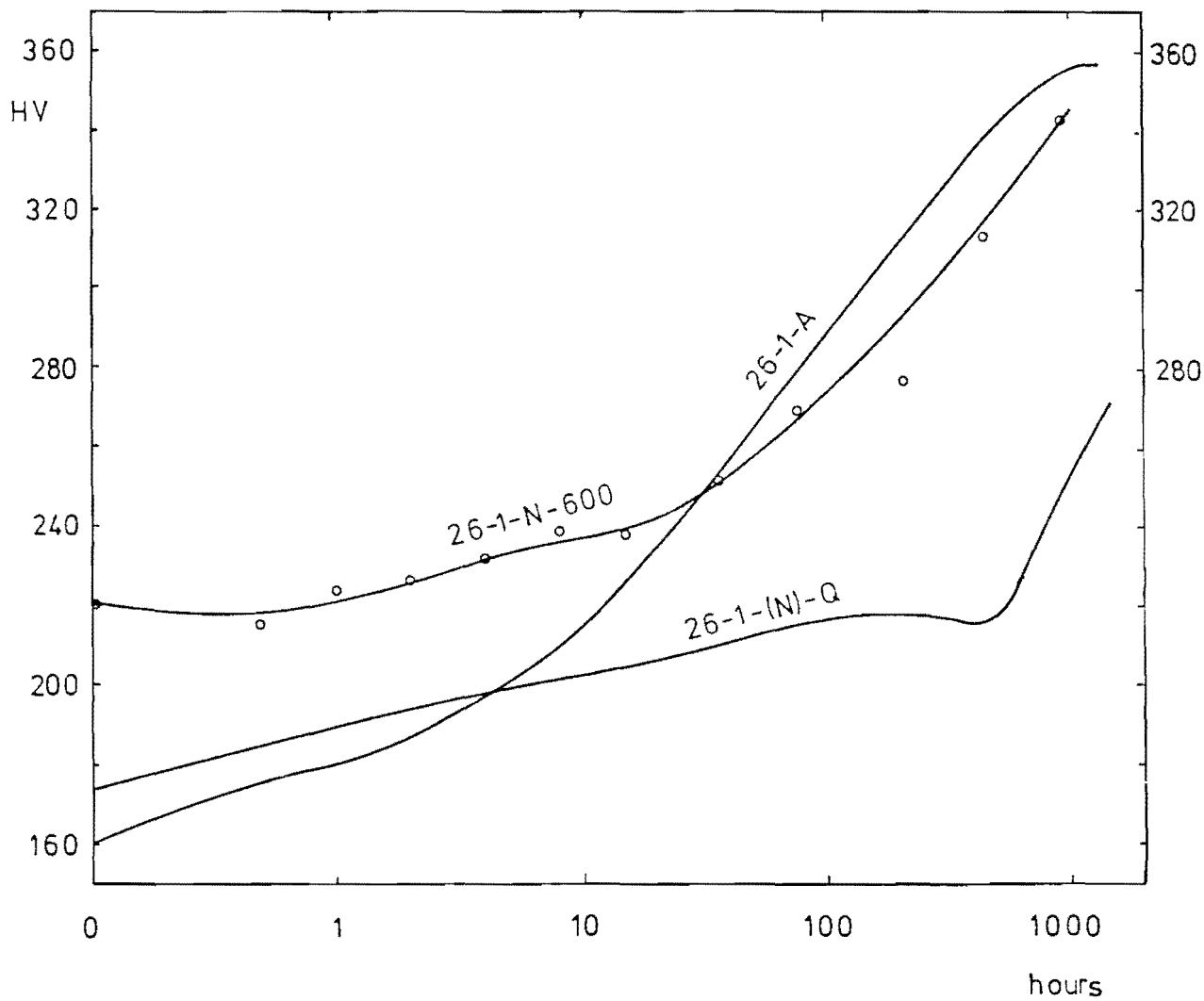

Figure 4.3. The 475 C ageing curve of the specimen of 26Cr-1Mo steel which had been hardened at 600 C by chromium nitride precipitation prior to commencement of 475 C ageing (specimen 26-1-N-600). Also shown are 475 C ageing curves labelled "26-1-A" and "26-1-(N)-Q" which are derived from the points in Fig. 4.1.

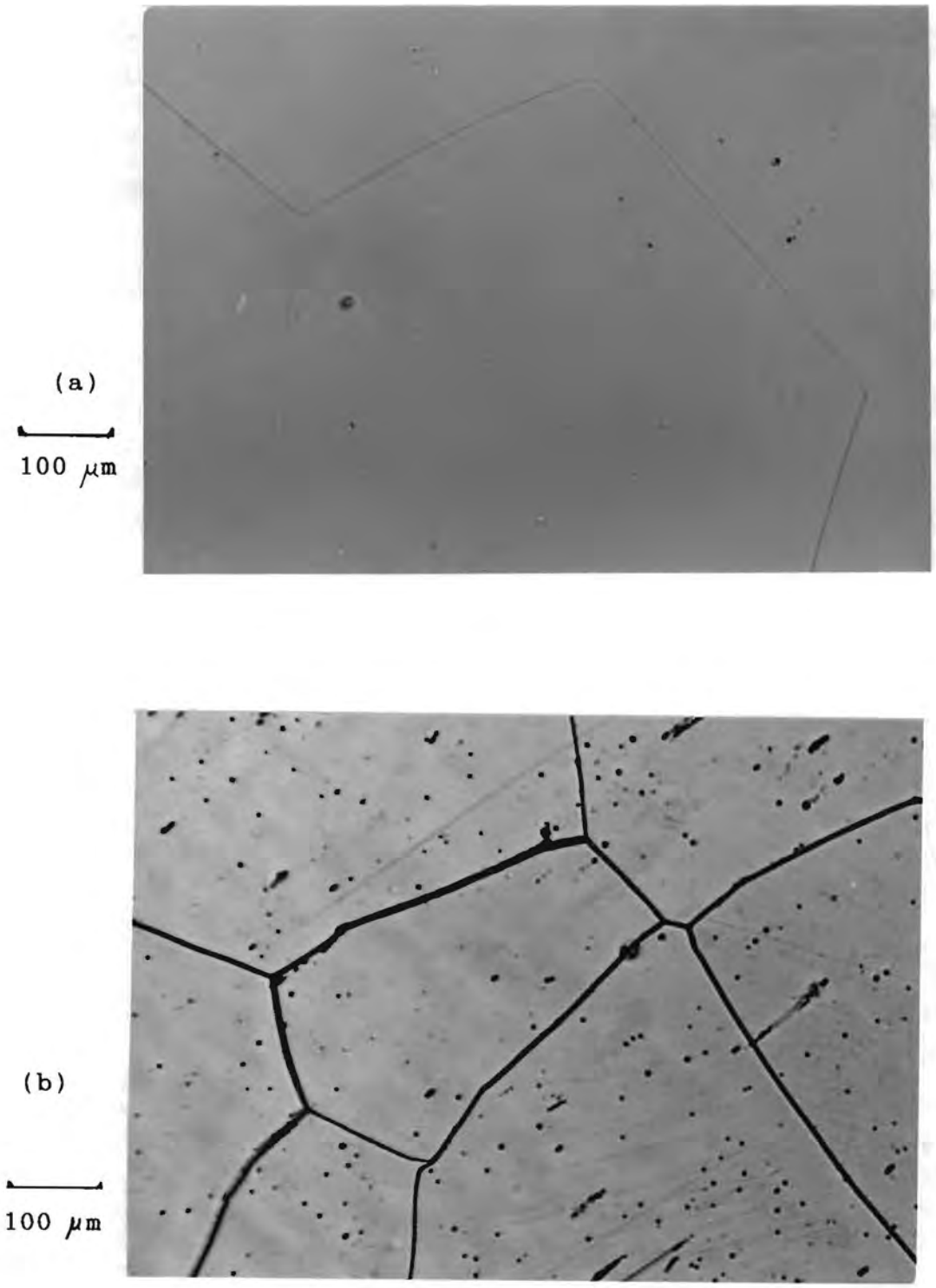

Figure 4.4 Optical micrographs of specimen 26-1-N-Q electro-etched in oxalic acid (a) before and (b) after ageing at 475 C for 940 hours, showing grain boundary etching in (b)

electrolytic etching, is evident in fig. 4.4. This pair of micrographs shows this steel both before and after 475 C ageing, both having been etched in oxalic acid in an identical manner. This suggests a reduction in the amount of chromium available in solid solution in regions immediately adjacent to the grain boundaries and inclusions.

4.3 The TEM Examination of Solution-Treated Specimens Aged at 475 C

TEM examinations were carried out on specimens which had been quenched from solution treatment (ie. specimens 26-1-Q and 26-1-N-Q) and subsequently aged at 475 C. These revealed microstructures that were superficially similar to those of the same material when examined before ageing. (These latter specimens were described in Section 3.2). However, careful examination at high magnification and resolution revealed significant additional features that can be attributed to the 475 C ageing: these were preferential precipitation at interfaces such as grain boundaries and inclusions, and an extremely small-sized strain centre uniformly distributed throughout the grain interiors. Both of these features were present in specimens aged for 310 and 940 hours, corresponding to hardness values of HV 235 and 255 respectively.

An example of preferential precipitation after the shorter (310 hour) period of ageing, is shown in fig. 4.5. It was present in an area up to about 1 μm from the grain boundary (whose intersections with the top and bottom of the foil are marked), and consisted of particles or strain centres up to about 20 nm in size.

After 940 hours at 475 C the grain-boundary precipitation was similar but more dense, as in fig. 4.6A. The grain boundary (characterized by fringes of narrow spacing) is at roughly right angles to the edge of the foil (defined by the narrowest thickness fringe). As the thickness fringes define

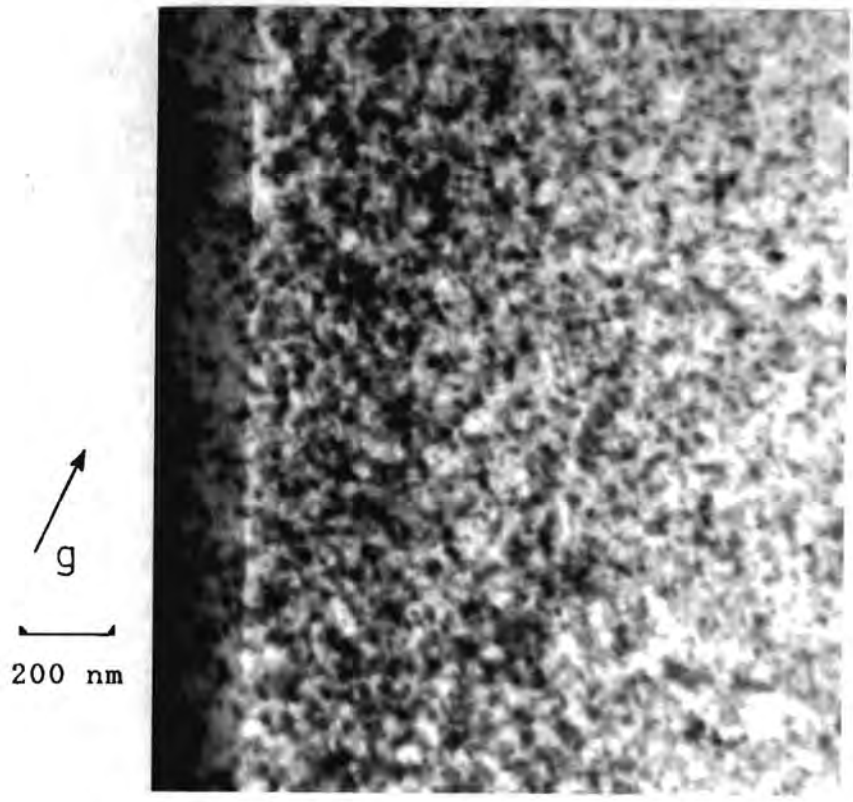

Figure 4.5 TEM micrograph of quenched specimen of 26Cr-1Mo steel (26-1-Q) aged at 475 C for 310 hours, showing preferential precipitation close to the grain boundary (position of which is marked).

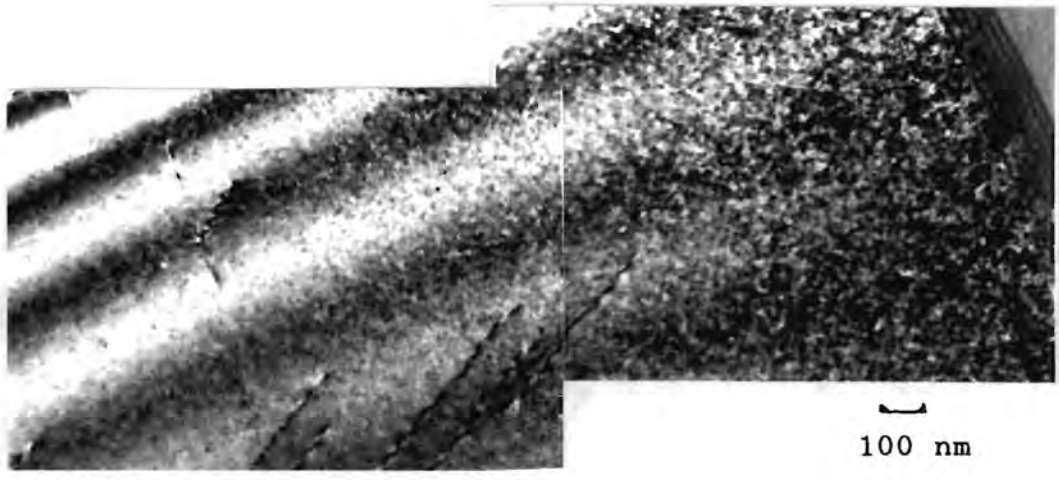

Figure 4.6(a) Specimen 26-1-N-Q aged at 475 C for 940 hours, showing a grain boundary at the extreme right of the micrograph and associated precipitation which decreases in density with distance away. Details are shown in figs. 4.6(b) and 4.6(c).

points of equal foil thickness, provided that the deviation from the Bragg condition does not change, it is clear that the density of precipitation is not related to foil thickness, but to distance from the grain boundary. (Details of this micrograph are shown in figs. 4.6B and 4.6C). The selected-area diffraction pattern associated with this grain boundary area is shown in fig. 4.7. The beam direction is close to ⟨111⟩ and the diffracted spots show streaks, visible here as three-pointed stars, in ⟨211⟩ directions. Because the lengths of the streaks do not increase with distance of the diffraction spot from the central (transmitted) spot, it can be concluded that the streaks arise from the presence of small scattering centres, rather than from lattice strains (Hirsch et al, 1965). These scattering centres are most probably the numerous small precipitates visible close to the grain boundary in the micrographs discussed here.

The second feature observed by TEM in these aged specimens, is a much finer but more sparsely distributed centre of strain, visible uniformly throughout the grains. This has the appearance of small dots of black-white contrast, up to about 8 nm in size of strain field, and visible only in two-beam conditions. These strain centres are considered to be zones (in the sense of a pre-precipitation phase), with large specific strain fields (ie. per unit volume of zone).

An example of the zones after 310 hours of ageing is shown in fig. 4.8, where the black-white contrast is quite readily visible. (In reality the zones do not show much contrast: the dislocations present in this micrograph demonstrate the high level of contrast at which the micrograph was printed; the same applies to figs. 4.9(a) and 4.9(b).

Little change in the appearance of the zones occurs on further ageing at 475 C to a total period of 940 hours, merely an increase in visibility. This can be seen in fig. 4.6 in the region far away from the grain boundary, or in figs. 4.9(a) and 4.9(b). These two micrographs demonstrate

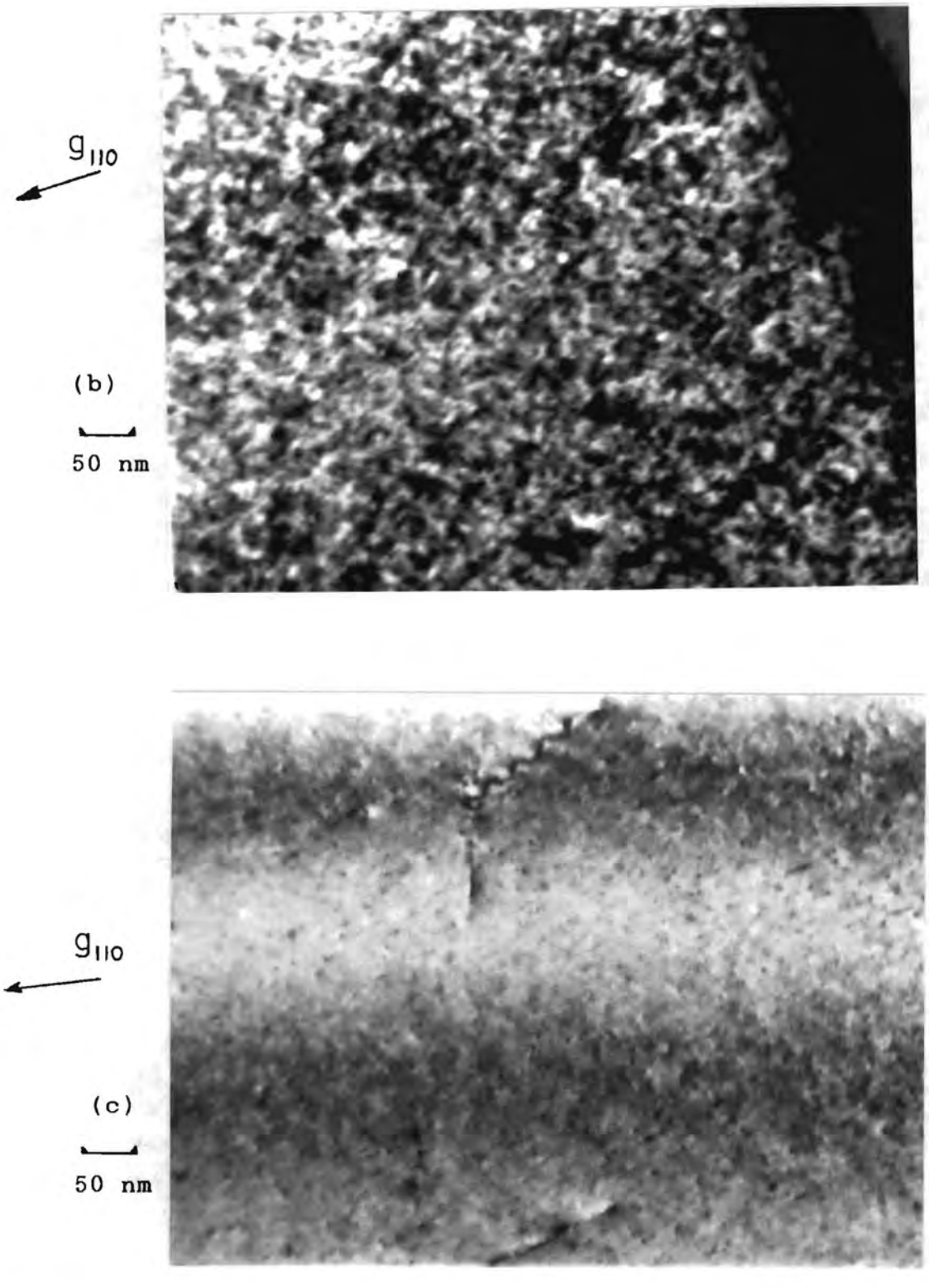

Figure 4.6 Details of areas of fig. 4.6(a). (b) shows heavy preferential precipitation, while (c) is centred about 16 μm away from the grain boundary. Small strain centres showing black-white contrast are visible in (c).

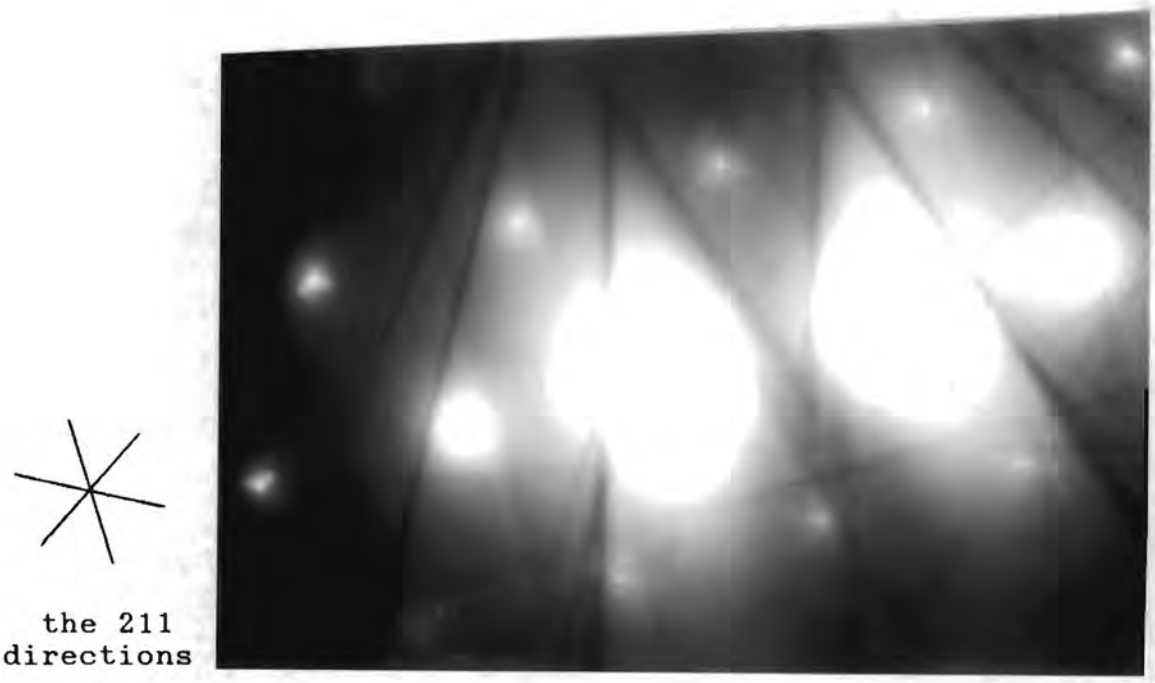

Figure 4.7 The selected area diffraction pattern associated with the grain boundary region shown in fig. 4.6(b). The pattern is 111 with g-vector 110. The spots which are diffracting weakly, show streaking in six directions each of which projects onto ⟨211⟩.

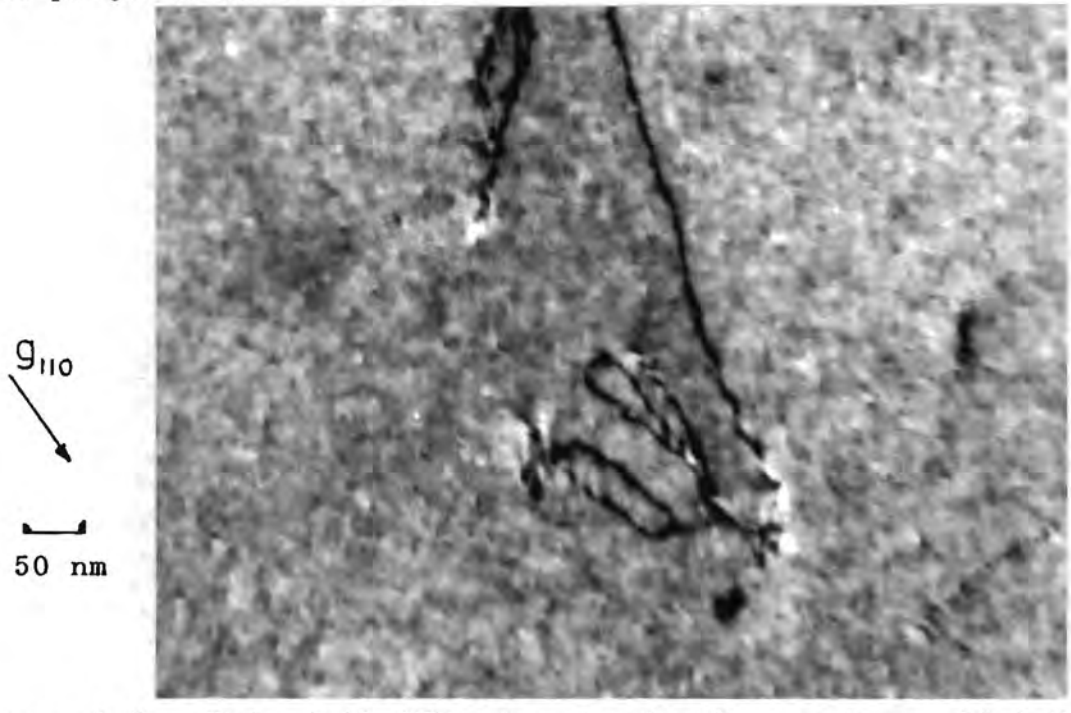

Figure 4.8 Thin-foil TEM micrograph of specimen 26-1-N-Q aged at 475 C for 310 hours. Small strain centres showing dot-like black-white contrast are visible.

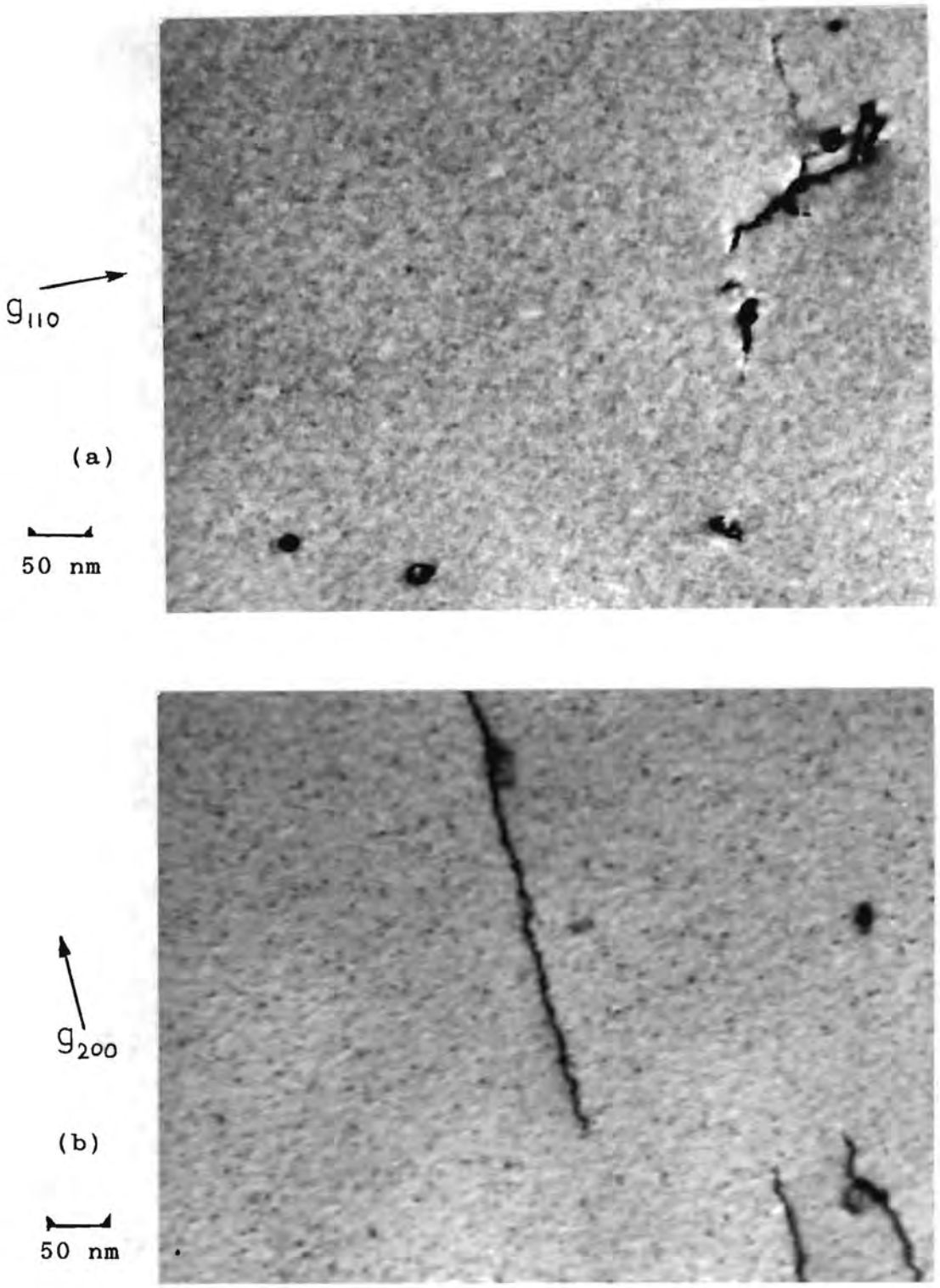

Figure 4.9 Specimen 26-1-N-Q aged at 475 C for 940 hours. (a) is imaged using the 110 g-vector, showing weak contrast modulations and some small dot-like strain centres. (b) is a nearby area of the same specimen imaged with 200 vector, showing prominent dot-like strain centres and some evidence of contrast modulations in <200> directions. The associated SADP's are shown in fig 4.10.

that, not only do the zones require two-beam diffraction conditions in order to be visible, but their visibility is dependent on the indices of the operating reflection. The micrographs were taken from adjacent regions of the same aged specimen of 26-1-N-Q and both at two-beam condition, with fig. 4.9(a) using the 110 and fig. 4.9(b) the 200 reflection. The corresponding diffraction patterns are shown in fig. 4.10. The zones obtained using the 200 reflection are considerably more prominent, and the black-white contrast is quite visible. It can be concluded that the zones have a larger component of strain field parallel to <100> than to <110>, and that their specific strain fields must be quite large for this amount of contrast to be produced from a zone less than 10 nm in size.

Precipitation on dislocations was frequently observed in these aged specimens. An example of this is shown in fig. 4.11 which corresponds to 310 hours of ageing. The precipitates are disc-shaped, and appear identical to those formed during the 700 C ageing of the nitrided and quenched steel. They are probably the same species of chromium nitride and are likely to contribute to some extent to embrittlement by immobilizing existing dislocations.

4.4 The TEM Examination of Annealed Specimens Aged at 475 C

The microstructural features of specimens 26-1-A - ie. those annealed at 800 C in order to remove the interstitials from solid solution and precipitate them as large incoherent chromium carbo-nitrides - have been described in Section 3.2. The features included the sparse distribution of precipitates, the freedom of the dislocations from precipitation, and the absence of strain centres within the matrix.

A TEM examination of the annealed specimens aged at 475 C for 310 hours showed that, when instrument magnifications below about 30 000 times were used, no apparent change in the

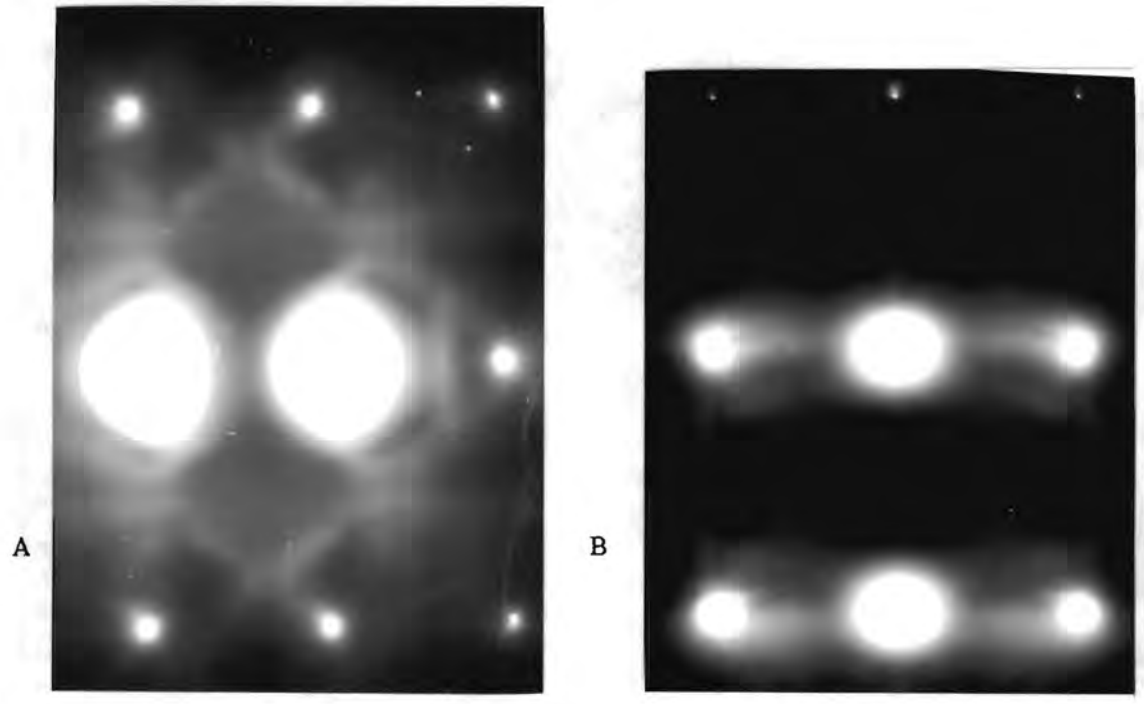

Figure 4.10 The selected area diffraction patterns associated with figs. 4.9(a) and (b). Pattern "A" with g-vector 110 corresponds to the former, pattern "B" (g-vector 200) to the latter.

Figure 4.11 TEM micrograph of specimen 26-1-Q aged at 475 C for 310 hours, showing precipitates which formed on dislocations during ageing.

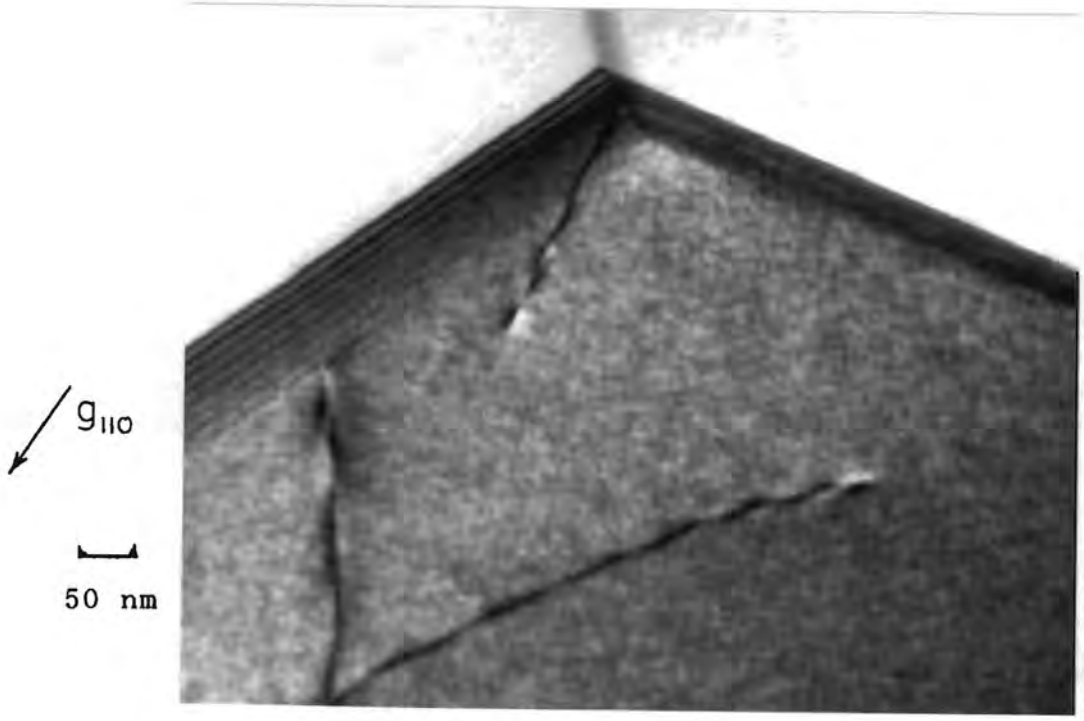

Figure 4.12 A specimen of the annealed 26Cr-1Mo steel (26-1-A) after ageing at 475 C for 310 hours. Only one of the three grains present is under a two-beam condition; it shows contrast modulations.

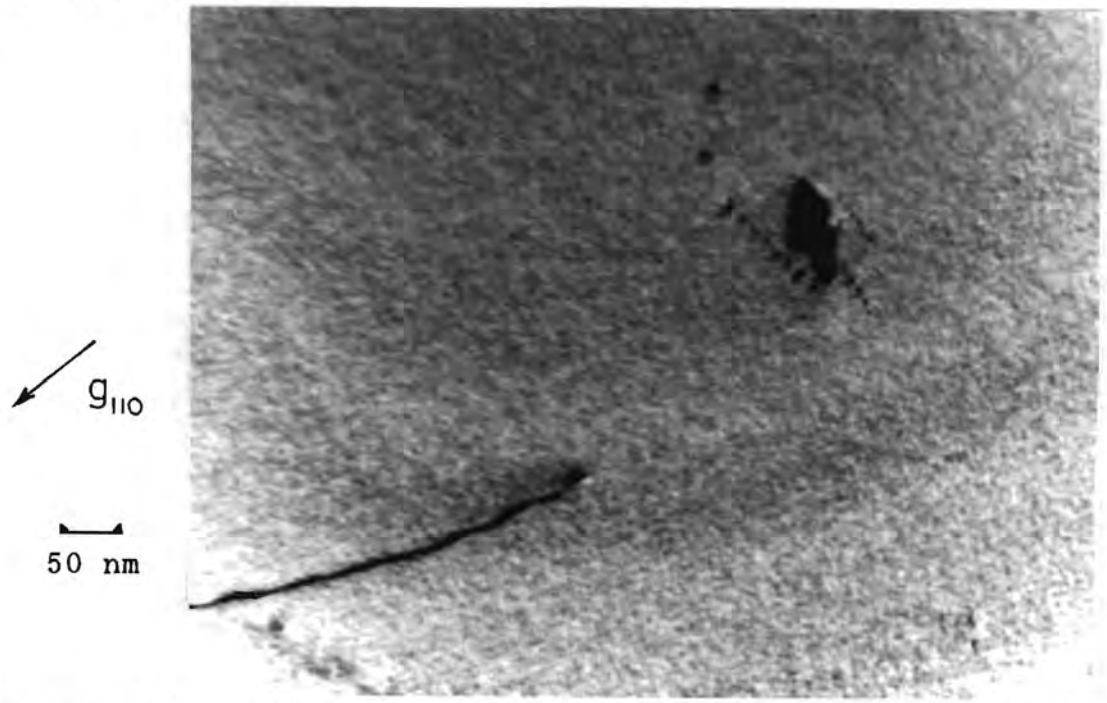

Figure 4.13 Heat treatment as for fig. 4.12, ie. specimen 26-1-A, but 475 C ageing time was 940 hours. The high hardness (HV 355) is associated with the contrast modulations. Also visible is an incoherent precipitate formed during the 800 C annealing.

features described above had occurred. However, examination using higher magnifications and two-beam diffraction conditions, revealed the presence of a fine modulation or "texture" within the grains of the steel, as shown in fig. 4.12. This feature was of very low contrast and not easily visible compared with the zones described in Section 4.3 and shown in fig. 4.8. The example shown in fig. 4.12 illustrates the requirement of appropriate diffraction conditions for visibility of the texture: the darkest of the three grains present shows texture imaged with a 110 g-vector while the other grains are not orientated for two-beam conditions. The uniformity of the texture throughout this grain, the cleanness of the grain boundary, and the absence of dot-like strain centres due to the presence of zones, are quite striking when compared with the microstructures of the corresponding specimens which had been quenched from 1100 C prior to ageing (figs. 4.5 and 4.8).

Longer exposure at 475 C, up to 940 hours, produced not only a further hardness increase but also increased contrast in the texture visible in TEM. Figure 4.13 shows such a specimen with the relatively high hardness of HV 355, imaged under a two-beam condition using a 110 g-vector. Under these conditions a texture showing a poorly-defined periodicity of about 7 nm is visible. This texture is consistently present in all specimens of 26-1-A which have been aged at 475 C for long periods; its presence appears to be unaffected by the discontinuities such as incoherent precipitates, dislocations or grain boundaries. It is the only microstructural feature observed that could account for the hardness change from HV 165 to 355 that occurred during ageing.

Imaging of these aged specimens using the 200 g-vector increases the contrast of the modulations, which lie along the <100> direction (ie. parallel to the g-vector). These are visible in fig. 4.14(a), which is taken from a specimen aged to hardness HV 370. The modulations have a spacing of about 6 nm, which agrees with the spacing measured on fig.

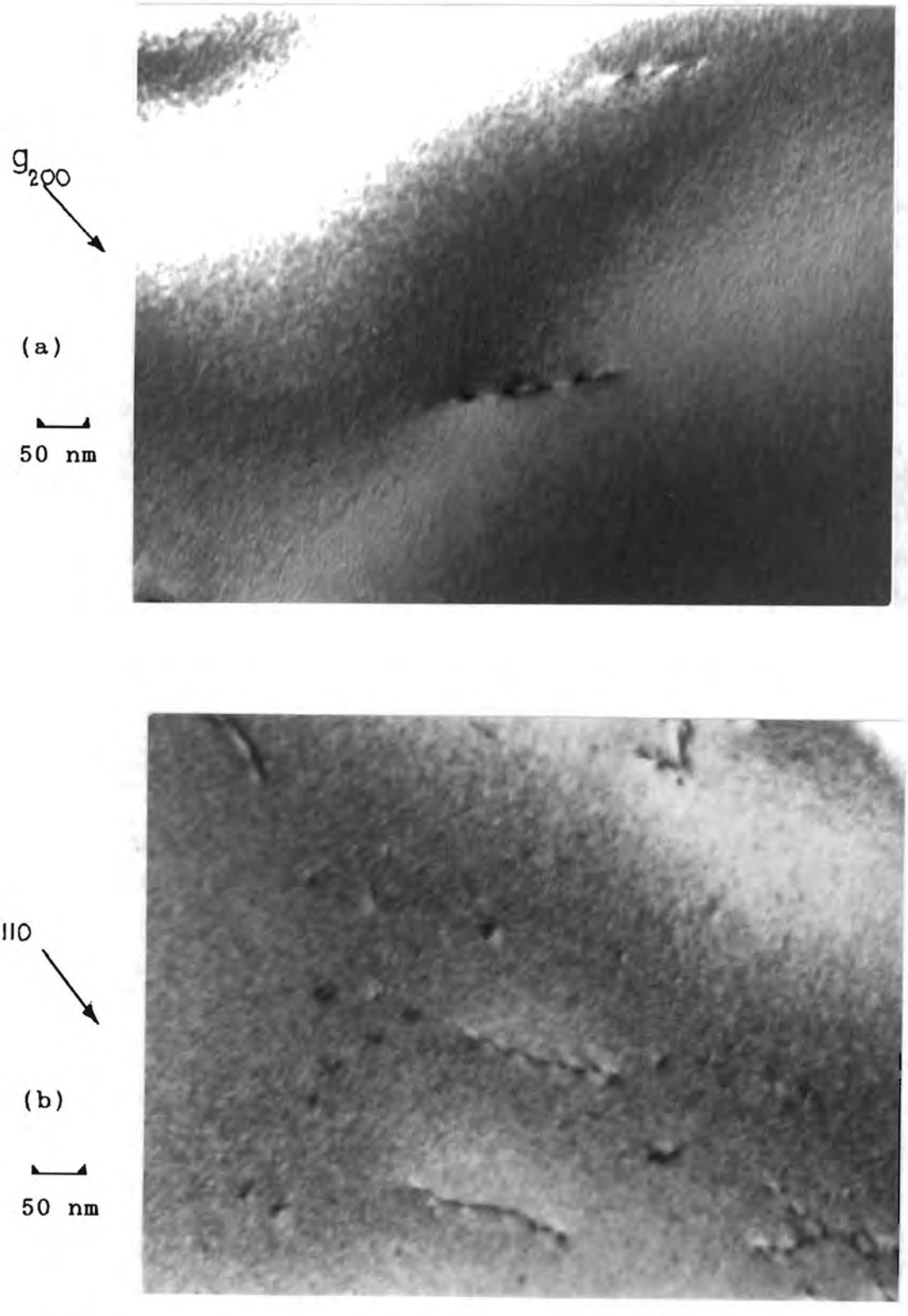

Figure 4.14 The specimen 26-1-A aged at 475 C for 940 hours to HV 370. (a) is imaged by means of a 200 reflection revealing the modulation spacing of about 6 nm. (b) is imaged using the 110 reflection.

4.13 (a different specimen, though subjected to identical heat treatment and ageing). The spacing also agrees with the measurements on other micrographs of the same specimen taken using different diffraction vectors (eg. fig. 4.14(b), where the g-vector is 110). The origin of these modulations is discussed in the following chapter.

4.5 The TEM Examination of a Dual-Aged Specimen

A 475 C ageing treatment was applied to a specimen of 26-1-N-600 for a period of 940 hours to give a final hardness of about HV 340. This complex heat treatment therefore comprised nitriding and quenching from 1100 C, precipitation hardening at 600 C for 8 hours to increase the hardness from about HV 170 to HV 220 through Cr_2N zone formation, and finally the 475 C ageing treatment to give a hardness of HV 340. Essentially, a 475 C reaction was superimposed upon an existing microstructure consisting of a high density of small coherent chromium nitride zones with relatively large strain fields.

Despite the substantial hardness increase that occurred on ageing at 475 C, little if any change was seen in the microstructure as observed by TEM, compared with prior to ageing. An example of the aged structure is shown in fig. 4.15, where strain centres up to about 11 nm in size are present in a quite high density. Comparison with micrographs of specimens 26-1-N-600, figs. 3.11 to 3.13, confirms that the appearance of the characteristic 600 C Cr_2N zones has not changed significantly, with the exception of a possible increase in size, during the 940 hours of ageing at 475 C.

The zones attributed to the earlier 600 C hardening were found to have a planar morphology, lying on $\{100\}$ habit planes. They are visible in fig. 4.15(b) where the foil orientation is close to $\langle 100 \rangle$ and the precipitates which inhabit two of the three $\{100\}$ planes occur in profusion. (The third plane is nearly parallel with the foil and this

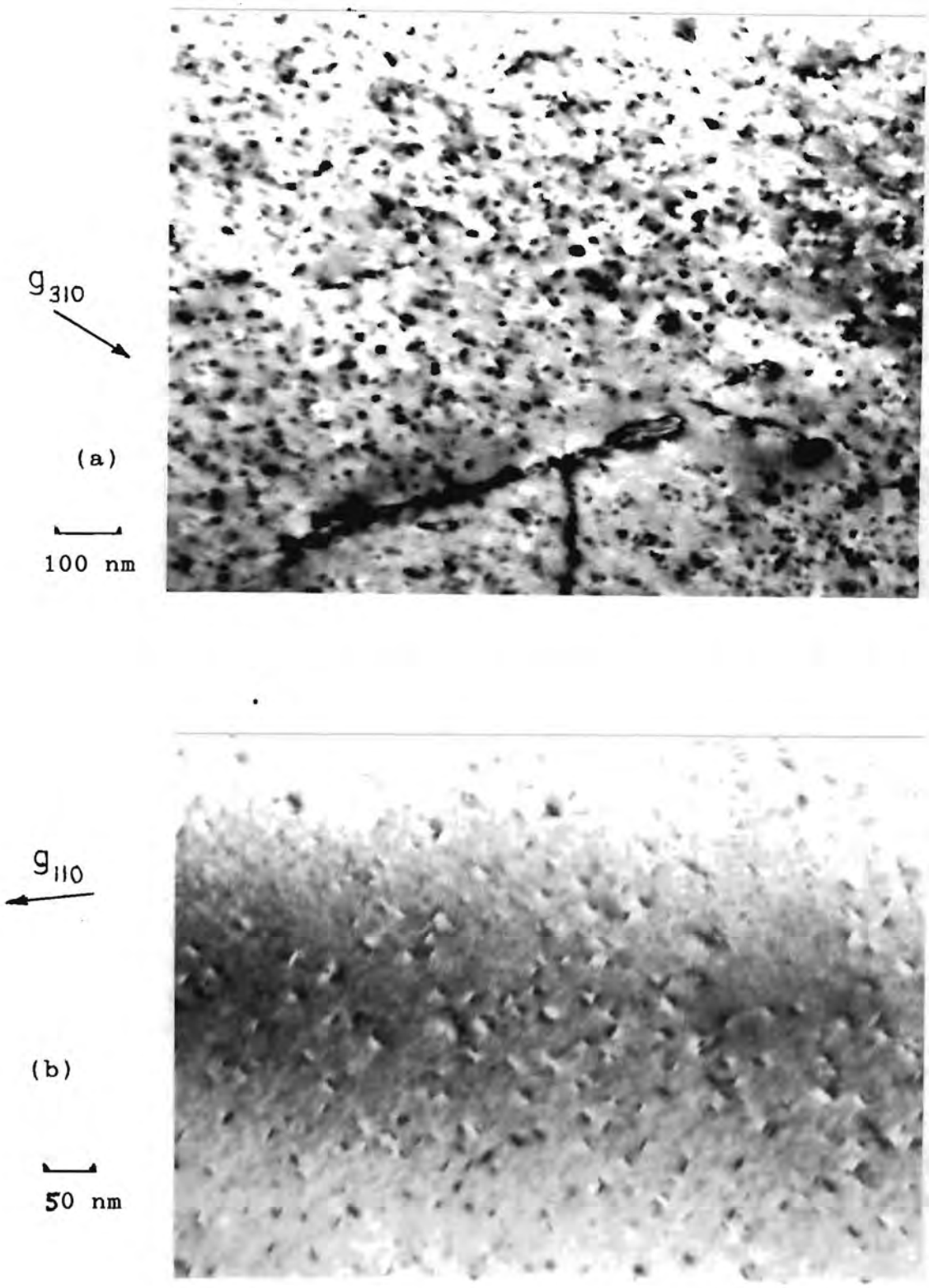

Figure 4.15 The specimen 26-1-N-Q, initially hardened at 600 C and then aged at 475 C to a hardness of HV 340, (a) showing the small coherent precipitates formed at 600 C, and (b) with foil orientation fairly close to (100). The precipitates appear to be planar and inhabit the three {100} planes.

orientation of precipitate is seldom seen for both diffraction and geometric reasons.) There is little or no evidence of contrast modulations in between the zones, or any other microstructural feature which might account for the large increase in hardness during 475 C exposure.

4.6 The Age Hardening at 550 C

A number of specimens of the 26Cr-1Mo steel were subjected to ageing at 550 C after one of the following preliminery heat treatments:

Annealed	(specimen 26-1-A);
1100 C quenched	(26-1-Q);
Nitrided and quenched	(26-1-N-Q);
600 C hardened	(26-1-N-600 and 26-1-600)

Ageing was carried out for 540 hours and the hardness measured at intervals as shown in fig. 4.16. (Also included in this figure are, in broken lines, the 475 C ageing curves for similar starting material.)

Consideration of fig. 4.16 leads to two significant conclusions concerning ageing at 550 C compared with 475 C. Firstly, the difference in hardening rate between the quenched (26-1-Q and 26-1-N-Q) and the annealed (26-1-A) specimens is less pronounced than at 475 C. Secondly, the rate of hardening of specimen 26-1-A is much reduced compared with its rate at 475 C, while the rates for 26-1-Q and 26-1-N-Q are greatly increased. In fact, at 550 C the quenched specimens age faster than the annealed, which is a reversal of the situation at 475 C. As TEM was not performed on these specimens, the microstructural changes responsible for the trends in hardening could not be confirmed. This is discussed further in Chapter 6.

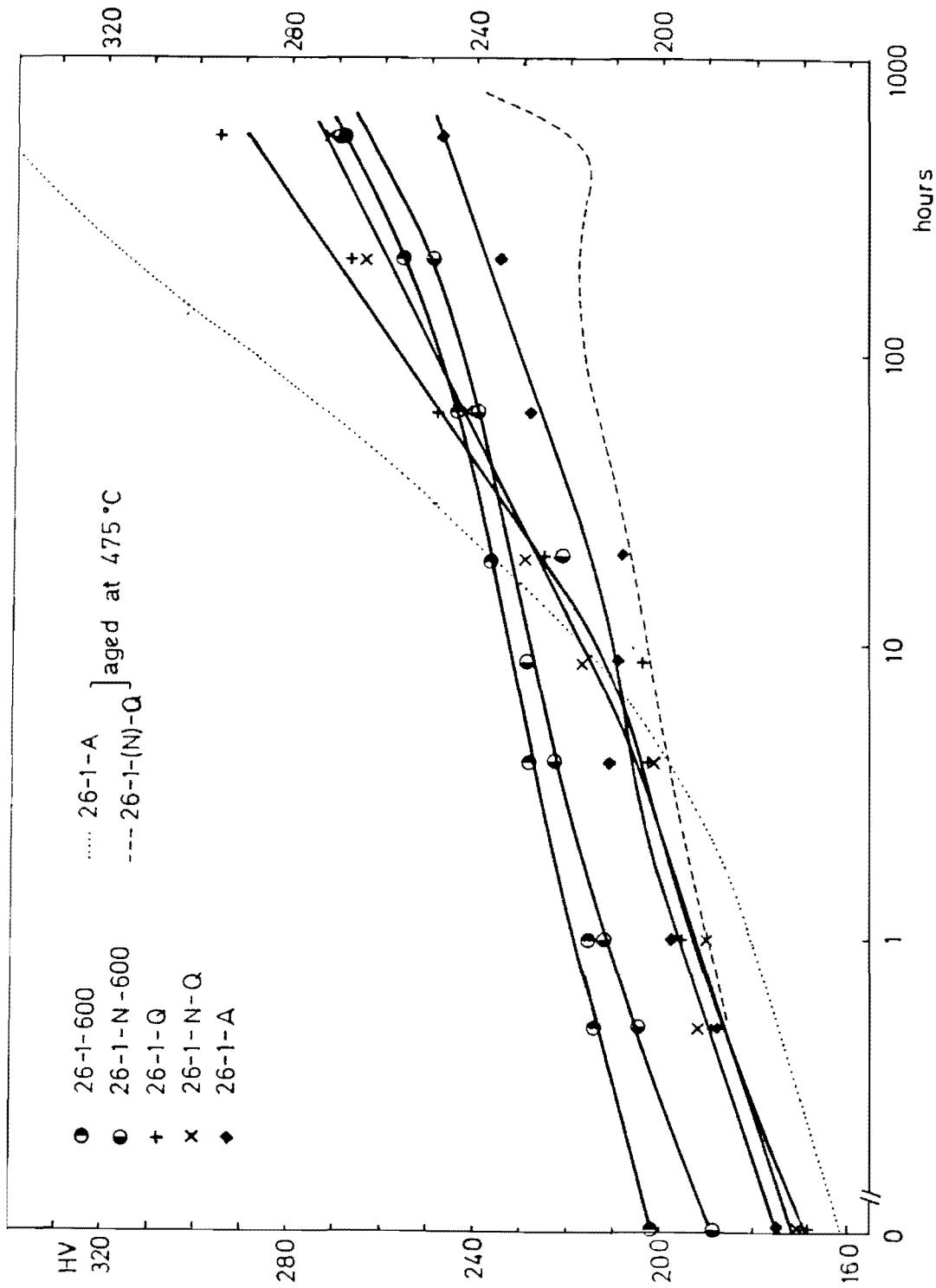

Figure 4.16 The 550 C age hardening curves for the 26Cr-1Mo steel subjected to various preliminery heat treatments. Also shown (broken lines) are the 475 C hardening curves derived from the data in fig. 4.1. There is less effect of preliminery heat treatment when aged at 550 C than 475 C.

4.7 The 475 C Hardening: 26Cr-1Mo Steel ex Climax Molybdenum

Specimens of the very low interstitial electron-beam refined steel from Climax Molybdenum were subjected to the standard preliminery heat treatments described in the introduction to the present chapter, and aged at 475 C for an extended period.

Hardening occurred to a similar extent to that found in the AL 26Cr-1Mo steel, with a hardness of HV 360 being reached after 540 hours of ageing. As in the other case, the specimens 26-1-A (two such specimens were examined) hardened at a faster rate than specimens 26-1-Q or 26-1-N-Q. In particular, the nitrided and quenched one hardened at the slowest rate. The lengths of time required to reach certain hardness values are shown in Table 4.1, from which it can be concluded from Table 4.1 that the greater the amount of interstitials in solid solution (specimens 26-1-N-Q, followed by 26-1-Q), the slower the rate of hardening beyond a hardness of about HV 200.

TABLE 4.1

Hardness	Ageing Time at 475 C in Hours			
	26-1-A	26-1-A	26-1-Q	26-1-N-Q
HV 180	0,2	0,1	0,4	<0,1
HV 195	1,4	1,8	3,0	1,1
HV 240	14	18	47	125
HV 280	44	60	150	230

Table 4.1: The ageing time at 475 C required to reach various hardness values for different specimens of 26Cr-1Mo steel (electron-beam refined).

4.8 The X-Ray Diffraction Studies of 26Cr-1Mo Steels

XRD measurements were made on specimens of both types of 26Cr-1Mo steel after various preliminery heat treatments and

at different stages of ageing at both 475 C and 550 C. While a very good resolution was obtained on suitable specimens - in fact the Kα doublet of copper at 44 degrees of 2θ was resolved - the XRD traces from the quenched specimens tended to be poorly resolved, probably as a result of grain growth having occurred during solution treatment at 1100 C. Furthermore the 200 reflection tended to be of low intensity and very broad compared with the 110 and 211. This can be attributed to lattice distortions in <100> due to both interstitial and precipitated nitrogen, which unfortunately obscured possible information from the XRD traces.

There was little evidence of sideband formation associated with the Bragg peaks in the aged specimens, such as are often associated with spinodal decomposition. The few sidebands present were somewhat ambiguous and will not be discussed here. Certainly the broadening of the 200 peaks mentioned above would have obscured any sidebands associated with <100> compositional modulations. However, secondary XRD peaks were found to be associated with the Bragg peaks in the low-interstitial (electron-beam refined) 26Cr-1Mo steel aged at 475 C for 940 hours and in the nitrided 26Cr-1Mo steel aged at 550 C for 540 hours. The secondary peaks reported here were well-resolved doublets of slightly different lattice parameter to the main peak (to the extent that they were partly coincidental with the main peak).

Figure 4.17 shows secondary peaks in the low-interstitial 26Cr-1Mo steel aged at 475 C in the 1100 C quenched and the 800 C annealed conditions. The figures are taken from the XRD traces of the 211 peaks obtained using Mo Kα radiation. In both cases the secondary peaks are at lower 2θ values than the main α_1 and α_2 peaks. The associated lattice parameters (a_o) were calculated from the positions of the secondary peaks by means of the the Bragg equation. These are represented in fig. 4.18, together with the results of a second measurement on the specimen of 26-1-Q aged at the temperature of 475 C, and of measurements on the same

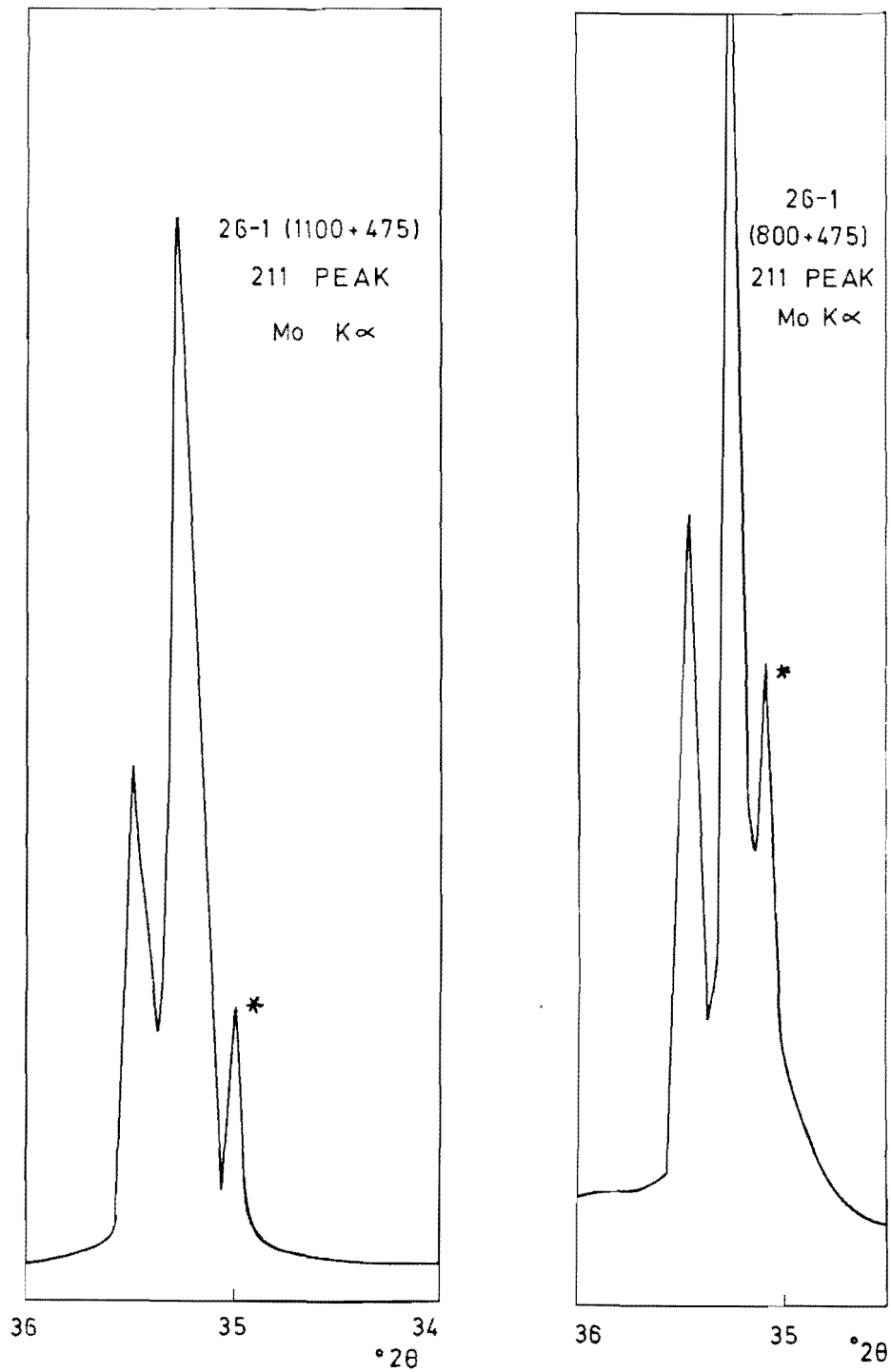

Figures 4.17 (a) (left) and (b) (right), showing the XRD trace across the 211 Bragg peak of the 26Cr-1Mo steel in the quenched and in the annealed conditions respectively. Both peaks have well-resolved α_1-α_2 doublets as well as a secondary α_1 peak at lower 2θ values, marked *.

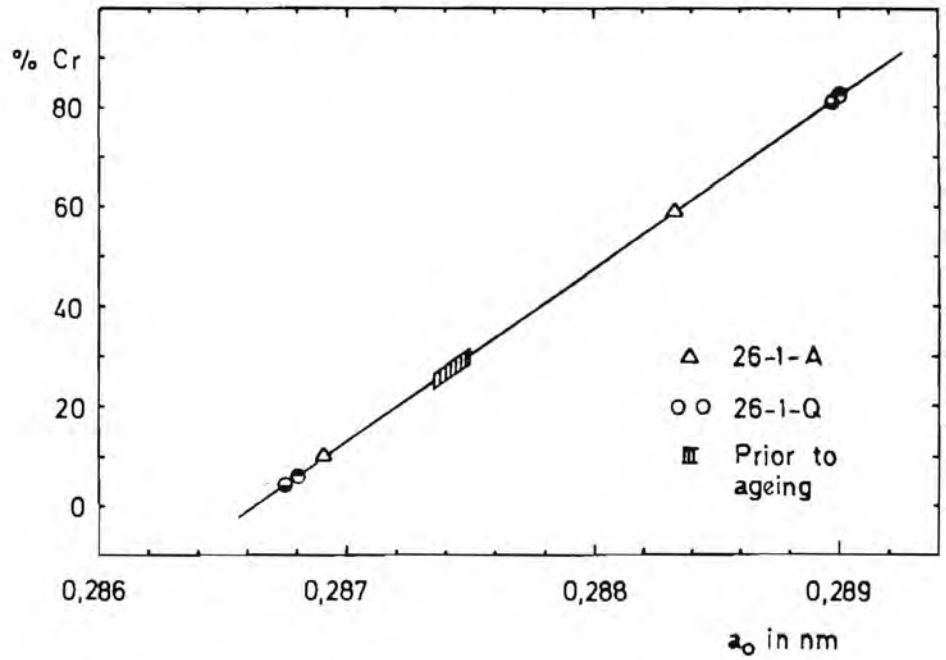

Figure 4.18 The lattice parameter measurements, of main and secondary peaks, and corresponding calculated chromium contents of the 26Cr-1Mo steel, both before and after 475 C ageing. Cr-rich and Cr-depleted zones formed during ageing.

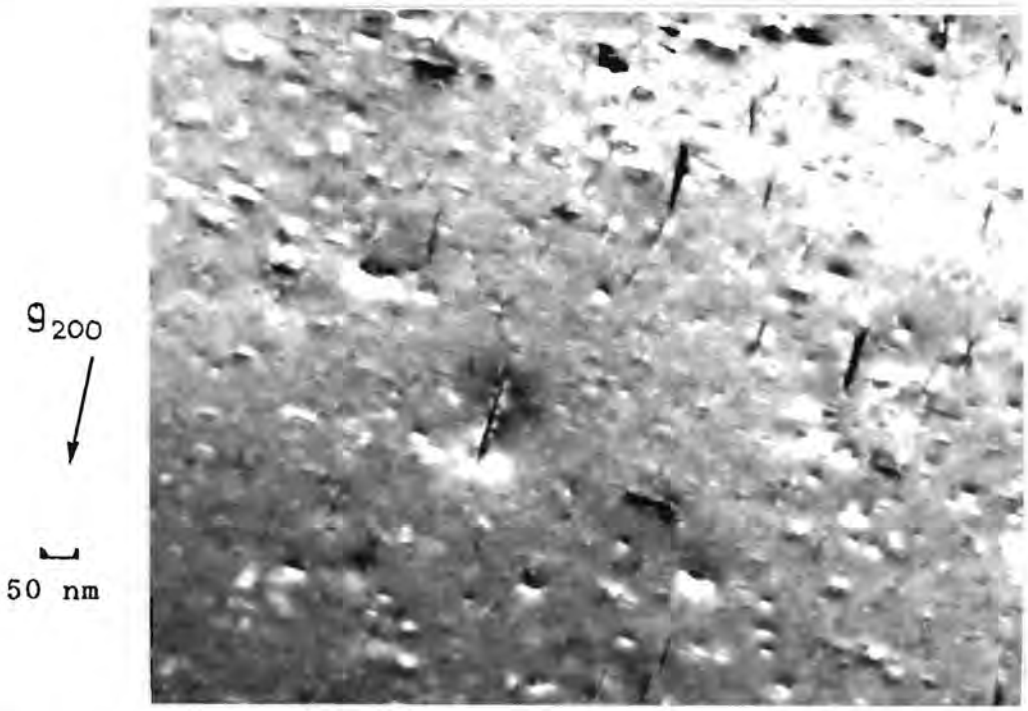

Figure 4.19 Dark field TEM micrograph of the 30Cr steel, quenched and aged at 475 C for 940 hours to HV 400. Foil orientation is (100); coherent planar precipitates lying on {100} planes are present.

materials prior to ageing. The straight line represents the chromium content as a function of a_o, based on a fixed Cr:Mo ratio of 26:1 and variations in the iron content. In calculating this relationship, standard a_o values have been used and Vegard's law assumed; the relationship is therefore possibly not exact. This line should represent any extent of decomposition into Cr-rich or Cr-depleted phases, but does not allow for any strong segregation of molybdenum.

It follows from fig. 4.18 that the 475 C ageing has resulted in decomposition into chromium-rich and chromium-depleted phases. In the case of 26-1-Q, the chromium contents are about 80% and 6% in precipitate and matrix repectively, while in specimen 26-1-A these were determined to be about 60% and 18% respectively. Concerning the "prior to ageing" value shown on fig. 4.18: this represents the spread of three measurements taken on specimens prior to 475 C ageing. This particular a_o value of 0,2874 nm, obtained from XRD, is in good agreement with the value of 0,28739 calculated from standard published data for Fe, Cr and Mo.

Similar secondary XRD peaks have been reported in other alloy systems which undergo decomposition; these are discussed in Chapter 5.

4.9 The 475 C Ageing of the 30Cr Steel

Specimens of the 30Cr steel, referred to in Section 2.1 as having a relatively high interstitial content, were aged at 475 C in either the 800 C annealed condition ("30Cr-A") or the 1100 C solution-treated and quenched condition ("30Cr-Q"). Both specimens showed substantial hardening over the 940 hours of exposure at 475 C: 30Cr-A increased in hardness from HV 220 to HV 390, and 30Cr-Q from Hv 280 to 400. (The high as-quenched hardness of 30Cr-Q, viz. HV 280, illustrates the detrimental properties, known as high temperature embrittlement, that result when a high-chromium steel with high carbon content is quenched from a temperature of

considerable carbon solubility.

TEM examination of the 475 C aged specimens revealed substantially different microstructures for the two preliminery heat treatments. If allowance is made for the considerably higher carbon content of the 30Cr steel compared with the 26Cr-1Mo steels, the microstructural features of the aged specimens of 26-1-(N)-Q and 30Cr-Q are consistent with each other, as are those of specimens 26-1-A and 30Cr-A.

The 475 C aged specimen of 30Cr-Q contained a high density of coherent planar precipitates, lying on $\{100\}$ lattice planes, and typically 80 nm in size. These are visible in fig. 4.19, which is a TEM micrograph with the foil orientated close to $\langle 100 \rangle$ and a g-vector of 200. With this foil orientation, one set of discs is in the plane of the foil, the other two are respectively parallel to and normal to the g-vector. Also present are much smaller strain centres, typically about 15 nm in size, with the appearance of planar zones on $\{100\}$ These probably account for some of the measured hardening at 475 C.

The specimen 30Cr-A showed, in its 475 C aged condition, numerous needle-shaped precipitates large enough to be incoherent with the matrix, and which were observed to have formed during the 800 C anneal. In addition, two-beam diffraction conditions revealed matrix strain contrast modulations similar to those found in specimens 26-1-A after 475 C ageing, but somewhat more clearly visible. An example is shown in fig. 4.20, where measurement of the modulations gives a spacing between them of about 12 nm. This type of contrast was homogeneously distributed throughout the specimen irrespective of lattice discontinuities such as the dislocation visible in fig. 4.20, and would appear to have been formed by spinodal decomposition at 475 C.

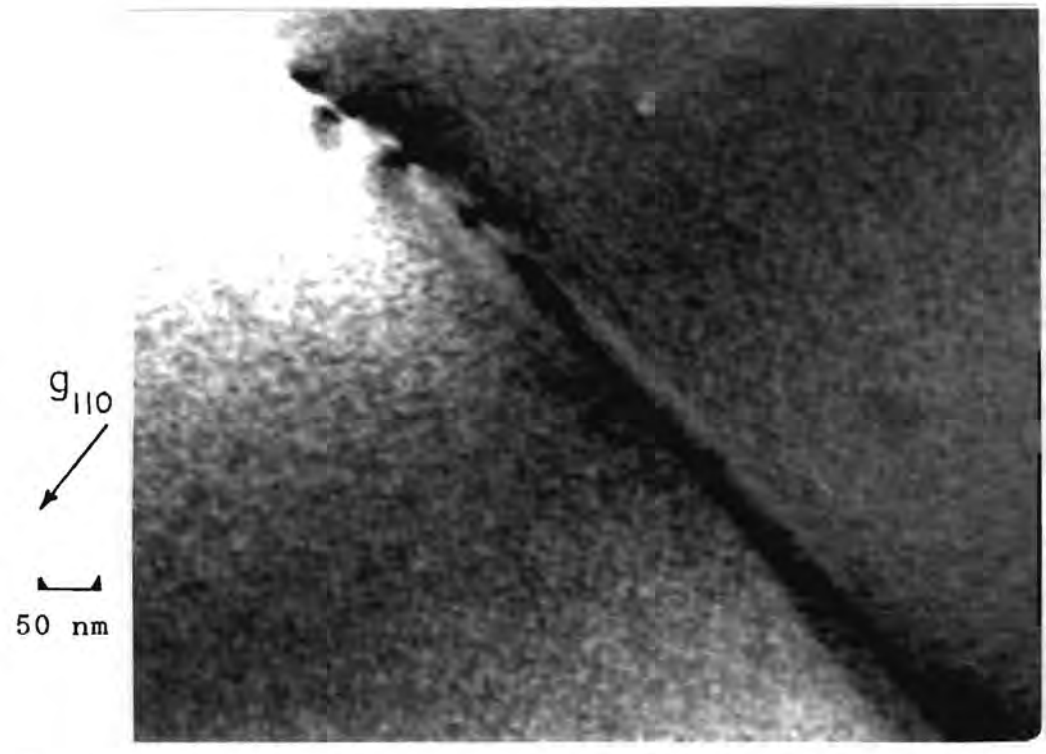

Figure 4.20 The annealed specimen of 30Cr steel, aged at 475 C for 940 hours to HV 390, showing matrix strain contrast modulations. (Dark field micrograph.)

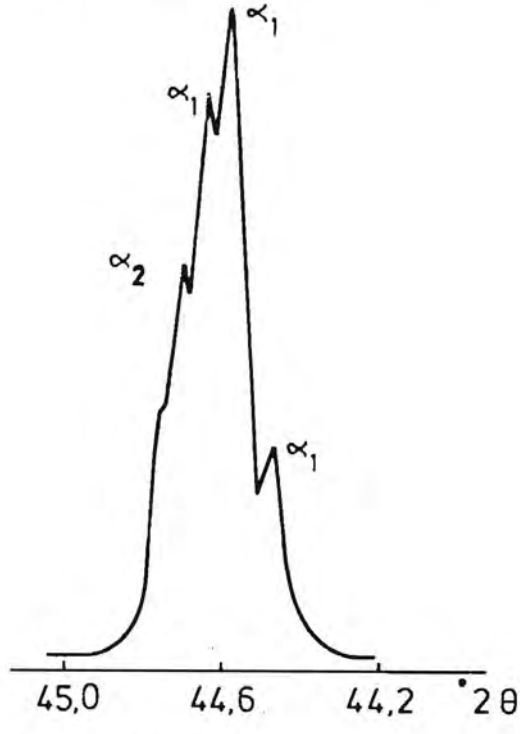

Figure 4.21 The XRD trace across the 110 peak of the 30Cr steel, annealed and then aged at 475 C, showing two secondary diffraction peaks flanking the main peak.

4.10 The X-Ray Diffraction Studies of the 30Cr Steel

High-resolution XRD scans of the 30Cr steel aged at 475 C were carried out on specimens which, prior to ageing, had been in both the annealed (30Cr-A) and the quenched (30Cr-Q) conditions. Secondary diffraction peaks - often multiple ones - were found to be associated with certain Bragg reflections, and their existence was confirmed by a repetition of the XRD scans on the same specimen.

The specimen 30Cr-A showed, after 475 C ageing, secondary peaks about the 110 (Cu K_α radiation) and 220 (Mo K_α) Bragg reflections, one of which is reproduced as fig. 4.21. The trace shows three α_1 peaks, each of which corresponds to a slightly different lattice parameter. If the corresponding chromium contents of the Fe-Cr alloy are calculated similarly to the 26Cr-1Mo steel described in Section 4.8, these peaks are found to correspond to chromium contents of 31% for the main peak and 11% and 67% for the secondary peaks. These results, together with another 110 and a 220 measurement, are presented in fig. 4.22 as lattice parameters and, through the simple Fe-Cr composition line, as approximate chromium contents. Close examination of this figure confirms that the specimen has decomposed into Cr-rich and Cr-depleted phases, relative to the original chromium content of 30%. A measurement of a_o on a 211 peak which had no secondary peaks, and hence represented the overall lattice parameter of the specimen, is also plotted on fig. 4.22: this is calculated to correspond to a composition of 40% chromium.

The quenched specimen 30Cr-Q showed secondary peaks at lattice parameters corresponding to calculated chromium contents of about 15% and 60% after 475 C ageing. These would appear to represent decomposition into Cr-rich and Cr-depleted zones, similar to the specimen 30Cr-A but to a slightly lesser extent. The results of three measurements of Bragg peaks with associated secondaries, as well as the lattice parameter for a peak free of secondaries, are given

in fig. 4.23. No explanation can be given for the absence of secondary peaks in the case of this 211 Bragg reflection.

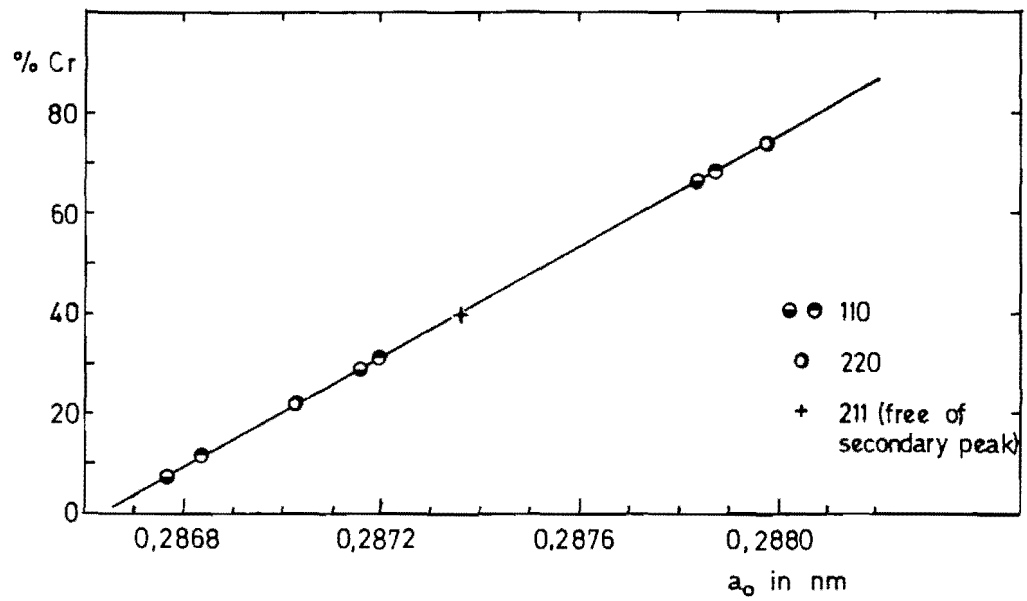

Figure 4.22 The lattice parameter measurements and corresponding calculated chromium contents, of the 30Cr steel aged at 475 C in the annealed condition. Decomposition into Cr-rich and Cr-depleted zones has occurred.

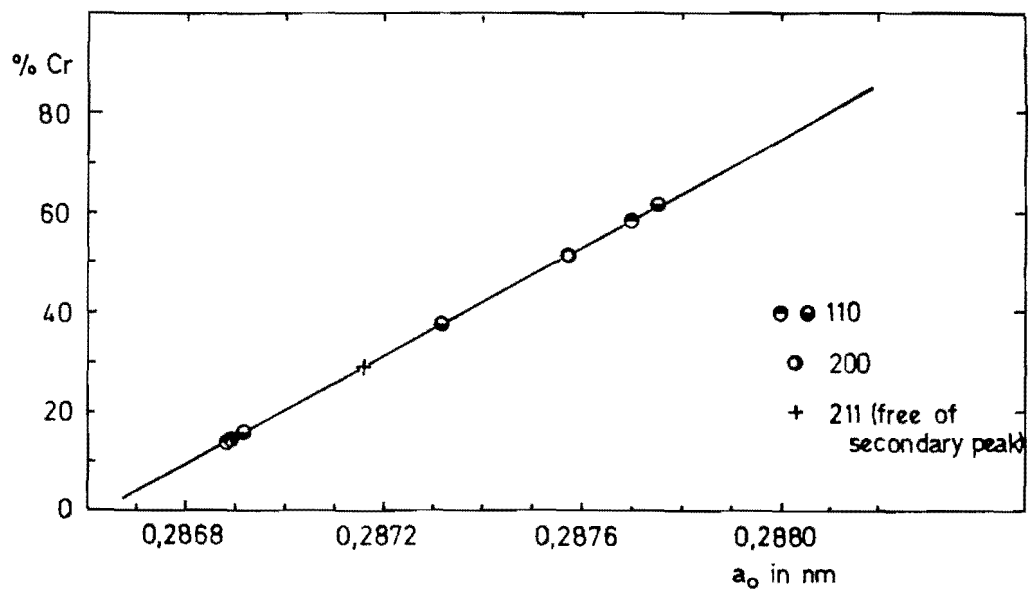

Figure 4.23 As for fig. 4.22, but the specimen was quenched prior to ageing (30Cr-Q). Decomposition is evident.

Chapter 5

DISCUSSION: AGE HARDENING DUE TO PRECIPITATION OF INTERSTITIALS

According to the phase diagram for the Fe-26Cr-N system (fig. 1.1), rapid quenching of the 26Cr-1Mo steel from either solution treatment or nitriding at a temperature of 1100 C should produce specimens containing a supersaturation of interstitial nitrogen, while annealing at 800 C should remove virtually all nitrogen and carbon from solid solution through precipitation as compounds of chromium. The interstitial nitrogen content, which comprises that distributed randomly or in zones (pre-precipitation phases) as defined by Krawitz and Sinclair (1975), was calculated from lattice parameters derived from XRD measurements, according to the factor given by Hendry et al (1979). Taking the interstitial nitrogen content of the annealed material as zero, this content was found to vary from about 0,02% for as-received and quenched material ("26-1-Q") to 0,03% - 0,04% for nitrided and quenched ("26-1-N-Q").

The XRD measurements on specimens quenched from 1100 C also revealed a considerably greater lattice parameter in <100> compared with other lattice directions such as <211>. This lattice expansion in <100> can be accounted for if one assumes that the interstitials are present at octahedral sites in the lattice, distributed either randomly or in zones.

The absence of grain boundary etching when specimens quenched from 1100 C were electro-etched in oxalic acid, and the absence of precipitation during direct observations of grain boundaries by TEM, confirm that grain-boundary precipitation of chromium nitrides did not occur during quenching from solution-treatment temperature. However numerous dislocations, lying in <110> directions are observed. These may have formed during quenching as a means of accomodating

the supersaturation of interstitials present in solid solution, through the formation of dislocation-solute atmospheres. This mechanism has been suggested by Demo (1971), to explain his observation of precipitation on dislocations present in a high-interstitial 27Cr steel after quenching from 1100 C. This heat treatment regime gives a small hardness increase - of about 8 points HV - relative to specimens annealed at 800 C, and is probably due to the increased flow stress associated with the interaction of interstitials with mobile dislocations.

The present results can be compared with those of Grubb and Wright (1979) on low- and high-interstitial 26Cr steels quenched from solution treatment at 1290 C. While the present 26Cr-1Mo steel has a similar carbon content to their low-interstitial alloy, its nitrogen content (200-400 ppm) is some 3 to 8 times greater than theirs (47ppm). Nevertheless, similar microstructures were obtained in the two steels in question, suggesting that small quantities of nitrogen (up to about 300 ppm) are not precipitated at grain boundaries during a rapid water quench. By contrast, their high-interstitial steel had similar nitrogen content to the present case but several times greater carbon content (300 ppm); it showed evidence of grain boundary precipitation and even some intragranular precipitates when quenched from high temperature. These observations suggest less of a tolerance of interstitial carbon than nitrogen in these steels, resulting in ejection of carbon to the grain boundaries during cooling from temperatures of substantial carbon solubility, even when the cooling rate is quite rapid.

Annealing at 800 C for 2-4 hours produces the softest condition for the 26Cr-1Mo steel, with virtually all interstitials compounded in the form of roughly cube-shaped incoherent chromium-rich precipitates situated within the grains as well as at the grain boundaries. No evidence of continuous, or even semi-continuous, grain-boundary films was found, although the grain boundary precipitation was observed

to be quite prolific, and resulted in some loss of grain boundary corrosion resistance.

The classical age hardening behaviour of the ferritic stainless steel-nitrogen system is demonstrated by the substantial hardening that occurs when quenched specimens are aged at temperatures of 600-800 C for appropriate periods of time. Peak hardness values are associated with specific microstructures, these being characterized by a high distribution density of small coherent precipitates with relatively large strain fields (5-10 nm in size) and visible only in TEM. The hardness increase over the as-quenched condition is due primarily to the increased flow stress, which itself results from the fact that a significant volume fraction of the matrix is in a strained condition and hence impedes dislocation motion. A further hardening arises from the immobilization of existing dislocations through the formation of precipitates on them.

The small strain centres which are responsible for the peak hardness measured after ageing at 600 C for about 6 hours, are clearly the initial stage of formation of chromium nitride precipitates and can be considered equivalent to GP [1] zones formed in an Al-Cu age hardening alloy. In the latter case the GP [1] zone is a plate-like cluster of copper atoms segregated onto {100} planes of the aluminium matrix. In the present case the zones grow with further ageing into planar precipitates of CuAl , with an increased hardening effect. In the Fe-26Cr-N system, growth of zones into planar precipitates leads to softening as soon as their sizes exceed about 15 nm, ie. beyond about 0,2 hours at 700 C or 6 hours at 600 C. The softening is also related to the decrease in distribution density of the precipitates.

At the temperature of 600 C the changes in precipitate size and density occur very slowly: after 270 hours exposure the precipitate strain fields have grown only to about 15 nm in size, which coincides with the hardness decrease to within

about 20 points (HV) above the as-quenched condition. At 700 C complete softening - to the level found in specimen 26-1-A - occurs on prolonged ageing, in this case for a period greater than about 10 hours. However, despite the low hardness measured in this condition (HV 150), dislocation movement is apparently still impeded by the presence of the small coherent precipitates. This observation serves to emphasise a conclusion that can be made: that precipitation hardening in these steels does not occur significantly unless there is a sizeable volume fraction of strain fields associated with a dense distribution of very small precipitates (size of strain field not exceeding about 20 nm).

With precipitate growth to a size of about 30 nm, they can be identified as planar discs lying on {100} planes. This morphology is maintained until ageing temperature is high enough (about 750 C) for the size of the precipitates formed to be about 80 nm. At this stage there is loss of total coherency through the formation of a dislocation loop around the disc, as shown in fig. 3.13. This serves to accomodate the increasing lattice misfit between the chromium in the disc and the surrounding iron-rich matrix, similar to what is observed to occur with GP [2] zones in aged Al-Cu alloys. At higher temperatures, growth of the precipitate normal to its habit plane commences.

The planar precipitate morphology has been reported by Grubb and Wright (1979) in the low-interstitial 26Cr steel quenched from solution treatment and aged at 540 C for 10 minutes. In view of the expected reduction in precipitate growth rate of about an order of magnitude when the ageing temperature is reduced from 600 C down to 540 C (due to reduced diffusion rates), and the present observations that precipitates formed at 600 C only begin to assume planar morphology after about 100 hours of ageing, the observations of Grubb and Wright are surprising. The differences can only be ascribed to either their higher solution treatment temperature, or else to the

absence of molybdenum from their steel.

Chapter 6

DISCUSSION: THE 475 C HARDENING REACTION

6.1 Summary of Results

The vacuum melted 26Cr-1Mo steel (ex Allegheny Ludlum) undergoes hardening when aged at 475 and 550 C for long periods. The rate of hardening at both temperatures is dependent on previous heat treatment, ie. on the state of the interstitials in the steel. The TEM examination of the 475 C aged specimens reveals the development of different types of microstructure which are exclusively characteristic of either the quenched or the annealed preliminery treatments.

On ageing at 475 C, the solution treated and quenched (1100 C) specimens show an initially slow rate of hardening until a period of about 500 hours has elapsed, when a discontinuity in the hardening rate results in further hardness increases occurring relatively rapidly. The differences in nitrogen content among the as-received and the nitrided specimens, 26-1-Q and 26-1-N-Q respectively, do not appear to change the hardening kinetics; this result is consistent with their similar microstructures as observed in TEM.

The quenched and 475 C aged specimens show a very dense preferential precipitation at interfaces such as grain boundaries. These fine precipitates scatter the electron beam strongly and are probably chromium rich, in which case the resultant depletion of alloying chromium would account for the heavy etching at these interfaces that is apparent in optical microscopy. A more important feature of the quenched and aged specimens is the high density of small strain centres, visible only under two-beam conditions, and which are present extensively throughout the grains. These zones have strain fields up to 10 nm in size and which are highly strained (judging from the degree of contrast produced) in an isotropic manner which is greatest along

<100> directions. They form during the first 300 hours of ageing and change relatively little thereafter; their formation appears to coincide with the initial slow rate of hardness increase up to about HV 220 measured during this period. The zones have similar appearance and hardness values, to the small chromium nitride precipitates formed during 600 C ageing of quenched specimens, described in Chapter 3.

By contrast, the 800 C annealed specimens have a rapid initial rate of hardening at 475 C which becomes consistently slower as ageing proceeds until the peak at about HV 360 is reached. At any given ageing time, the annealed specimens are considerably harder than their quenched counterparts. They develop a different form of microstructure during ageing, compared with the corresponding quenched specimens. The features observed in TEM can best be described as contrast modulations along <100> directions, visible with difficulty after 300 hours of ageing and more easily after longer periods. The modulations form uniformly throughout the specimen, irrespective of crystallographic discontinuities such as grain boundaries. They are very small, with a periodicity of only about 6 nm (ie. only about 20 unit cells), and do not show the large lattice strains associated with the zones present in the quenched specimens described above.

In the case of a previously 600 C hardened specimen, whose microstructure contains a high density of small chromium-nitrogen zones with associated matrix strain fields, the first twenty hours of ageing at 475 C proceed similarly to the quenched specimens (ie. at a slow rate of hardness increase). Thereafter an increase in rate occurs and the hardness increases with the faster rate associated with the annealed specimens. This specimen shows little further change in microstructure after prolonged ageing at 475 C. The small precipitates with large strain fields, present after 600 C ageing, have not changed in appearance and are

clearly not associated with the large hardness increase found after 475 C ageing.

The XRD measurements on the 475 C aged specimens reveals the existence, through the presence of secondary peaks close to the Bragg reflections, of separate phases whose lattice parameters vary slightly from those of the matrix. The compositions of these phases were calculated from standard values of lattice parameters of the elements, with the ratio Cr:Mo assumed constant at 26:1 and the Fe:Cr ratio varying. The secondary peaks were found to correspond to domains of either high or low chromium contents: in the quenched specimen these are approximately 80% and 6% Cr respectively, and in the annealed, 60% and 18%. Similar peaks were also observed in the XRD trace from a quenched specimen aged at 550 C for an extended period.

Ageing at a temperature of 550 C results in considerable hardening in both the annealed and the quenched specimens. The rates of hardening in the quenched cases are greater at 550 C than at 475 C; however in the annealed case, the rate is slower at 550 C than at 475 C. Thus contrary to what was found at 475 C, the hardening rate at 550 C is slower in the annealed case than in the quenched. The ageing at 550 C of specimens already hardened by chromium nitride precipitation at 600 C, results in further hardening although at a reduced rate compared with ageing of the same (600 C hardened) material at 475 C. This provides evidence that a hardening mechanism other than nitride precipitation, is operative at 550 C.

The electron-beam refined 26Cr-1Mo steel (Climax Molybdenum) demonstrates similar 475 C ageing behaviour to the vacuum melted equivalent, being affected by the type of preliminery heat treatment used. In particular, prior quenching from solution treatment at 1100 C results in a lower rate of hardening at 475 C than does annealing at 800 C, and nitriding at 1100 C retards the ageing even more.

The 30Cr steel of moderately high interstitial content hardens considerably - to final values of HV 390-400 - on ageing at 475 C. TEM examination reveals different microstructures after ageing, depending on whether the specimen was previously quenched from 1100 C or annealed at 800 C; these microstructures were consistent with those encountered in corresponding 26Cr-1Mo steels after ageing. The quenched specimen contained a high density of coherent precipitates, planar in morphology and lying on {100} planes, as well as a smaller species of strain centre which was also present in large numbers. The annealed specimen showed a matrix strain contrast, identical to that observed during TEM examination of annealed specimens of the 26Cr-1Mo steel which had been aged similarly. The strain contrast modulations have a periodicity of about 12 nm, and are characterized by a uniformity of distribution irrespective of the presence of discontinuities such as dislocations or large incoherent precipitates.

High-resolution XRD measurements made on the 475 C aged specimens of 30Cr steel, produced secondary Bragg peaks similar to those found in the aged 26Cr-1Mo steels. Calculation of chromium contents from the lattice parameters derived from the peak positions, gives chromium-rich and chromium-depleted zones, containing about 60% and 15% chromium respectively in the quenched specimen and 67% and 11% in the annealed.

6.2 Discussion of Results: 26Cr-1Mo steel

The experimental rsults summarized above provide information on aspects of the 475 C hardening reaction which, as far as is known, have not been published previously. The first aspect is the effect of the state of the interstitials on the mechanism and kinetics of the chromium-rich phase formation and on the associated microstructure; the second is the detection of this chromium-rich phase formation, and the measurement of lattice parameter and hence chromium content

thereof, by the technique of XRD. In addition, valuable information has been obtained from the TEM examination of aged specimens, which can be related to ageing at temperatures above the spinodal. A consideration of all of these results allows one to conclude that two mechanisms of decomposition into chromium-rich phases are possible when the 26Cr-1Mo steel is aged at 475 C. These mechanisms are chromium nitride zone formation, and spinodal decomposition into chromium-rich ferrite (known as α') within a chromium-depleted ferrite matrix. The two mechanisms are discussed below.

The 475 C age hardening results shown in fig. 4.1 are remarkable for the time delay of a few hundred hours before the hardness will increase above about HV 220, found in specimens 26-1-(N)-Q. The specimens 26-1-A, on the other hand, harden at a much faster rate from the onset of ageing. The specimens quenched from solution treatment or nitriding (26-1-(N)-Q) have, after ageing for about 300 hours, microstructures similar to those found in quenched specimens aged at 600 C for about 10 hours, and which have similar measured hardness. These observations can be explained as follows.

In the presence of interstitial nitrogen, 475 C exposure results in the nucleation and growth of small chromium nitride zones, similar to those shown to form when these steels are aged at 600 - 700 C in the quenched state. These zones are very small and are present in a high density due to the large degree of supersaturation of interstitial nitrogen, and to the slow kinetics of growth, at 475 C. They are associated with large strain fields ("large" meaning somewhat larger than the actual zone size) which produce strong contrast under appropriate diffraction conditions in TEM. As a result of the formation of the zones and strain fields, a certain degree of hardening occurs during the first 100 hours of exposure at 475 C. During ageing for another 100 - 200 hours, the zones grow in size and largely deplete the matrix

of interstitial nitrogen; no further increase in hardness is provided by the chromium nitride zones. In any case, in the 26Cr-1Mo steel of only 0,02-0,04% nitrogen content, the amount of hardening due to this mechanism is not great, with a maximum hardness of about HV 220 being measured.

In the case of the 800 C annealed steels - both 26Cr-1Mo and 30Cr - there is virtually no nitrogen or carbon present in solid solution prior to ageing. Exposure at 475 C results in an immediate commencement of hardening which is continuous until peak hardness has been reached. Despite the relatively high hardness after about 300 hours of ageing, TEM reveals only barely visible microstructure at this stage. Even at peak hardness (HV 360), the structure can only be seen with difficulty. This lack of contrast is to be expected when phases rich in chromium are formed, for the reasons of small lattice strain and similar atomic scattering factors as outlined in Section 1.2. This microstructure is characteristic of spinodally decomposed alloys, eg. an Fe-20%Mo alloy (Miyazaki et al, 1980) which of course also has a b.c.c. structure and a miscibility gap. The observations on 475 C ageing in the annealed high-chromium steels are therefore consistent with a spinodal decomposition into chromium-rich phases in an iron-rich matrix.

Thus the formation of chromium-rich ferrite only occurs in the absence of interstitial nitrogen, but is responsible for a greater degree of hardening than is nitride zone formation. It applies to the annealed specimens from the onset of ageing at 475 C, and the quenched specimens after about 500 hours of ageing (on depletion of interstitials in solid solution). In the former case the change in mechanism is signified by the sudden discontinuous increase in the rate of hardening, as shown in fig. 5.2. In the annealed case the hardening rate is significantly higher during the initial hardening period (and in fact the rate is described by a different index in the logarithmic rate equation) than that which applies to the chromium nitride precipitation mechanism. This is attributed

to the fact that in the annealed case, the mechanism is spinodal decomposition. The precipitates are spaced about 7 nm apart and have chromium contents of about 60% after ageing for long enough periods for equilibrium to be approached.

The 475 C ageing behaviour of the specimen 26-1-N-600, ie nitrided and quenched, and hardened at 600 C to form a microstructure of chromium nitride zones, can be explained in terms of the above mechanisms. The 600 C ageing has removed most of the interstitial nitrogen from solid solution. When subsequently exposed at 475 C, hardening proceeds slowly by the nitride precipitation mechanism until about 20 hours has elapsed, at which point presumeably all of the interstitials have been removed. Thereafter the kinetics correspond to those applying to the formation of chromium-rich ferrite (see fig. 4.2) and hardening proceeds by this mechanism.

The 550 C ageing behaviour is characterized by an increased rate of hardening, relative to 475 C, in the 26-1-(N)-Q specimens, and a decreased rate, relative to 475 C, in the 26-1-A. These hardening behaviours can be interpreted as follows: the quenched specimens (26-1-Q and 26-1-N-Q) are, when held at a temperature of 550 C, in a similar non-equilibruim condition, (due to a supersaturation of interstitials) as at 475 C. The heterogeneous nucleation mechanism operates at both temperatures; however at the higher temperature the kinetics of zone formation are faster and hence hardening occurs at a faster rate.

The annealed specimens, on the other hand, undergo spinodal decomposition inside the miscibility gap (at 475 C). The higher temperature of 550 C is closer to the spinodal curve and thus the driving force for decomposition is much less and so decomposition and the observed result, hardening, occur at a slower rate. The fact that specimens 26-1-N-600 and 26-1-600, which have been hardened through the formation of a high density of small coherent nitride precipitates, do in fact harden more at 550 C, is further proof that at this

temperature a hardening mechanism other than chromium nitride precipitation is operative. Thus the results of age hardening at 550 C confirm that at this temperature the 26Cr-1Mo steel lies within the miscibility gap of the Fe-Cr phase diagram.

The use of XRD to confirm the occurrence of spinodal decomposition has been reported for several alloy systems. Krull et al (1972) aged an alloy of 6 atomic percent titanium in copper and studied the resultant microstructure by means of XRD and TEM. With progression of ageing they found initially the appearance of symmetrical sidebands which were associated with <100> compositional modulations. With continued ageing the discrete Bragg reflections of a Ti-rich phase, together with those of the Ti-depleted matrix, were present on the XRD trace. TEM confirmed that the secondary diffraction peaks were associated with the presence of Ti-rich precipitates.

An alloy of 20% molybdenum in iron undergoes spinodal decomposition when aged at a temperature within the miscibility gap (Miyazaki et al, 1980). Similar to the Cu-Ti case above, the first stage of decomposition consists of <100> compositional modulations, visible in TEM, which result in the presence of sidebands associated with the 200 Bragg reflection in XRD. With ageing time the prominence of the observed striations increases, and a second XRD peak replaces the sideband satellites. This diffraction doublet is observed in every main Bragg reflection, suggesting the coexistence of two b.c.c. structure phases with lattice parameters corresponding to Mo enrichment and Mo depletion. This latter observation is particularly significant as the Fe-Cr system has many similarities with the Fe-Mo.

The present XRD results confirm the formation of chromium-rich phases (containing about 60% chromium) within a chromium-depleted matrix (about 18% Cr) during ageing of annealed specimens at 475 C. As far as is known, the

observation of chromium-rich ferrite in aged ferritic stainless steels, using the technique of XRD, has not been reported previously. By comparison, in the segregation into molybdenum-rich phases reported in the analogous Fe-20%Mo system (Miyazaki et al, 1980) secondary peaks are more readily observed because of the greater difference in constituent lattice parameters than the Fe-Cr system.

The XRD measurements on the 1100 C quenched specimens give an even greater degree of segregation after 475 C ageing, with chromium contents of 80% and 6% in precipitate and matrix respectively. This is somewhat surprising as the hardness increase on ageing was less in these than in the annealed specimens; the only explanation that can be offered is that the large lattice distortions associated with the chromium nitride zones, have a real or apparent effect on the lattice parameters of the chromium-rich ferrite and of the depleted matrix. Nevertheless, chromium contents of 60-80% for the chromium-rich phase are consistent with the miscibility gap shown on the accepted Fe-Cr phase diagram.

The TEM examinations of thin foils taken from aged specimens, are remarkable for the differences in appearance between the quenched and the annealed materials. The impressive TEM contrast of the chromium nitride zones in the quenched and aged material, arises from the large lattice strains associated with the zones: the diffracted electron beam passing through the strained lattice, undergoes a phase shift relative to the phase of the beam passing through the unstrained matrix. On the other hand, as discussed in Chapter 1, chromium-rich ferrite precipitates strain the lattice very little, and produce weak contrast which arises from their structure factor differing from that of the matrix. Consequently such precipitates should only be visible when they are of the order of 10 nm in size, and even then they should be of low contrast relative to the matrix.

The TEM images of the 800 C annealed and 475 C aged specimens

(both 30Cr and 26Cr-1Mo steels) do indeed show a contrast modulation with a periodicity of about 6-8 nm but which is quite weak. Nevertheless, comparison with micrographs of spinodally decomposed alloys of different compositions, shown in the papers referred to in Section 1.3 of this thesis, confirms that the present TEM images are consistent with those produced by spinodal decomposition.

We now consider the present work in relation to some of the published results of research into the 475 C hardening reaction, particularly in the context of the hardening mechanisms discussed above.

The thin-foil TEM study of an aged 21Cr steel carried out by Blackburn and Nutting (1964), has been described in Chapter 1. The steel contained 0,02% each of carbon and nitrogen and was quenched from 1100 C: it was thus similar to the 1100 C quenched 26Cr-1Mo steel used in the present study, but had lower chromium and molybdenum contents and higher carbon. Ageing at 475 C produced a hardness increase and microstructural changes: after 150 hours the hardness was HV 220 and the associated TEM microstructure consisted of numerous small coherent precipitates with large associated matrix strain fields. Further ageing caused these precipitates to grew into discs lying on $\{100\}$ matrix planes.

Comparison with the present results suggests that Blackburn and Nutting observed the hardening and microstructure associated with chromium nitride and carbide precipitation, with similar rates of hardening measured as are found in specimens 26-1-(N)-Q in the present study. However, it is likely that the ultimate hardness of almost HV 300 encountered after several thousand hours of ageing, was due to the formation of precipitates of chromium-rich ferrite, although no features associated with the α' phase were recognized in TEM.

The results of Lagneborg (1967) on a 30Cr steel containing

0,025% of nitrogen, aged at 475 C when in the 1050 C quenched condition, confirm the relatively slow rate of hardening of specimens aged in this condition. A hardness increase of only HV 40 was measured over the first 50 hours of 475 C ageing, which corresponds exactly with the increase measured in the present study during chromium nitride zone formation in the quenched specimens. Micrographs of the structure associated with this initial period of ageing, show a strongly-contrasting fine precipitation, similar to that seen in the quenched and aged specimens in the present study. While Lagneborg attributes this microstructure to chromium-rich ferrite, its appearance suggests that it is chromium nitride precipitation, particularly as it was visible after only one hour of ageing.

Lagneborg found, on ageing at 550 C for a period of as little as 1 hour, a high density of small precipitates whose morphology was either disc-like or, when ageing was carried out immediately after quenching, spherical. The discs have a strong resemblance to the chromium nitride discs, formed in the quenched 26Cr-1Mo steel on ageing for short periods at 600-700 C, in the present study. The large strain fields and short time for formation at 550 C, suggest that they are chromium nitrides rather than chromium-rich ferrite.

Plumtree and Gullberg (1976) studied the 475 C reaction of a low-interstitial 25Cr steel containing only about 0,01% nitrogen, which had been quenched from 850 C prior to ageing at 475 C. A thin-foil TEM micrograph taken after only 50 hours of ageing, shows small strain centres which are present in large numbers and appear to be disc-shaped. They are similar in appearance to the strain centres present in specimens 26-1-(N)-Q after ageing at the same temperature, with both cases showing relatively strong strain contrast. Despite the prominent microstructure, the hardness is only HV 210, which is close to the maximum found to be associated with chromium nitride zones in the present study. It therefore seems likely, from the morphology and strong

contrast of the strain centres, and from the relatively low hardness of the specimen, that Plumtree and Gullberg observed chromium nitride precipitation rather than the formation of chromium-rich ferrite.

The results of the work of Hendry et al (1979) on the ageing of a 22Cr steel with varying interstitial nitrogen contents, referred to in Section 1.2, appear at first sight to contradict the essence of the present results. While the present results show that the 475 C reaction is affected by the presence of interstitial nitrogen, and in fact the formation of and hardening by chromium-rich ferrite precipitates are delayed until all interstitials have formed precipitates or zones which have a lesser hardening effect, Hendry et al find opposite results. They propose that hardening of the 22Cr steel at 500 C occurs solely as a result of chromium nitride formation, and that the degree of hardening increases with interstitial nitrogen content. With the highest nitrogen content of 0,08%, hardening to over HV 300 was found; they were the first to show that the total contribution to 475 C hardening can arise from the formation of Cr-N zones from interstitial nitrogen, and to propose an important role for nitrogen in the reaction. By contrast, the present study shows that the main contribution to hardening at 475 C arises from the presence of chromium-rich ferrite precipitates, and not from chromium nitrides.

Hendry et al found that in all specimens of different nitrogen contents, the hardening occurred within the first 100-150 hours of ageing with no further increases during the duration of the test (ie to a total time of 540 hours). However, an examination of fig. 4.1 of the present work confirms that hardening by nitride precipitation should indeed occur during the first 100 hours, and particularly so at the higher temperature of 500 C). It also confirms that hardening by formation of chromium-rich ferrite should only commence after about 500 hours has elapsed. Considering the higher temperature and lower chromium content they used -

factors which would both tend to slow down the rate of spinodal decomposition - it is possible that a longer ageing period would have resulted in spinodal decomposition in their specimens. An alternative explanation is that the composition-temperature used lies outside of the coherent spinodal.

They found a greater degree of hardening to be produced by the Cr-N clusters, than did the present study. While they measured hardness values of HV 250 and at least 300, for nitrogen contents of 0,02% and 0,04% respectively, in the present study the precipitation of chromium nitrides never produced hardness values any greater than HV 220, despite the similar nitrogen contents. Possible reasons for the discrepancy are in the load used in hardness testing (50 gram used by Hendry et al compared with 10 kg in the present study), and in the compositions of the steels where the chromium and molybdenum contents differ.

The ageing reaction of a titanium-stabilized variant of the 26Cr-1Mo steel (type AL26-1S) was studied by Nichol et al (1980). The steel contained 0,03% carbon and 0,02% nitrogen, most of which were precipitated as harmless titanium carbo-nitrides during a preliminery annealing treatment at 870 C. The effectiveness of the annealing in removing interstitials from solid solution, is confirmed by the presence of large particles of titanium carbonitrides together with some chromium carbides, in this material prior to ageing.

Prolonged ageing at a temperature of 482 C resulted in large changes in mechanical properties, generally within the first 100 hours, which were indicative of severe embrittlement, for example increases in hardness and strength. However, TEM on thin foils taken from material aged for this period showed no evidence of strain centres or contrast modulations, despite the high measured hardness of equivalent to about HV 280. Microstructural features were however present after 1000 hours of ageing, in the form of matrix contrast modulations

along {100} matrix planes, with a perodicity which appears to be about 10 nm. This TEM contrast is quite similar,in both appearance and measured periodicity, to that observed in the present study in specimens 26-1-A aged at 475 C, as described in Section 4.4.

These results can be considered to confirm the findings of the present study, viz. that in the absence of interstitials, exposure at 475 C results in microstructural changes occurring within the first 100 hours which have severe hardening effects. These changes, however, are only visible in TEM after considerably longer ageing periods, when they appear as contrast modulations which can be attributed to spinodal decomposition into chromium-rich precipitates within a chromium-depleted matrix.

6.3 Conclusions

1. The low-interstitial 26Cr-1Mo steel undergoes hardening at the temperature of 475 C by two mechanisms: nucleation and growth of chromium nitride zones with large strain fields in the surrounding lattice, and spinodal decomposition into chromium-rich ferrite (α') within a chromium-depleted matrix. The former mechanism occurs preferentially when interstitial nitrogen is present. An effect of this is to delay the onset of spinodal decomposition until all interstitials have been precipitated.

2. The formation of chromium nitride zones leads to relatively small hardness increases which occur slowly, eg. of HV 50 over a period of several hundred hours in a 26Cr-1Mo steel containing up to 0,04% nitrogen. The zones are readily visible in TEM as small centres of contrast within matrix strain fields. They are identified as as Cr-N clusters on {100} lattice plains, and are identical in all respects except size, to the precipitates produced in these steels on ageing at temperatures up to 750 C.

3. The TEM observations by various authors (viz. Blackburn and Nutting (1964), Lagneborg (1967), and Plumtree and Gullenberg (1976)) of microstructural features associated with 475 C hardening, and interpreted as chromium-rich ferrite, would appear in the above cases to be chromium nitride zones and associated strain fields.

4. Spinodal decomposition resulting in the formation of chromium-rich ferrite, proceeds from the onset of ageing at 475 C. This is associated with substantial hardening, which can be measured within minutes of the commencement of ageing. The rate and extent of hardening by this mechanism exceed those of the chromium nitride precipitation: an overall hardness increase of about HV 200 is measured after about 1000 hours of ageing.

5. The spinodally decomposed structure is not readily visible in TEM, even after about 300 hours of ageing. However, after about 900 hours, contrast modulations are present in the TEM image under two-beam conditions. The weakness of the contrast is attributed to the small degree of lattice strain arising from the similarities in lattice parameters of zone and matrix and the small degree of structure factor contrast which is due to the similarity in atomic scattering factors of Fe and Cr, although ultimately it is the small size of the zones that renders them elusive to TEM observation. The modulation spacing is measured at 6-7 nm (present work) and 10 nm (Nichol et al).

6. Precision XRD measurements on the aged specimens reveal the existence of secondary Bragg reflections which arise from the presence of phases of different lattice parameter from the matrix. By analogy with results from other alloy systems including Fe-20%Mo, these confirm that spinodal decomposition has occurred. It can be concluded from the lattice parameters that the precipitates formed when annealed specimens are aged, contain about 60% chromium within an iron-rich matrix of 18% chromium. The quenched and aged

specimens are calculated to have about 80% chromium in the zones; this high value is possibly due to the presence of nitrogen and the resultant lattice expansion which it causes.

7. A specimen hardened at 600 C by the formation of chromium nitride precipitates, will undergo further (and greater) hardening by spinodal decomposition when subsequently aged at 475 C. As the microstructure of the chromium nitrides does not alter, this proves that the major 475 C hardening effect is due to the formation of chromium-rich ferrite.

8. The observation of age hardening at 550 C by both nitride precipitation and spinodal decomposition, leads to the conclusion that this temperature lies within the coherent spinodal for the 26Cr-1Mo steel composition.

9. The commercial purity 30 Cr steel, when aged at 475 C in the annealed condition (ie. no interstitials in solid solution), undergoes spinodal decomposition which results in considerable hardening due to the formation of chromium-rich zones. The zones have a spacing of about 12 nm and a composition, as calculated from XRD measurements, of about 67% chromium within an iron-rich matrix containing about 11% chromium

LITERATURE CITED

Ashby, M.F. and Brown, L.M.: Philos. Mag., Vol 8, 1963, p 1083.

Baerlecken, E.B., Fischer, W.A. and Lorenz, K.: Stahl und Eisen, Vol 81, 1961, pp 768-778.

Binder, W.O. and Spendelow, H.R., Trans. ASM, Vol 43, 1951, pp 211-229.

Blackburn, M.J. and Nutting, J.: J. Iron and Steel Institute, Vol 202, 1964, pp 610-613.

Bond, A.P.: Trans AIME, Vol 245, 1969, pp 2127-2134.

Brewer, L. and Chang, S-G.: ASM Metals Handbook, 8th Ed., Vol 8, 1973, p 422.

Chandra, D. and Schwartz, L.H.: Metall. Trans., Vol 2, 1971, pp 511-519.

Cornie, J.A., Datta, A. and Soffa, W.A.: Metall. Trans., Vol 4, 1973, pp 727-733.

Demo, J.J.: Corrosion, Vol 27, 1971, pp 531-544.

Demo, J.J.: Structure, Constitution, and General Characteristics of Wrought Ferritic Stainless Steels, ASTM STP 619, ASTM, 1977.

De Fontaine, D.: Acta Metall., Vol 17, 1969, p 477-482.

De Nys, T. and Gielen, P.M.: Metall. Trans., Vol 2, 1971, pp 1423-1428.

Grobner, P.J.: Metall. Trans., Vol 4, 1973, pp 251-260.

Grubb, J.F. and Wright, R.N., Metall. Trans. A, Vol 10A, 1979, pp 1247-1255.

Hendry, A., Mazur, Z.F. and Jack, K.H.: Metals Science, Vol 13, 1979, pp 482-486.

Hirsch, P.B., Howie, A., Nicholson, R.B., Pashley, D.W. and Whelan, M.J.: Electron Microscopy of Thin Crystals, Butterworths, 1965.

Hodges, R.: Corrosion-NACE, Vol 27, 1971, pp 119-127.

Imai, Y., Izumiyama, M. and Masumoto, T.: Sci. Rep. RITU, Metal Soc. of Japan, 1964.

Krawitz, A. and Sinclair, R.: Philos. Mag., Vol 31, 1975, p 697.

Krull, W.E., Starke, E.A. and Newman, R.W.: Mater. Sc. and

Eng., Vol 9, 1972, pp 211-216.
Kubaschewski, O. and Chart, T.G.: J. Institute of Metals, Vol 93, 1964-65, p 329.
Lagneborg, R.: Trans. ASM, Vol 60, 1967, pp 67-78.
LaSalle, J.C., and Schwartz, L.M.: Acta Metall., Vol 34, 1986, pp 989-1000.
Leitch, J.E. and Ball, A.: Proc. Electron Microscopy Soc. S. Africa, Vol 9, 1979, pp 47-48.
Livak, R.J. and Thomas, G.: Acta Metall., Vol 19, 1971, pp 497-505.
Lula, R.A., Lena, A.J. and Kiefer, G.C.: Trans ASM, Vol 46, 1954, pp 197-230.
Marcinkowski, M.J., Fisher, R.M. and Szirmae, A: Trans. AIME, Vol 230, 1964, pp 676-689.
Martin, J.W. and Doherty, R.D.: Stability of Microstructure in Metallic Systems, Cambridge, 1976.
Mityazaki, T., Takagishi, S., Mori, H. and Kozakai, T.: Acta Met., Vol 28, 1980, pp 1143-1153.
Nichol, T.J., Datta, A. and Aggen, G.: Metall. Trans. A, Vol 11A, 1980, pp 573-585.
Plumtree, A. and Gullberg, R.: J. Testing and Evaluation, Vol 2, 1974, pp 331-336.
Plumtree, A. and Gullberg, R.: Metall. Trans. A, Vol 7A, 1976, pp 1451-1457.
Rajkay, L.: Proc. ASTM, Vol 67, 1967, pp 158-169.
Roy, R.B. and Solly, B.: Scan. J. Metallurgy, Vol 2, 1973, pp 243-248.
Semchyshen, M., Bond, A.P. and Dundas, H.J.: Proc. Symp. Towards Improved Ductility and Toughness, Kyoto, Japan, 1971, pp 239-253.
Thielsch, H.: Welding J. Research Suppl., Vol 34, 1955, pp 22S-30S.
Williams, R.O. and Paxton, H.W.: J. Iron Steel Institute, Vol 185, 1957, pp 358-374.
Williams, R.O.: Trans. AIME, Vol 212, 1958, pp 497-502.
Wright, R.N.: Welding J. Research Suppl., Vol 50, 1971, pp 434S-440S.
Wolfe, R.A. and Paxton, H.: Trans. AIME, Vol 230, 1964, p 1426.

APPENDIX A

Elektronmikroskopievereniging van Suidelike Afrika PORT ELIZABETH (1979)

THE MICROSTRUCTURE OF AN AGED FERRITIC STAINLESS STEEL CONTAINING NITROGEN

J.E. Leitch and A. Ball

Department of Metallurgy and Materials Science, University of Cape Town

The ferritic stainless steels are of interest because of their better resistance to stress corrosion cracking and lower cost compared with austenitic grades. However their use has been restricted by poor toughness associated with the presence of residual carbon and nitrogen. Reasons proposed for this embrittlement after high temperature exposure include grain boundary precipitation of carbides and nitrides during subsequent slow cooling[1], precipitation on existing dislocations[2] and hardening by fine precipitates[3]. This study is being undertaken to clarify the behaviour of nitrogen in a high-chromium ferritic stainless steel.

Nitrogen was diffused into a low-interstitial Fe-26Cr-1Mo alloy at 10 Pa and 1100°C, followed by water quenching and ageing at temperatures up to 800°C. Changes in mechanical properties were monitored by hardness tests (Fig.1) and microstructural changes were observed by TEM. Ageing proceeded slowly at temperatures below 600°C, while at 600°C a hardness peak was reached followed by very gradual softening. Ageing at 700°C proceeded rapidly to peak hardness followed by softening to the as-quenched hardness value, while at 800°C the overaged condition showed a hardness well below the as-quenched value.

The microstructures associated with ageing are shown in the bright field TEM micrographs (Figs. 2-5). Ageing at 600°C for 6 hours (HV 193) produced a high density of fine precipitates amongst a few larger coherent precipitates (Fig.2). Dislocations are decorated and their immediate neighbourhoods are denuded of fine precipitates. This indicates that migration to sinks and coalescence is occurring. The microstructure is characteristic of a precipitation hardening alloy aged to peak hardness; as could be predicted from the 600°C ageing curve, little change in this structure was observed after ageing for several hundred hours. Fig.3 shows the structure of an overaged specimen (700°C for 4 hours to give HV 159). Numerous coherent precipitates with characteristic lobes of contrast are present and since their lines of no contrast are not always perpendicular to $\underline{g}$, the strain fields are anisotropic and the particles non-spherical. Figs. 4 and 5 show a grossly overaged specimen (800°C for 4 hours, HV 145) which contains large incoherent nitride precipitates characteristic of an overaged alloy, and some smaller coherent precipitates, possibly of a different species. The grain boundaries of this specimen were heavily precipitated (Fig. 5).

It can be concluded that the principal hardening mechanism in these alloys is precipitation hardening by small coherent precipitates. Ductility may be restored through overageing at 700°C or above to produce large incoherent precipitates particularly at the grain boundaries.

J.E.L. acknowledges financial support from the N.I.M.

REFERENCES:

1. Pollard, B., 1974, Metals Technol. 1, 31.
2. Demo, J.J., 1971, Corrosion 27, 531.
3. Plumtree, A. and Gullberg, R., 1974, J. Testing Eval. 2, 331.

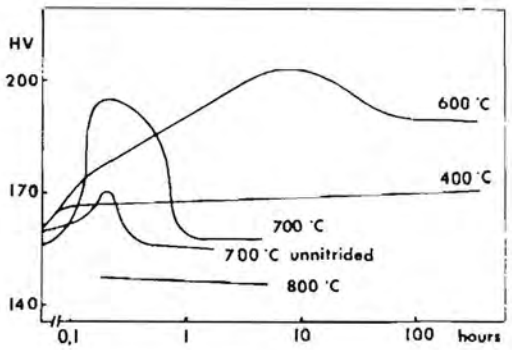

Fig.1. Vickers hardness as a function of ageing time for Fe-26Cr-1Mo alloy containing nitrogen.

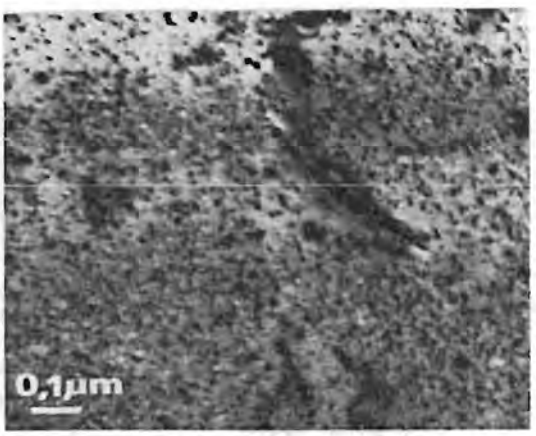

Fig.2. Aged at 600°C for 6h.

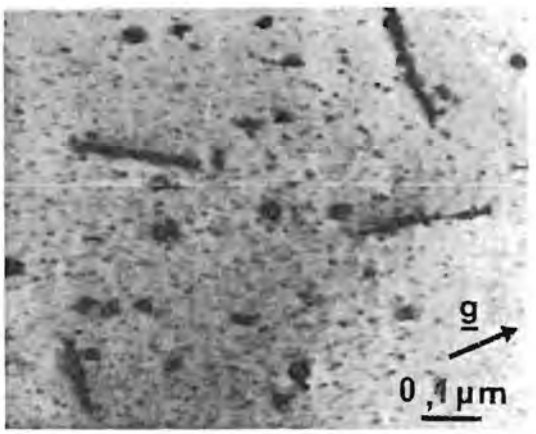

Fig.3. Aged at 700°C for 4h.

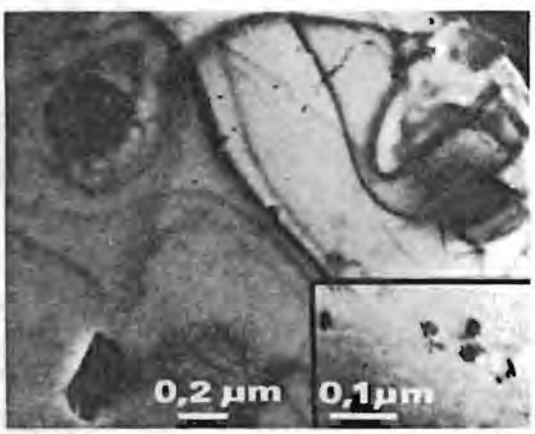

Fig.4. Aged at 800°C for 4h with inset showing detail.

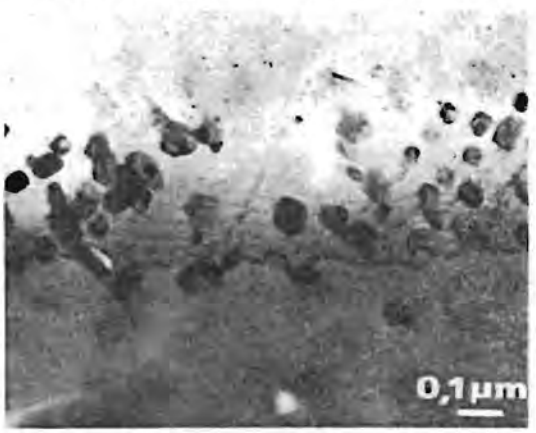

Fig.5. Aged at 800°C for 4h showing grain boundary precipitates.